

# On the deactivation of cobalt-based Fischer-Tropsch synthesis catalysts

**Citation for published version (APA):**

Moodley, D. J. (2008). *On the deactivation of cobalt-based Fischer-Tropsch synthesis catalysts*. [Phd Thesis 1 (Research TU/e / Graduation TU/e), Chemical Engineering and Chemistry]. Technische Universiteit Eindhoven. <https://doi.org/10.6100/IR637807>

**DOI:**

[10.6100/IR637807](https://doi.org/10.6100/IR637807)

**Document status and date:**

Published: 01/01/2008

**Document Version:**

Publisher's PDF, also known as Version of Record (includes final page, issue and volume numbers)

**Please check the document version of this publication:**

- A submitted manuscript is the version of the article upon submission and before peer-review. There can be important differences between the submitted version and the official published version of record. People interested in the research are advised to contact the author for the final version of the publication, or visit the DOI to the publisher's website.
- The final author version and the galley proof are versions of the publication after peer review.
- The final published version features the final layout of the paper including the volume, issue and page numbers.

[Link to publication](#)

**General rights**

Copyright and moral rights for the publications made accessible in the public portal are retained by the authors and/or other copyright owners and it is a condition of accessing publications that users recognise and abide by the legal requirements associated with these rights.

- Users may download and print one copy of any publication from the public portal for the purpose of private study or research.
- You may not further distribute the material or use it for any profit-making activity or commercial gain
- You may freely distribute the URL identifying the publication in the public portal.

If the publication is distributed under the terms of Article 25fa of the Dutch Copyright Act, indicated by the "Taverne" license above, please follow below link for the End User Agreement:

[www.tue.nl/taverne](http://www.tue.nl/taverne)

**Take down policy**

If you believe that this document breaches copyright please contact us at:

[openaccess@tue.nl](mailto:openaccess@tue.nl)

providing details and we will investigate your claim.

# On the Deactivation of Cobalt-based Fischer-Tropsch Synthesis Catalysts

PROEFSCHRIFT

ter verkrijging van de graad van doctor aan de  
Technische Universiteit Eindhoven, op gezag van de  
Rector Magnificus, prof.dr.ir. C.J. van Duijn, voor een  
commissie aangewezen door het College voor  
Promoties in het openbaar te verdedigen  
op donderdag 6 november 2008 om 16.00 uur

door

Denzil James Moodley

geboren te Port Shepstone, Zuid-Afrika

Dit proefschrift is goedgekeurd door de promotor:

prof.dr. J.W. Niemantsverdriet

Copromotor:

dr. J. van de Loosdrecht

Denzil J Moodley

Technische Universiteit Eindhoven, 2008

A catalogue record is available from the Eindhoven University of Technology Library

ISBN: 978-90-386-1399-4

Copyright © 2008 by Denzil J Moodley

The research described in this thesis was carried out at the Schuit Institute of Catalysis within the Laboratory of Inorganic Chemistry and Catalysis, Eindhoven University of Technology, The Netherlands. Financial support was provided by Sasol Technology (Pty) Ltd.

Cover design by Denzil J Moodley and Paul Verspaget (Verspaget & Bruinink).

Front: A slurry bubble column Fischer-Tropsch synthesis reactor.

Back: The Oryx Gas-to-Liquid plant in Ras Laffan, Qatar.

Permission to use drawings was obtained from Sasol Ltd.

Printed at the Universiteitsdrukkerij, Eindhoven University of Technology.

*Dedicated to my parents*



---

# Contents

---

<b>Chapter 1</b>	Introduction and outline	1
<b>Chapter 2</b>	Experimental Techniques	19
<b>Chapter 3</b>	The impact of cobalt aluminate formation on the deactivation of cobalt-based Fischer-Tropsch synthesis catalysts	35
<b>Chapter 4</b>	The formation and influence of carbon on cobalt-based Fischer-Tropsch synthesis catalysts: <i>A Review</i>	55
<b>Chapter 5</b>	Carbon deposition as a deactivation mechanism of cobalt-based Fischer-Tropsch synthesis catalysts under realistic conditions	91
<b>Chapter 6</b>	Factors that influence carbon formation on Co/Al <sub>2</sub> O <sub>3</sub> catalysts	117
<b>Chapter 7</b>	Opportunities to study the behaviour of cobalt nanoparticles by using model FTS catalysts: <i>Initial results and outlook</i>	137
<b>Summary</b>		157
<b>Samenvatting</b>		161
<b>Acknowledgements</b>		165
<b>List of Publications</b>		169
<b>Curriculum Vitae</b>		171



---

# Chapter 1

---

## Introduction and outline

### 1.1 Fischer-Tropsch synthesis –a brief historical overview and current prospects

The early 20<sup>th</sup> century was an exciting period in the development of catalysis. The development of the ammonia synthesis process marked the start of large scale heterogeneous catalysis as well as high pressure continuous processing [1]. It was also during this time that the reaction of mixtures of H<sub>2</sub>/CO (synthesis gas or syngas) to hydrocarbons was discovered. Sabatier and Serendens reported in 1902 that methane can be formed by passing syngas over nickel and cobalt [2]. The production of liquid hydrocarbons from syngas, over a cobalt oxide catalyst was first claimed, at least qualitatively, in a patent granted to BASF in 1913 [3]. At that time much research was conducted towards developing a process for the conversion of Germany's abundant coal reserves into fuels and chemicals. The German research efforts yielded two important discoveries. The first was the direct liquefaction of coal with H<sub>2</sub> at about 477 °C and up to 700 bar in the presence of finely divided iron catalysts by Friedrich Bergius in Rheinau-Mannheim [4]. The second discovery in the 1920's, was the production of hydrocarbons (synthol) in measurable amounts from syngas over alkalized iron catalysts at 100-150 bar, 400-450 °C by Franz Fischer and Hans Tropsch at the Kaiser-Wilhelm (presently Max Plank) Institute for Coal Research in Mülheim [5]. Later, Fischer and Tropsch succeeded in producing mainly hydrocarbons with cobalt and iron catalysts at much milder conditions (1 bar, 250-300 °C) [6]. This was a significant finding as they had hoped to produce liquid hydrocarbon motor fuels.

The patent rights for the Fischer-Tropsch synthesis (FTS) were acquired by Ruhrchemie AG in 1934 and soon after, the industrial application of the FT process



started in Germany [7]. By 1938 there were nine plants in operation utilizing cobalt-based catalysts at atmospheric pressure, having a combined capacity of about 13 000 bbl/day [8]\*. These synthetic fuels were utilised by Germany during the second World War and there is no doubt that the FTS was both a scientific and technological success. Even though these plants ceased to operate after the war, interest in the process remained due to the perception that the reserves of crude oil were very limited. After this period the commercialisation of the iron catalyst dominated, with cobalt being sidelined. Ruhrchemie and Lurgi formed an Arbeitsgemeinschaft (ARGE) that optimised the fixed bed iron catalyst to produce wax [9]. Based on syngas produced from methane, a gas-to-liquids (GTL), FTS plant with a capacity of 7 200 bbl/day was built and operated by Hydrocarbon Research Inc. in Brownsville, Texas, during the 1950s but a sharp increase in the price of methane caused the plant to be shut down [10].

South Africa, like Germany had no crude oil but plenty of coal that could be mined cheaply. Based on the world-wide prediction of increasing crude oil prices, Sasol's first FTS plant based on coal (approximately 2 200 bbl/day), employing iron-based catalysts, came on stream in 1955 in Sasolburg, South Africa [11]. However, even before construction of this plant was completed, the huge oil fields of the Middle East were discovered and consequently the predicted rise in the price of crude oil did not materialise and interest in the FTS all but disappeared. The oil embargo by OPEC (Organization of the Petroleum Exporting Countries) in the early 1970's led to a huge increase in the price of oil and, hence, the economics of the FTS in South Africa improved dramatically which led to the construction of two new and much larger Sasol coal-to-liquid (CTL) plants which came on stream in 1980 and 1982 in Secunda, South Africa. [11]. This period also marked the "rediscovery" of cobalt and much research efforts were put into the development of new cobalt catalysts for application in low temperature FTS [12]. Additionally there was a focus on converting the largely untapped natural gas reserves into transportable liquid products. In 1993, a 22 000 bbl/day GTL plant went into full production at Moss gas (now PetroSA) in Mossel Bay, South Africa using the licensed iron catalyst and circulating fluidised bed (i.e. CFB) reactor technology from Sasol [11]. A few months

---

\* 1 bbl/day is approximately equivalent to 50 tons/yr

later Shell began operating a 12 000 bbl/day plant in Bintulu, Malaysia that converted natural gas into high quality synthetic oil products and speciality chemicals using cobalt-based catalysts [13]. The latest large scale GTL plant, employing cobalt catalysts, in operation since 2007, is the Oryx-GTL plant in Qatar, with a nominal capacity of 34 000 bbl/day, which is a joint venture between Sasol and Qatar Petroleum [14].

Many companies have invested heavily into developing propriety FTS technology with a preference towards cobalt-based FTS catalysts, either for their own use or for licensing [15, 16]. These include Shell [13, 17], ExxonMobil [18], BP [19], Syntroleum [20], Rentech [21], ENI/IFP/AXENS [22] and ConocoPhillips [23]. Sasol is by far the largest producer of synthetic fuels and chemicals via the FTS and has commercial experience with both CTL and GTL technology. The total production from Sasol's plants including licensed technology is in excess of 200 000 bbl/day. Remarkably, today, 80 years after Fischer and Tropsch made their discovery there is renewed interest in the process that bears their name. There are various factors that have contributed to this:

- The rising price of crude oil. At the time of writing the oil price is over \$100 barrel. This fact makes the production of synthetic fuels from alternative sources attractive.
- Legislative constraints on fuel quality. Synthetic fuels, both produced from natural gas and coal are much cleaner than those derived from crude oil, while still being of a high quality. For example CTL diesel [24] has a sulphur content of less than 5 ppm, aromatic content of less than 1% and a cetane number of more than 70.
- Geopolitical reasons. Some countries may want to reduce their dependence on crude oil. The United States, heavily dependent on the Middle East for crude oil, has at its disposal the largest coal reserves in the world estimated at 270 billion recoverable tons [25]. CTL technology may play an important part in producing synthetic fuels in the future.
- The China and India factor. These countries are home to more than a third of the world's population and are experiencing major economic growth. Their

energy needs will increase drastically in the future. Both have large amounts of reserves of coal (combined amount of 200 billion tons) that can be converted to synthetic fuels. It is interesting to note that Sasol has announced plans to set-up CTL plants in both India and China in the near future [26, 27].

- Biomass-to-liquids (BTL) and the carbon neutral economy. Biomass is the only long-term carbon containing renewable for liquid fuels or for synthesizing chemicals. The European Union plans to increase the fraction of biogenic fuels from 2% in 2005 to 8% in 2020 [28]. The FTS can be used to produce synfuels from gasified biomass. In 2007, Choren, a bioenergy company built a 300 bbl/day BTL plant that uses Shell's FTS technology to transform biomass to biodiesel [29].

## 1.2 Overview of Gas-to-liquids (GTL) technology

Gas-to-liquids is the process of converting natural gas into transportable liquids and has gained considerable interest in the last decade. There are several key factors that drive growth in the GTL industry [16, 30, 31]:

- The need to monetize the large amount of existing stranded natural gas reserves.
- The market demand for cleaner fuels and new cheaper chemical feedstocks.
- Technological development by existing and new role players which is leading to cost effectiveness of FTS technology from development of more active catalysts and improved reactor systems.
- Increased interest from gas-rich host countries.
- The need to diversify economies and to create new employment opportunities.

The GTL process can be divided into three steps; syngas generation, syngas conversion and hydroprocessing [30]. Syngas generation typically accounts for more than 50% of the capital expenditure in the process [32]. The methane molecule is very stable and the reaction is very endothermic and therefore a high energy input is required. Syngas can be generated from steam reforming, partial oxidation, autothermal reforming or combined two step reforming of methane [30]. It should be noted that the air separation unit (ASU) contributes to a large part of the cost of

syngas generation. Syngas conversion is at the heart of the process and the aim here is to produce paraffinic wax using low temperature FTS, preferably on cobalt catalysts. The high activity of cobalt combined with the exothermicity of the reaction makes heat removal a key issue in this step. In the hydroprocessing step the wax is hydroisomerised/hydrocracked to produce high quality diesel ( $C_{11}$ - $C_{18}$ ) and naphtha ( $C_5$ - $C_{10}$ ). As mentioned before, diesel produced via GTL is virtually free of sulphur and aromatic compounds, has a high cetane number and low particulate,  $NO_x$  and CO emissions [31].

There are currently two commercial GTL plants that employ cobalt-based FTS catalysts. Since 1993, Shell has operated the Shell Middle Distillate Synthesis (SMDS) plant based on offshore methane in Bintulu, Malaysia, which has a current capacity of 14 700 bbl/day [13,17, 33]. The syngas is generated by the non-catalytic partial oxidation of methane at high pressures and temperatures around 1500 °C. The FTS step is carried out in multi-tubular fixed bed reactors using a supported cobalt-based catalyst. There are a large number of narrow tubes per reactor, which help to cope with the reaction heat released [32]. Operation is at about 30 bar and 200-230 °C and the objective is to produce high quality waxes [32]. The waxes are worked-up either to produce different wax specialities or hydrocracked over a catalyst to high quality diesel and kerosene ( $C_{10}$ - $C_{13}$ ) fuels.

The second commercial GTL plant is the Oryx-GTL plant with a nominal capacity of 34 000 bbl/day which is located in the northern gas field in Ras Laffan, Qatar. The plant which was inaugurated in 2006 operates on the Sasol Slurry Phase Distillate (SPD<sup>TM</sup>) process (Figures 1.1 and 1.2). Syngas generation is done by reforming of natural gas in a Haldor Topsøe autothermal reformer with oxygen from an air separation unit and steam in a flame, followed by a catalyst. In the FT section a highly active and selective supported cobalt-based catalyst is operated in a slurry bubble column reactor with approximate outside dimensions of 60 m in height and 10 m in width. The Sasol slurry phase reactor [34] is an integral part of the SPD process and carries out the synthesis reaction at low temperatures (220-240 °C) and pressures of 20-30 bar. The process involves bubbling hot syngas through a liquid slurry of catalyst particles and liquid reaction products. Heat is removed from the reactor via coils within the bed producing medium pressure steam. Liquid products are removed

from the reactor and the liquid hydrocarbon wax is separated from the catalyst. The gas stream from the top of the reactor is cooled to recover light hydrocarbons and reaction water. There are several advantages of using slurry bubble column over fixed bed reactors and these include [35, 36, 37]:

- Isothermal, gradientless reactor with better temperature control/heat removal due to large liquid volume;
- low maintenance/operating cost due in part to simple design and absence of moving components;
- lower pressure drop , < 2 bar compared to 3-7 bar for a fixed bed;
- ability to use fine catalyst particles (< 300  $\mu\text{m}$ ) allowing large surface area per unit volume and better liquid–solid mass transfer;
- higher yield per reactor volume and higher potential for scaling up; and
- higher on-line factor where the catalyst can be added and removed continuously, allowing longer runs without reactor shutdown.

In the product upgrading step, the liquid hydrocarbon is hydrocracked to produce diesel and naphtha using Chevron Isocracking<sup>TM</sup> technology.

It has been estimated that GTL (using FTS) is profitable at an oil price of around \$30 per barrel [38], but this is a moving target given rapidly increasing engineering and construction costs. The oil price has continued increasing steadily for the last few years and is now well above \$100 per barrel. Additionally, it is estimated that the world's vast natural gas reserves, estimated to have an oil equivalent of at least 1 000 billion barrels, could meet human needs for at least another 60 years [31]. Significantly, about half of these reserves are uncommitted, which makes them ideal for monetisation through GTL technology [31]. It is therefore believed that GTL technology has a significant role to play in the global energy future. Many multinational companies have shown interest in GTL and some have announced plans to build plants. Table 1.1 shows the current and proposed GTL plants. The largest plants will be built in Qatar, which has 15% of the world's gas reserves [39].

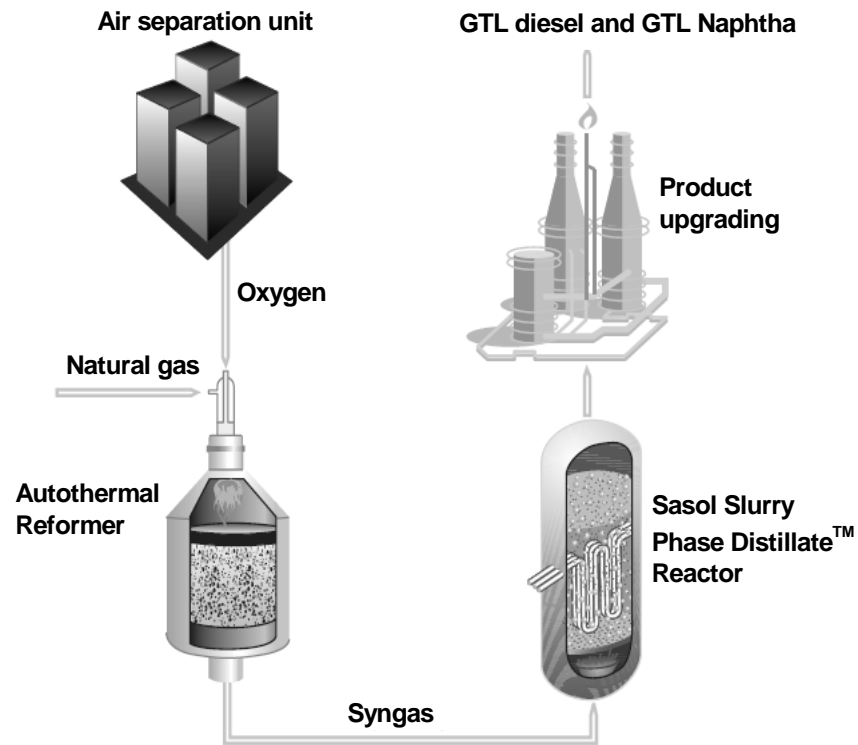


**Figure 1.1** An overview of the Sasol Slurry Phase Distillate (SPD<sup>TM</sup>) process [31].

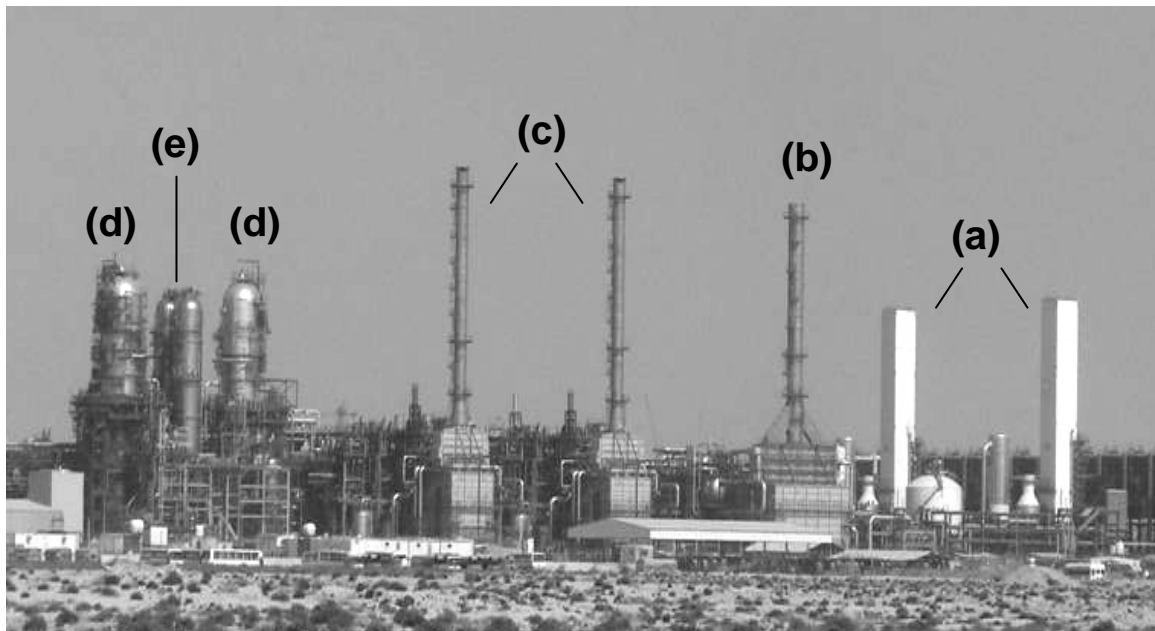


**Figure 1.2** The Oryx-GTL plant in Ras Laffan, Qatar with a nominal capacity of 34 000 bbl/day (a) Air separation units (b) Gas superheater (c) Autothermal reformers (d) Slurry bubble column FTS reactors (e) Catalyst hoppers.

**Table 1.1** *Currently operating and recently announced FTS plants based on natural gas, together with the location, companies and technologies involved.*

Country (Location)	Owner	Technology	Production (bbl/day)	Start-up
South Africa (Mossel Bay)	PetroSA	Sasol CFB (Fe)	36 000	1992
Malaysia (Bintulu)	Shell	SMDS Fixed bed (Co)	14 700	1993
South Africa (Sasolburg)	Sasol	Sasol Slurry and Arge technology (Fe)	5 000 (solely chemicals)	2004 (Changed over from coal to natural gas)
Qatar (Ras Laffan)	Sasol/Qatar Petroleum (Oryx-GTL)	Sasol SPD Slurry bed (Co)	34 000	2007
Nigeria (Escarvaros)	NNPC/Chevron (E-GTL)	Sasol SPD Slurry bed (Co)	34 000	2009 (Construction in progress)
Qatar (Ras Laffan)	Qatar Petroleum/Shell (Pearl)	SMDS Fixed bed (Co)	70 000	2009 (expansion to 140 000 bbl/day in 2011)
Trinidad (Pointe-à- Pierre)	World GTL/ Petrotrin	Use of existing multi-tubular fixed bed reactors from gas-to- methanol plants (Co)	2 250	Production expected in last quarter 2008

### 1.3 FTS catalysts

The overall process in FTS is comprised of a network of the elementary bond-breaking and bond-formation steps. These include CO and H<sub>2</sub> dissociation as well as hydrogenation and chain growth (carbon coupling) on the metal surface. The balance of the bond-breaking and bond-formation processes on the metal surface dictates the choice of metal. Transition metals to the left in the periodic table will easily dissociate CO, but the products, i.e., surface carbon and oxygen, are too strongly bound to the surface thus blocking subsequent hydrogenation and carbon coupling reactions.

Transition metals to the right, on the other hand, are not active enough to dissociate CO. The optimal metals are those which can promote CO dissociation, along with a balanced degree of surface carbon hydrogenation and carbon coupling in order to produce longer chain hydrocarbon products.

It is known that the Group 8 transition metals are active for FTS. However, the only FTS catalysts, which have sufficient CO hydrogenation activity for commercial application, are composed of Ni, Co, Fe or Ru [40]. The choice of active metal has important implications for the selectivity of the catalyst and its cost. Iron catalysts are known to make large amounts of carbon dioxide via the water gas shift (WGS) reaction and as such are generally considered unsuitable for operation from natural gas derived syngas [41]. The production of CO<sub>2</sub> also is an environmental concern. On the other hand, the WGS activity of a Fe catalyst gives it flexibility for use with coal or biomass derived synthesis gas which has a low H<sub>2</sub>/CO ratio. Fe catalysts tend to produce predominantly linear alpha olefins as well as a mixture of oxygenates such as alcohols, aldehydes and ketones. Of the other metals active for CO hydrogenation, nickel is too hydrogenating and consequently produces excessive amounts of methane. It also has a tendency to form carbonyls and sub carbonyls at FTS conditions which facilitates sintering via atom migration [42]. Ruthenium is the most active FTS catalyst, producing long chain products around 140 °C [43, 44], however it is expensive and relatively rare and this precludes its use industrially.

Cobalt catalysts are a good choice for FTS from natural gas derived synthesis gas and have a good balance between cost and stability. The water-gas shift activity of cobalt-based catalysts is low and water is the main oxygen containing reaction product. Cobalt-based catalysts are very suitable for wax formation in slurry bubble columns and can operate at high per pass conversion.

### ***1.3.1 Cobalt catalysts in the FTS***

The first cobalt catalyst used at Mülheim was a 100 Co/18 ThO<sub>2</sub>/100 kieselguhr catalyst [7]. There is evidence that Otto Roelen (famous for discovering the oxo synthesis), a PhD student of Franz Fischer, played an important role in the preparation of the technologically relevant catalysts [7, 45]. It was reported that the best way to



prepare these cobalt catalysts was by co-precipitating the nitrates of cobalt and thorium (or zirconium or magnesium) with a basic solution in the presence of kieselguhr to yield an intimate mixture of the oxides supported on the kieselguhr. This catalyst can be considered as the forerunner of modern cobalt catalysts. Interestingly, the modern cobalt catalysts are similar to the one prepared by Fischer and his co-workers, i.e. they consist of promoted cobalt on an oxide support.

An inspection of literature and patents on cobalt-based catalysts will lead one to come up with the following composition for the state-of-the-art catalysts [12, 40, 46]. Almost all companies with FTS catalysts have a similar formulation for them:

- a) Cobalt as the FT active metal (typically 10-30 wt%)
- b) A second metal as a promoter (usually a noble metal e.g. Pt, Ru and Pd)
- c) A structural oxidic promoter (e.g. Zr, Ba and La)
- d) A high surface area refractory oxidic support (most likely modified)

Cobalt is expensive and to maximize its use, it needs to be well dispersed on the support. Iglesia et al. [47-49] reported that for relatively large cobalt particles ( $d > 10$  nm) there was a linear correlation between FTS reaction rates and metal dispersion. Recently, Bezemer et al. [50] observed lower FTS turnover frequencies with cobalt particles smaller than 6 - 8 nm. It seems that the lower activity of small cobalt particles is caused by the fact that small particles have a modified electronic structure because of the quantum size effect or do not possess the domains that contain the active sites for the FTS. There seems to exist an optimum cobalt particle size in the range 8-10 nm.

As metallic cobalt is considered the active phase in the FTS, a high degree of reduction is required. Small cobalt particles when supported on traditional oxidic carriers like silica ( $\text{SiO}_2$ ), alumina ( $\text{Al}_2\text{O}_3$ ) and titania ( $\text{TiO}_2$ ) are difficult to reduce due to a strong interaction with the support. Therefore catalysts are often promoted with noble metals (e.g. Ru, Pt or Pd) which lead to much easier reduction of the cobalt oxide particles. Noble metals have also been claimed to lead to the formation of bimetallic particles and alloys which influence activity and selectivity, enhance cobalt dispersion, inhibit catalyst deactivation by keeping the surface clean (Ru) and allow

easier regeneration of the cobalt surface [51]. The noble metal promoter is usually kept around 0.1-0.5 wt% due to cost but also due to the fact that higher amounts may cause blocking of the cobalt if intimate mixing of the metals occurs. Structural promoters affect the formation and stability of the active phase of a catalyst material. It has been shown for Co/SiO<sub>2</sub> catalysts that promotion with Zr results in a decreased cobalt-silica interaction leading to a higher degree of reduction of cobalt and increase in the metallic atoms on the surface [52, 53]. Zr promotion of Co/Al<sub>2</sub>O<sub>3</sub> catalysts is claimed to prevent the formation of cobalt aluminate [54].

The support provides mechanical strength and thermal stability to the cobalt crystallites, while facilitating high cobalt dispersion. The properties of the support are also an important factor for producing good catalysts. For alumina it has been shown that ideal properties are high purity, low acidity, and relatively high surface area (150 - 250 m<sup>2</sup>/g) [55, 56]. The pore size of the support can also influence the size of the cobalt crystallites as shown by Saib et al. [57]. Recently, van Steen and Claeys reported that the desired support pore size for the optimum cobalt crystallite size should be around 12-16 nm [58]. The support also needs to be robust during FTS conditions, in the presence of several bars of steam that will occur at high conversion levels. Van Berge et al. [59] found that an alumina-supported cobalt FTS catalyst was susceptible to hydrothermal attack that is inherent to realistic FTS conditions. Hydrothermal attack on the exposed and unprotected support material resulted in contamination of the produced wax with ultra fine cobalt rich particulate matter and may also result in an increase in the rate of activity decline. This problem was solved by pre-coating the support with a silica structural promoter, which was achieved by impregnating tetra ethoxy ortho silicate (TEOS) dissolved in ethanol, drying under vacuum and calcining in air at 500 °C [59]. The supported catalyst should also be resistant to attrition especially in the slurry bubble column environment. Wei et al. [60] noted that the attrition resistances of supported cobalt catalysts followed the sequence: Co/Al<sub>2</sub>O<sub>3</sub> > Co/SiO<sub>2</sub> > Co/TiO<sub>2</sub>.

The most common technique to prepare supported cobalt catalysts is incipient wetness impregnation of the support with a cobalt salt solution of the appropriate concentration, drying, calcining to decompose the nitrate to the oxide and finally reduction with hydrogen [41]. Other methods such as slurry impregnation [61],

kneading [62] and deposition-precipitation [63] of cobalt compounds have also been reported. In order to prepare a catalyst with good activity and dispersion, each of these preparation steps needs to be optimised. The conditions during calcination of impregnated cobalt precursors have a significant influence on the performance of the final catalyst. Van de Loosdrecht et al. [64] reported high metallic cobalt surface areas and high catalytic activities when the concentration of nitrogen oxides and water was kept low during calcination by employing a high flow rate. Similarly, the flow rate during reduction should be kept high to avoid high partial pressures of the water product which results in sintering [12, 41]. High calcination temperatures ( $> 350\text{ }^{\circ}\text{C}$ ) result in the diffusion of cobalt ions into the support, producing irreducible compounds [65], while it was reported that too high reduction temperatures ( $> 365\text{ }^{\circ}\text{C}$ ) for the original Co/ThO<sub>2</sub>/Kieselguhr catalyst caused extensive loss of surface area due to sintering [66].

### ***1.3.2 Deactivation of cobalt-based catalysts***

Unfortunately cobalt FTS catalysts like many other systems lose their activity with time on stream. Figure 1.3 shows an activity profile for a proprietary Co/Al<sub>2</sub>O<sub>3</sub> catalyst tested at realistic conditions [67]. It is commonly observed that during the first few days the rate of activity decline is rapid then followed by a slow steady deactivation [68, 69].

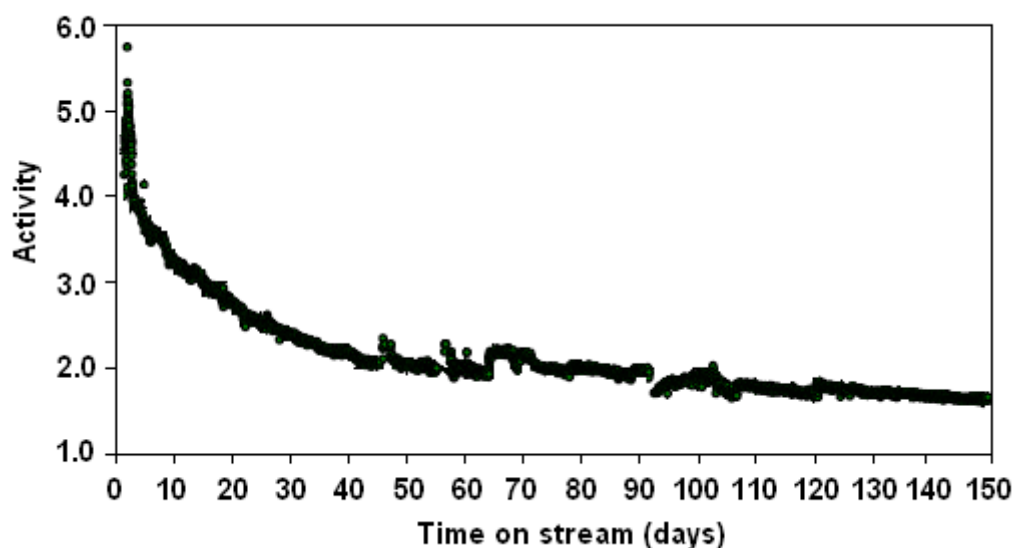


**Figure 1.3** *Typical activity profile of a proprietary Co/Al<sub>2</sub>O<sub>3</sub> catalyst tested in a slurry reactor under realistic FTS conditions for an extended period (adapted from [67])*

There are various possible mechanisms by which cobalt FTS catalysts can lose their activity:

- **Poisoning** Sulphur, chloride and nitrogen-containing compounds poison cobalt [41]. Since this deactivation is synthesis gas related it can be prevented/reduced by cleaning up the feed stream. Shell reports that ZnO guard beds can be used to effectively remove sulphur from the feed stream [70].
- **Oxidation of cobalt/support compound formation.** Water is the main FTS by-product and accounts for more than 50 wt% of all products. Oxidation of the active metal by the product water has been widely postulated as a deactivation mechanism [71]. Although bulk thermodynamics predicts that cobalt will not be oxidized [72], recent thermodynamic analysis, taking into account surface free energies, shows that particles smaller than 4.4 nm will oxidize under FTS conditions [73]. It has been shown experimentally that particles larger than 4-5 nm do not undergo oxidation at realistic FTS conditions [74]. The formation of irreducible cobalt support compounds is thermodynamically favorable and has been put forward as a possible cause of activity decline [75].

- **Sintering of the active phase.** During the FTS, cobalt nanoparticles may agglomerate and this will result in loss of active surface area [76, 77]. This process may be facilitated by the presence of water.
- **Fouling by wax.** During low temperature FTS over cobalt-based catalysts long chain waxes are produced. One of the plausible reasons for the activity decline is the build up on the surface and in the catalyst pores of these waxes which inhibit adsorption and slow down diffusion rates [41, 78].
- **Deposition of inert/deactivating carbon phases.** It has been previously reported that inert carbon phases can form during extended runs and cause blocking of the active phase [79]. The formation of bulk cobalt carbide may also result in a decrease in activity [80].
- **Surface reconstruction.** Adsorbates may strongly chemisorb on the metal surface and cause the surface to rearrange to a more stable configuration [81]. Large scale changes during model FTS conditions have been observed on a flat cobalt surface which has been ascribed to the intrusive nature of CO [82].

It is interesting to note that many of the deactivation mechanisms that plague modern cobalt catalysts were already identified for the original Co/ThO<sub>2</sub>/kieselguhr catalyst operating in the first commercial plants in the late 1930's. According to Roelen [83], deactivation was due to sulphur, pore blocking by heavy wax, carbon deposition and sintering. Additionally, he noted that oxidation of cobalt did not occur over a period of six months nor was there any cobalt silicate formation.

## 1.4 Outline of the Thesis

Cobalt catalysts are the preferred choice of catalysts for GTL processes. Due to the high cost of cobalt high catalyst stability is required. An understanding of the deactivation mechanisms at play is important as this allows one to tailor process conditions to ensure extended catalyst lifetimes. The knowledge of deactivation mechanisms could also be used to rationally design new catalysts with enhanced activity and stability. The research described in this thesis involved investigating the deactivation of cobalt-based FTS catalysts. Attention was focused on cobalt aluminate formation and carbon deposition as possible deactivation mechanisms.

- **Chapter 3** focuses on cobalt aluminate formation during FTS. Catalyst samples were drawn from a demonstration unit slurry reactor operating under realistic FTS conditions (230 °C, 20 bar, % (H<sub>2</sub>+CO) conversion between 50-70 %, feed gas composition of ca. 50 vol. % H<sub>2</sub> and 25 vol. % CO) and quantitatively characterized with X-ray adsorption near edge spectroscopy (XANES). The influence of varying water partial pressures, in laboratory scale reactors, on the formation of cobalt aluminate was investigated with XANES and X-ray photoelectron spectroscopy (XPS).
- A review (**Chapter 4**) on carbon deposition on cobalt-based FTS catalysts was undertaken to bring together existing open and patent literature on this topic to provide a clearer picture on the formation and influence of carbon on cobalt-based FTS catalysts.
- In **Chapter 5** samples of cobalt catalysts tested in a demonstrated unit slurry reactor, over an extended period, were characterized for carbon deposits. This involved wax extraction of the catalysts, then applying temperature programmed (TP) techniques to study the accumulation of the carbon. The location of carbon deposits was also studied via a combination of energy-filtered transmission electron microscopy (EFTEM), H<sub>2</sub> chemisorption and low energy ion scattering (LEIS).
- As a follow up on the topic of carbon deposition, **Chapter 6** involved an investigation into the factors that influence carbon deposition on cobalt-based catalysts. We report on the impact of temperature and H<sub>2</sub>/CO ratio on the build-up of carbonaceous species on Co/Pt/Al<sub>2</sub>O<sub>3</sub> catalysts using both model and realistic FTS tests. The influence of upset conditions on carbon deposition and its subsequent effect on catalyst structure was also investigated.
- A strong point of Chapter 3 and 5 is that samples of the catalyst studied were taken from a large scale reactor at realistic conditions, which makes the results industrially relevant. However, real systems are complex and often to obtain fundamental information, the complexity needs to be reduced using model catalysts. **Chapter 7** discusses some preliminary results of new potential techniques that are able to shed light on the reactivity and morphology of cobalt nanoparticles by using both spherical and flat model catalysts.

## 1.5 References

- [1] I. Chorkendorff, J.W. Niemantsverdriet, *Concepts of Modern Catalysis and Kinetics*, Wiley-VCH, Weinheim, 2007.
- [2] P. Sabatier, J.B. Senderens, *J. Soc. Chem. Ind.* 21 (1902) 504.
- [3] A. Mittasch, C. Schneider, German Patent 293 787 (1913), to BASF.
- [4] F. Bergius, J. Billwiller, German Patent 301 231 (1919).
- [5] F. Fischer, H. Tropsch, *Brennstoff-Chem.* 4 (1923) 276.
- [6] F. Fischer, H. Tropsch, *Brennstoff-Chem.* 7 (1926) 97.
- [7] A.N. Stranges, "Germany's Synthetic Fuel industry 1927-45", Presentation at AIChE 2003, New Orleans, LA. ([www.fischertropsch.org](http://www.fischertropsch.org)).
- [8] N.R. Golumbic, Review of Fischer-Tropsch and Related Processes for Synthetic Liquid Fuel Production, Information circular, 1947 ([www.fischertropsch.org](http://www.fischertropsch.org)).
- [9] M. Dry, in: J. Anderson, M. Boudard (Eds.), *Catalysis Science and Technology*, Vol. 1, Springer, Berlin, 1984.
- [10] M.E. Dry, *Catal. Today* 71 (2002) 227.
- [11] M.E. Dry, *Endeavour* 8 (1984) 2.
- [12] C.H. Bartholomew "History of Cobalt Catalyst Design for Fischer-Tropsch Synthesis" Presentation at AIChE 2003, New Orleans, LA ([www.fischertropsch.org](http://www.fischertropsch.org)).
- [13] H.M.V. van Wechem, M.M.G. Senden, *Stud. Surf. Sci. Catal.* 81 (1994) 43.
- [14] *Petroleum Review*, 60 (714), July 2006, p. 7
- [15] J. Zhang, J. Chen, Y. Li, Y. Sun, *J. Nat. Gas Chem.* 11 (2002) 99.
- [16] T.H. Fleisch, R.A. Sills, M.D. Briscoe, *J. Nat. Gas Chem.* 11 (2002) 1.
- [17] J. Eilers, S.A. Posthuma, S.T. Sie, *Catal. Lett.* 7 (1990) 253.
- [18] B. Eisenberg, R.A. Fiato, *Stud. Surf. Sci. Catal.* 119 (1998) 943.
- [19] J.J.H.M. Font Freide, T.D. Gamlin, C. Graham, J.R. Hensman, B. Nay, C. Sharp, *Top. Catal.* 26 (2003) 3.
- [20] K.B. Arcuri, K.L. Agee, M.A. Agee, United States Patent 6 262 131 (2001), to Syntroleum.
- [21] E. Kintisch, *Science* 320 (2008) 306.
- [22] R. Zennaro, *Oil Gas* 2 (2007) 88.
- [23] R.L. Espinoza, Y. Jin, J. Kandaswamy, N. Srinivasan, United States Patent 7 012 104 (2006), to ConocoPhillips.
- [24] P.W. Schwaberg, I.S. Myburgh, J.J. Botha, P.N. Roets, L.P. Dancuart, in: *Proc. of the 11th World Clean Air Congress*, Durban, South Africa, September 1998.
- [25] "International Data: Coal"; Energy Information Agency, Washington, DC, 2007 (<http://www.eia.doe.gov/pub/international/iea2003/table82.xls>).
- [26] E. van de Venter, Sasol Coal-to-Liquids Developments, Presentation to Gasification Technologies Council Conference, October 2005, San Francisco.
- [27] J. Sarkar, *Platt's International Coal Report* 840 (2007) 17.
- [28] H. Leibold, A. Hornung, H. Seifert, *Powder Tech.* 18 (2008) 265.
- [29] *Chemische Rundschau* 11 (2006) 21.
- [30] A.C. Vosloo, *Fuel Proc. Tech.* 71 (2001) 149.
- [31] Sasol GTL Brochure ([www.sasol.com](http://www.sasol.com)).
- [32] M.E. Dry, in: I.T. Horvath (Ed.), *Encyclopedia of Catalysis*, Vol. 3, Wiley, New York, 2003. p. 347.
- [33] Information on SMDS in Bintulu (<http://www.shell.com>).
- [34] B. Jager, P. van Berge, A.P. Steynberg, *Stud. Surf. Sci. Catal.* 136 (2001) 63.
- [35] J.W.A. de Swart, R. Krishna, S.T. Sie, *Stud. Surf. Sci. Catal.* 107 (1997) 217.
- [36] B. Jager, R. Espinoza, *Catal. Today* 23 (1995) 17.
- [37] L. Sehabiague, R. Lemoine, A. Behkish, Y.J. Heintz, M. Sanoja, R. Oukaci, B.I. Morsi, *J. Chin. Inst. Chem. Eng.* 39 (2008) 169.
- [38] O. van Vliet, A. Faaij, W. Turkenburg, "Developments in Fischer-Tropsch diesel in a WTW chain perspective" Presentation at the International Conference on Transport and Environment, Milan, March 2007.
- [39] PennWell Corporation, *Oil Gas J.* 104 (2006) 47.
- [40] B.H. Davis, *Ind. Eng. Chem. Res.* 46 (2007) 8938.
- [41] M.E. Dry, *Stud. Surf. Sci. Catal.* 136 (2001) 63.
- [42] M. Agnelli, M. Kolb, C. Mirodatos, *J. Catal.* 148 (1994) 9.
- [43] M. Vannice, *J. Catal.* 37 (1975) 462.

- [44] C. Xiao, Z. Cai, T. Wang, Y. Kou, N. Yan, *Angew. Chem. Int. Edit.* 47 (2008) 746.
- [45] B. Cornils, W.A. Herrmann, M. Rasch, *Angew. Chem. Int. Edit.* 33 (1994) 2144.
- [46] R. Oukaci, A.H. Singleton, J.G. Goodwin Jr., *Appl. Catal. A* 186 (1999) 129.
- [47] E. Iglesia, *Appl. Catal. A* 161 (1997) 59.
- [48] E. Iglesia, S.C. Reyes, R.J. Madon, S.L. Soled, *Adv. Catal.* 39 (1993) 221.
- [49] S.L. Soled, E. Iglesia, R.A. Fiato, J.E. Baumgartner, H. Vroman, S. Miseo, *Top. Catal.* 26 (2003) 101.
- [50] G.L. Bezemer, J.H. Bitter, H.P.C.E. Kuipers, H. Oosterbeek, J.E. Holewijn, X. Xu, F. Kapteijn, A.J. van Dillen, K.P. de Jong, *J. Am. Chem. Soc.* 128 (2006) 3956.
- [51] F. Morales, B.M. Weckhuysen, *Catalysis (Royal Society of Chemistry)* 19 (2006) 1.
- [52] A. Feller, M. Claeys, E. van Steen, *J. Catal.* 185 (1999) 120.
- [53] G.R. Moradi, M.M. Basir, A. Taeb, A. Kiennemann, *Catal. Comm.* 4 (2003) 27.
- [54] H. Xiong, Y. Zhang, K. Liew, J. Li, *J. Mol. Catal. A* 231 (2005) 145.
- [55] H. Beuther, C.L. Kibby, T.P. Kobylinski, R.B. Pannell, United States Patents 4 413 064 (1983); 4 493 905 (1985); 4 585 798 (1986), to Gulf Research & Development Company and 4 605 680 (1986); 4 613 624 (1986), to Chevron Research Company.
- [56] T.P. Kobylinski, C.L. Kibby, R.B. Pannell, E.G. Eddy, United States Patents 4 605 676 (1986) and 4 605 679 (1986), to Chevron Research Company.
- [57] A.M. Saib, M. Claeys, E. van Steen, *Catal. Today* 71 (2002) 395.
- [58] E. van Steen, M. Claeys, *Chem. Eng. Technol.* 31 (2008) 655.
- [59] P.J. van Berge, J. van de Loosdrecht, E.A. Caricato, S. Barradas, Patent PCT/GB 99/00527 (1999), to Sasol Technology.
- [60] D.G. Wei, Y.L. Zhang, J.G. Goodwin, *Appl. Catal. A* 210 (2000) 129.
- [61] J. van de Loosdrecht, S. Barradas, E.A. Caricato, P.J. van Berge, J.L. Visagie, *Prep. Symp.-Am. Chem. Soc., Div. Fuel Chem.* 45 (2000) 587.
- [62] A. Hoek, A.H. Joustra, J.K. Minderhoud, M.F. Post, Great Britain Patent 2 125 062 (1983) to Shell Research Ltd.
- [63] C.M. Lok, *Stud. Surf. Sci. Catal.* 147 (2004) 283.
- [64] J. van de Loosdrecht, S. Barradas, E.A. Caricato, N.G. Ngwenya, P.S. Nkwanyana, M.A.S. Rawat, B.H. Sigwebela, P.J. van Berge, J.L. Visagie, *Top. Catal.* 26 (2003) 121.
- [65] W. Chu, P.A. Chernavskii, L. Gengembre, G. A. Pankina, P. Fongarland, A.Y. Khodakov, *J. Catal.* 252 (2007) 215.
- [66] V. Haensel, CIOs File No. 30, Item XXX-1, Kaiser Wilhelm Institut für Kohlenforschung, Mülheim, CIOs Target No. 30/6.01, Fuels and Lubricants, June 15, 1945 (<http://www.fischertropsch.org>).
- [67] White paper, "Fischer Tropsch Catalyst Test on Coal-Derived Synthesis Gas", Syntroleum Corporation. ([www.syntroleum.com](http://www.syntroleum.com)).
- [68] P.J. van Berge, R.C. Everson, *Stud. Surf. Sci. Catal.* 107 (1997) 207.
- [69] M.K. Niemela, A.O. Krause, *Catal. Lett.* 42 (1996) 161.
- [70] M.J. van der Burgt, J. van Klinken, S.T. Sie, in: *Proc. Synfuels Worldwide Symp.*, Washington, DC, 11–13 November, 1985.
- [71] J. van de Loosdrecht, B. Balzhinimaev, J.-A. Dalmon, J.W. Niemantsverdriet, S.V. Tsybulya, A.M. Saib, P.J. van Berge, J.L. Visagie, *Catal. Today* 123 (2007) 293.
- [72] P.J. van Berge, J. van de Loosdrecht, S. Barradas, A.M. van der Kraan, *Catal. Today* 58 (2000) 321.
- [73] E. van Steen, M. Claeys, M.E. Dry, J. van de Loosdrecht, E.L. Viljoen, J.L. Visagie, *J. Phys. Chem. B* 109 (2005) 3575.
- [74] A.M. Saib, A. Borgna, J. van de Loosdrecht, P.J. van Berge, J.W. Niemantsverdriet, *Appl. Catal. A* 312 (2006) 12.
- [75] G. Jacobs, P.M. Patterson, Y. Zhang, T. Das, J. Li, B. Davis, *Appl. Catal. A* 233 (2002) 215.
- [76] G.Z. Bian, N. Fujishita, T. Mochizuki, W.S. Ning, M. Yamada, *Appl. Catal. A* 252 (2003) 251.
- [77] M.J. Overett, B. Breedts, E. du Plessis, W. Erasmus, J. van de Loosdrecht, *Prepr. Pap.-Am. Chem. Soc., Div. Pet. Chem.* 53 (2008) 126.
- [78] I. Puskas, *Catal. Lett.* 22 (1993) 283.
- [79] J.J.H.M. Font Freide, T.D. Gamlin, R.J. Hensman, B. Nay, C. Sharp, *J. Nat. Gas Chem.* 13 (2004) 1.
- [80] R.B. Anderson, W.K. Hall, A. Krieg, B. Seligman, *J. Am. Chem. Soc.* 71 (1949) 183.
- [81] I.M. Ciobica, R.A. van Santen, P.J. van Berge, J. van de Loosdrecht, *Surf. Sci.* 602 (2008) 17.
- [82] J. Wilson, C. de Groot, *J. Phys. Chem.* 99 (1995) 7860.



## *Chapter 1*

- [83] British Intelligence Objectives Sub-committee. Interrogation of Dr Otto Roelen of Ruhrchemie A.G. B.I.O.S. – Final report No 447; Item no 30 (1945). (<http://www.fischer-tropsch.org>).

---

# Chapter 2

---

## Experimental Techniques

---

*In order to study the formation of cobalt aluminate, carbon deposition or the behaviour of cobalt nanoparticles under different reaction conditions as outlined in the previous chapter, appropriate analytical methods had to be selected. X-ray adsorption near-edge spectroscopy (XANES) was chosen to study the formation of cobalt aluminate as it is a powerful technique to differentiate phases in a catalyst and can be used in a pseudo in-situ manner on wax-covered cobalt-based FTS catalysts tested at realistic conditions. However, due to the wax layer present, it is difficult to analyse the catalysts for deleterious carbon deposits and subsequently a wax-extraction procedure was developed. X-ray photo-electron spectroscopy (XPS) was used to give information on the surface properties of wax-extracted and carbon-deposited catalysts. Temperature programmed (TP) techniques were applied to determine the amount and nature of the carbon deposits on the catalysts. The location of deleterious carbon was investigated with energy filtered transmission electron microscopy (EFTEM) and low energy ion scattering (LEIS). TEM and in-situ TEM was performed on model cobalt catalysts to gauge the potential of this technique to observe the behaviour of cobalt nanoparticles when treated under model conditions. The following section briefly describes the above-mentioned characterization and pre-treatment techniques used in this study.*

---

## 2.1 X-ray absorption near-edge spectroscopy (XANES)

X-ray absorption spectroscopy (XAS) is a useful method to investigate chemical composition and local structure [1, 2]. During the experiment the material under investigation is targeted with a monochromatic X-ray beam which is produced by synchrotron radiation. The basic process involves the photoelectric effect: a photon is absorbed by an atom or ion and an electron is emitted from an inner shell. A parallel monochromatic x-ray beam of intensity  $I_0$  passing through a sample of thickness  $x$  will get a reduced intensity  $I$  according to the expression:

$$\ln(I_0/I) = \mu x \quad (2.1)$$

where  $\mu$  is the linear absorption coefficient, which depends on the type of atoms and the density of the material. At certain energies where the absorption increases drastically, it gives rise to an absorption edge. Each such edge occurs when the energy of the incident photons is just sufficient to cause excitation of a core electron of the absorbing atom to a continuum state, i.e. to produce a photoelectron. Thus, the energies of the absorbed radiation at these edges correspond to the binding energies of electrons in the K, L, M, etc, shells of the absorbing elements. When the photoelectron leaves the absorbing atom, its wave is backscattered by the neighbouring atoms. Consequently the X-ray adsorption spectrum exhibits oscillation of fine structure that extends beyond the absorption edge.

An X-ray absorption spectrum (Figure 2.1) is generally divided into three sections: 1) pre-edge ( $E < E_0$ ); 2) X-ray absorption near edge structure (XANES), where the energy of the incident x-ray beam is  $E = E_0 \pm 50$  eV and 3) extended X-ray absorption fine structure (EXAFS), which starts approximately from 50 eV and continues up to 1000 eV above the edge. Analysis of the XANES region, near the adsorption edge, gives chemical information, oxidation state and sometimes co-ordination around the absorbing atom. The interpretation of the XANES region can be done with the help of spectra of reference compounds and constructing linear combinations of references to fit the spectrum of the sample being measured.

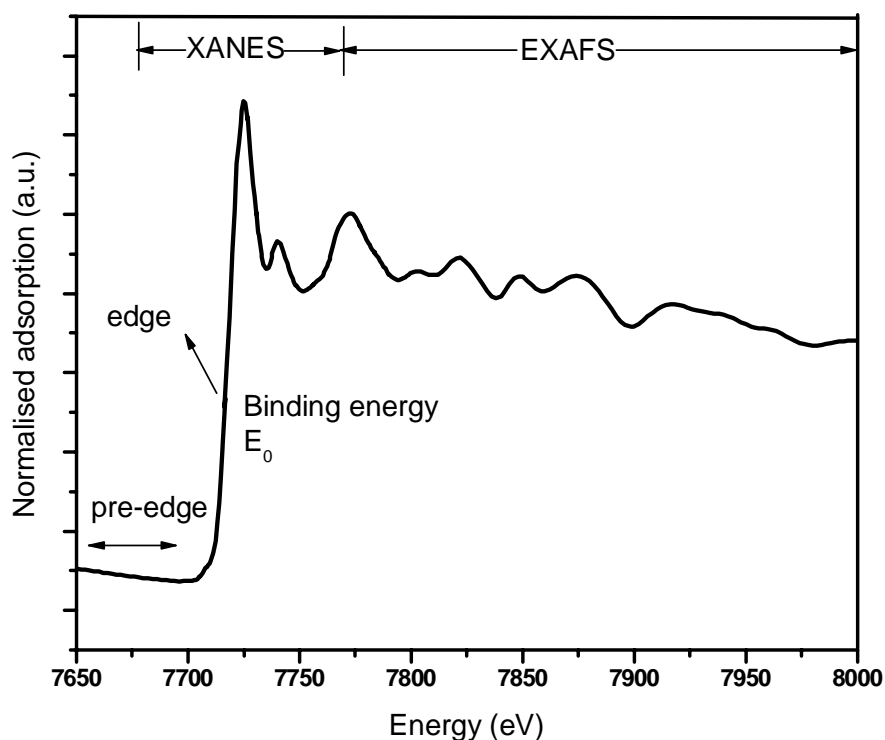


**Figure 2.1** *X-ray adsorption spectrum of a reference sample of CoO recorded at the Co K-edge.*

Figure 2.2 summarises previously reported XANES analyses [3] of the Co K-edge of cobalt reference compounds CoO, Co<sub>3</sub>O<sub>4</sub>, CoAl<sub>2</sub>O<sub>4</sub> and cobalt foil (Co<sup>0</sup>). The minor features in the pre-edge region are usually due to the electron transitions from the core level to the higher unfilled or half-filled orbitals. The pre-edge feature appears (ca. 7710 eV) for tetrahedral cobalt environments but is forbidden for octahedral environments [4], and arises from the 1s to 3d absorption transition. The intensity is inversely dependent on the degree of inversion symmetry in the first coordination shell, as well as the extent of occupancy of the 3d shell. Atoms in tetrahedral sites often exhibit pre-edge peaks due to lack of symmetry [5], while the peak is very low for octahedral environments, due to the centre of symmetry. Therefore, the intensities follow the order CoAl<sub>2</sub>O<sub>4</sub> > Co<sub>3</sub>O<sub>4</sub> > CoO, as the cobalt atoms in CoAl<sub>2</sub>O<sub>4</sub> are in a tetrahedral environment, the cobalt atoms in the spinel structure of Co<sub>3</sub>O<sub>4</sub> are in a mixed environment (one Co atom in a tetrahedral environment, while the other two are in octahedral), and the cobalt atoms in CoO are in an octahedral environment [4].

Another indicator of valence is the white line (the intensity overshoot that occurs at the edge). White lines are particularly prominent in XANES spectrum of transition metal ions with high oxidation states [2]. The oxidic reference compounds display a strong absorption white line with unique spectral features due to the presence of cobalt atoms in different Co–O environments and oxidation states. The intense white line is not present in the cobalt metal reference. It is clear from Figure 2.2 that by using XANES it is easy to distinguish between  $\text{Co}^0$ ,  $\text{CoO}$  and  $\text{Co}_3\text{O}_4$  and to a lesser extent  $\text{CoAl}_2\text{O}_4$ .

One of the attractive features of XANES is that the oxidation state of cobalt in wax-coated samples from a FTS reactor can be determined without pre-treatment that may affect the oxidation state of the sample [3]. This is due to the weak absorption of carbon atoms at the Co K-edge.

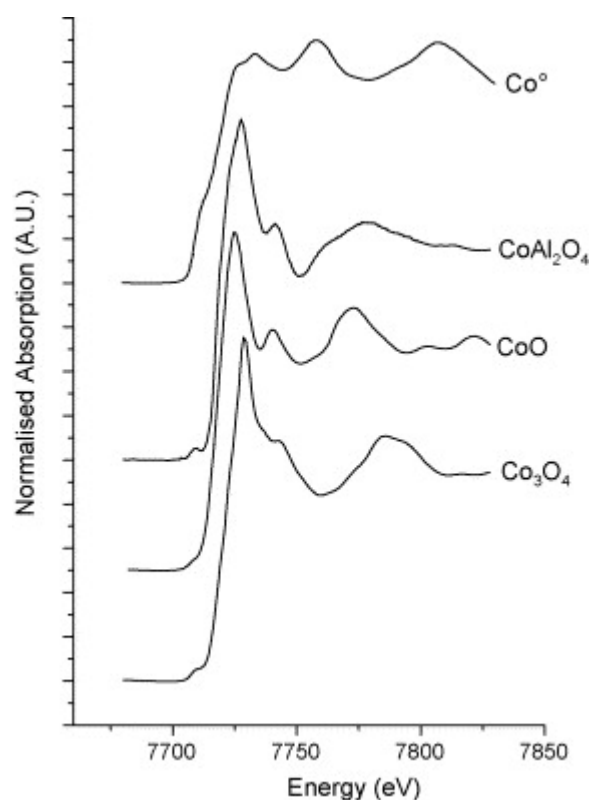


**Figure 2.2** Co K-edge XANES spectra of cobalt reference compounds (from [3]).

## 2.2 Wax-extraction procedure for spent cobalt catalysts.

During the low temperature FTS process with a cobalt catalyst, molten product hydrocarbon wax acts as the liquid phase in the reactor. The samples may be collected under nitrogen in this protective wax layer and allowed to congeal (Figure 2.2). This wax layer may interfere with several characterization techniques and in order to remove it, an extraction procedure was developed. Because of the air sensitivity of the samples, an approach was chosen based on techniques commonly used in organo-metallic synthesis. This approach made use of 'Schlenk' glassware. The procedures used ensured that an argon or vacuum atmosphere protected the air sensitive catalyst at all times.

Use was made of a P40 glass frit extraction apparatus (Figure 2.3). The glass frit set-up consisted of 3 sections: a 500 ml Schlenk flask, a 'filter' unit with an internal glass frit (porosity = 16 – 40  $\mu\text{m}$ ) and a water-cooled condenser. All glassware was placed in an oven overnight (125 °C) to remove moisture and then assembled. The entire system was allowed to cool and then evacuated and flushed with argon repeatedly. The joint between the flask and the filter unit was briefly opened under an argon flow and 200 ml of distilled tetrahydrofuran (THF), which was stored under an argon atmosphere, was injected and thoroughly degassed with argon. Then the joint between the filter unit and condenser was briefly opened while under an argon flow to add the catalyst-in-wax sample ( $\pm 1 \text{ cm}^3$ ). The system was again evacuated and filled with argon 3 times.

During the extraction process the solvent was heated with an oil bath and boiling THF vapour passed through the frit, condensed, and formed a liquid layer on top of the frit (surrounding the catalyst sample). The THF vapour bubbles ensured a well-mixed solvent-sample mixture. When a 0.5 to 1 cm liquid layer has formed, the system was drained. This was done by removing the oil bath, which lowered the solvent temperature below boiling point. After several cycles (formation of a liquid layer followed by drainage) the catalyst particles were sufficiently cleaned. The particles were dried under vacuum and poured into a small Schlenk tube (while under argon). This tube was evacuated, closed, and transferred into a glove box for storage. The advantage of this method is that it represents a well mixed solvent-wax system where clean THF is continuously recycled to the sample. Also compared to traditional

Sohxlet extraction, the progress is easily visible and the sample can be transferred easier under vacuum.

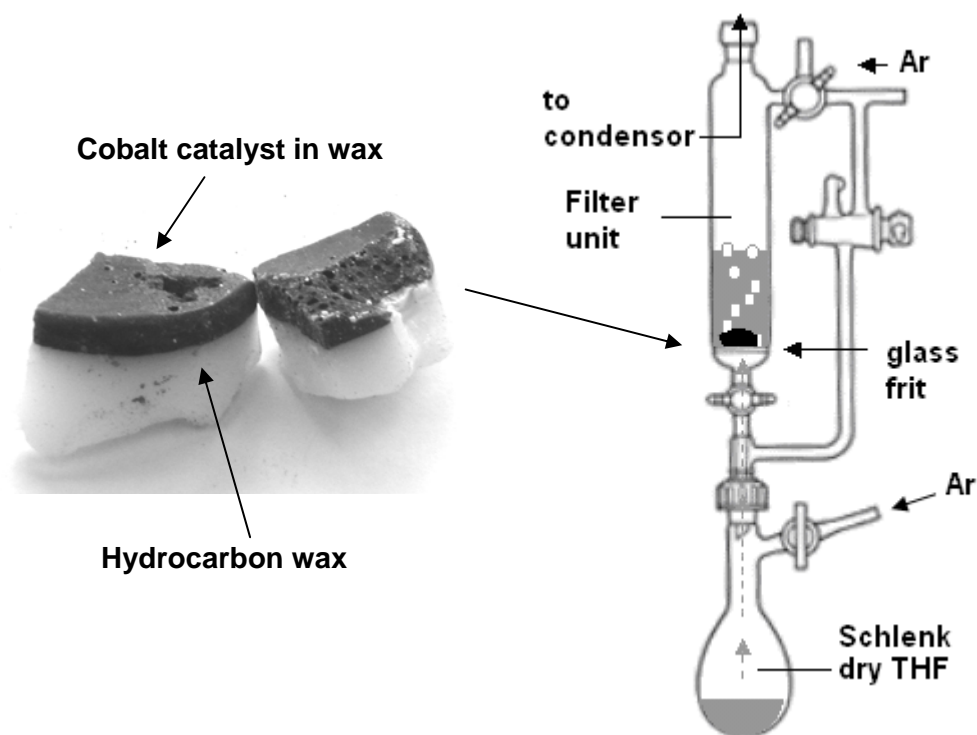


**Figure 2.3** A picture of catalyst in wax and representation of the glass frit set-up.

### 2.3 X-ray photoelectron spectroscopy (XPS)

XPS is a widely applied surface science technique that is used to probe the first few nanometers of the sample [2]. XPS is able to give information on the elements present and associated chemical bonds (chemical state) in the surface of the material. XPS like XAS is based on the photoelectric effect which involves the emission of electrons by atoms after the absorption of X-rays. The kinetic energy of the emitted photoelectron depends on the energy of the adsorbed light according to the following equation [2]:

$$E_k = h \nu - E_b - \phi \quad (2.2)$$

where

$E_k$  is the kinetic energy of the photoelectron

$h$  is Planck's constant

$\nu$  is the frequency of the absorbed radiation

$E_b$  is the binding energy of the photoelectron with respect to the Fermi level of the sample

$\phi$  is the work function of the spectrometer

If a material is irradiated with a source of known energy, the binding energy of the electron in the atom can be determined by measuring its kinetic energy after ejection. The binding energy of the electron is directly related to the atom it originates from and thus carries element specific information. Frequently used X-ray sources for XPS are Mg K $\alpha$  (1253.6 eV) and Al K $\alpha$  (1486.3 eV). In XPS the intensity,  $N(E)$ , of electrons is measured as a function of their kinetic energy, but in an XPS spectrum the intensity is usually plotted as a function of the binding energy. Figure 2.4 shows an XPS spectrum of a calcined silica supported cobalt catalyst which has been prepared by spin coating an aqueous solution of cobalt nitrate onto a SiO<sub>2</sub>/Si (100) wafer.

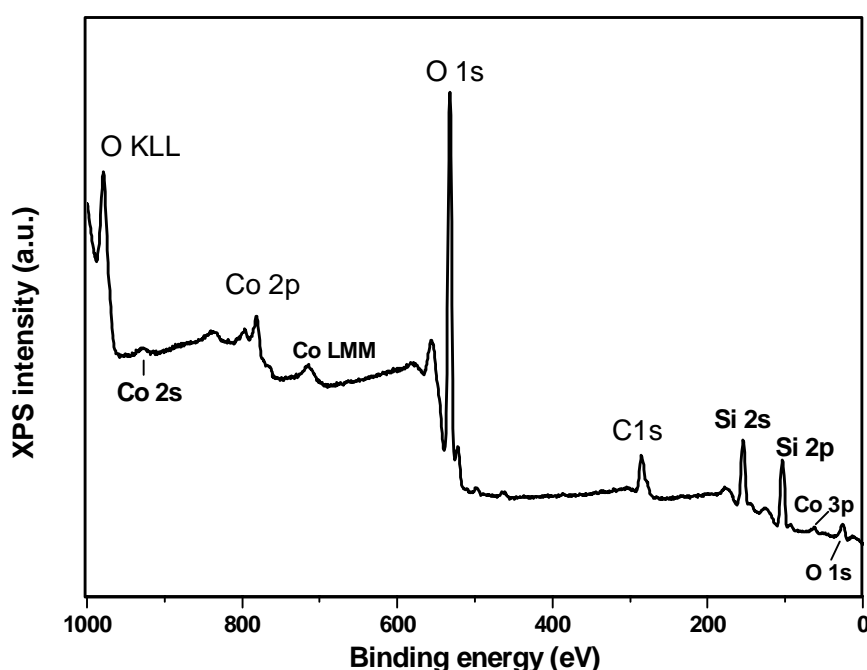


**Figure 2.4** Wide scan XPS spectrum of a calcined Co/SiO<sub>2</sub> flat model catalyst.

Peaks due to Co, Si, O and C (from the ever-present hydrocarbon contamination) are visible and can be assigned using binding energy tables. In addition to the photo-electron peaks, Auger peaks (for example Co LMM) are also visible. When the photoelectron is emitted the atom is in an excited state with a hole in



its core level. This core hole is filled by an electron from a higher shell. The energy released from this transition is taken up by another electron, the Auger electron which is emitted with an element specific kinetic energy.

Because the set of binding energies is characteristic of an element, XPS can be used to analyse the composition of samples. Binding energies are not only element specific but contain chemical information as well: the energy levels of core electrons depend on the chemical state of the atom. Figure 2.5 shows the Co 2p region of the XPS spectra for cobalt foil, CoO, Co<sub>3</sub>O<sub>4</sub> and cobalt aluminate. The binding energy peak of Co<sup>2+</sup> compounds is shifted 2 eV higher than metallic cobalt. The reason is that the electrons of the Co<sup>2+</sup> ion (two less in number than in Co<sup>0</sup>) feel a higher attractive force from the nucleus than those of a neutral Co<sup>0</sup> atom. The Co 2p core level spectrum is characterized not only by two components i.e. Co 2p<sub>3/2</sub> and Co 2p<sub>1/2</sub> (appearing due to spin-orbital splitting), but also features occurring at higher binding energies from the main photo line. This feature is called shake-up and occurs when a second electron in the 2p orbital goes into an excited state as a consequence of a sudden change in the atoms central potential produced by the photoelectron emission. Shake-up loss is common for oxides of Ni, Fe and Co and has diagnostic value as the precise loss structure depends on the environment of the atom. For example the high spin Co<sup>2+</sup> compounds such as CoO and CoAl<sub>2</sub>O<sub>4</sub> exhibit strong satellite lines which are located at about 5–6 eV above the photo line [6]. Contrary to that, a very weak satellite, shifted about 10–11 eV to higher binding energies from the main peak, is characteristic of the low spin Co<sup>3+</sup> compounds (Co<sub>3</sub>O<sub>4</sub> and CoOOH) [7]. The spectrum of metallic cobalt does not contain shake-up satellite structure at all.

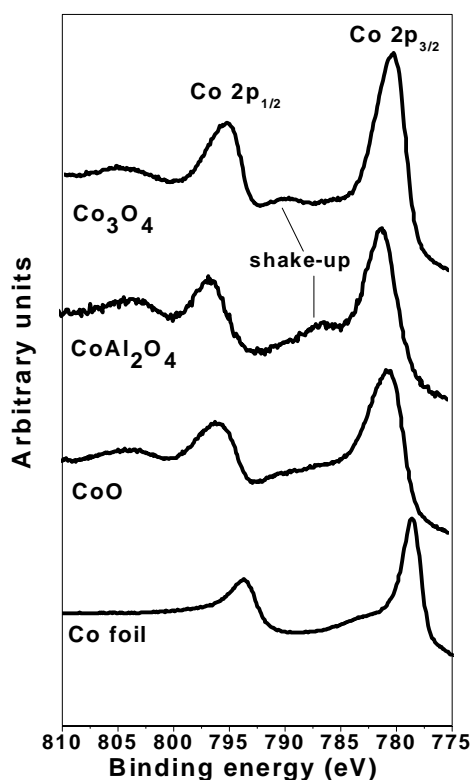


**Figure 2.5** *Co 2p region of XPS spectrum of in-house measured cobalt reference compounds.*

## 2.4 Temperature programmed (TP) techniques

Temperature programmed (TP) techniques involve monitoring a chemical reaction involving a carrier gas and the catalyst surface while the temperature is usually raised linearly [2, 8]. Several forms of these techniques exist and they provide a useful way to study carbon formation on catalysts. The main difference among these forms is the composition of the carrier gas. When oxygen is present in the carrier, the technique is called temperature programmed oxidation (TPO); if the carrier contains hydrogen, it is termed temperature programmed hydrogenation or reduction (TPH/R); if only an inert gas (helium or nitrogen) is the carrier gas, it is called temperature programmed desorption (TPD). These techniques are advantageous because they are experimentally simple and relatively inexpensive compared to many spectroscopic techniques yet they yield a wealth of information about real catalyst systems.

The instrumentation for these techniques is relatively simple (Figure 2.6). The reactor charged with catalyst is controlled by a processor which heats the reactor at

rates of typically 0.1-20 °C/min. In the case of TPH the catalyst containing carbonaceous deposits is heated in hydrogen and this reacts to form predominantly methane. The off gases are monitored by a mass spectrometer. The amount, reactivity, location and in some cases kinetics of carbon burn off can be determined by TP techniques.

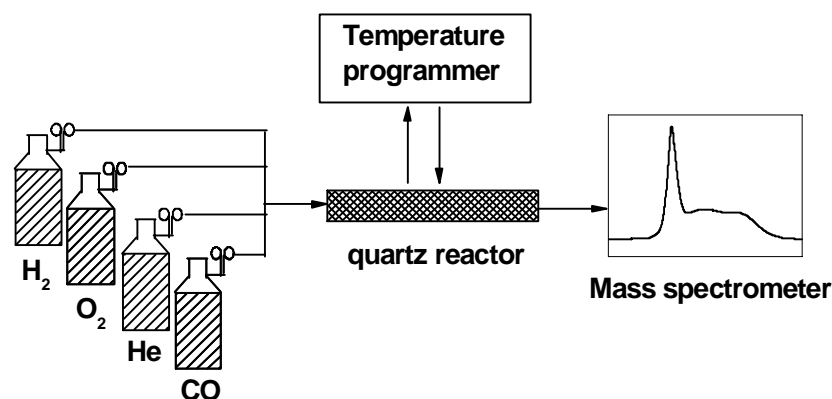


**Figure 2.6** *An experimental set-up for a TP technique apparatus equipped with a mass spectrometer (adapted from [2])*

Figure 2.7 shows a TPH methane profile of Co/Al<sub>2</sub>O<sub>3</sub> catalyst exposed to model FTS conditions. It is evident from the methane evolution that there are different carbonaceous species with varying reactivity towards hydrogen. In some cases the nature of carbonaceous phase can be determined by comparison to carbon references. For example it is known that graphite on cobalt is hydrogenated at around 630 °C, while amorphous, polymeric carbon is hydrogenated at around 430 °C.

Characterization of carbon by TPH is of special interest when hydrogen is one of the reactants, e.g. in reforming and FTS [8]. Usually in these reactions, the overall deactivation rate is the difference between the carbon formation rate, and the carbon gasification rate. If the former is greater than the latter, carbon accumulates on the catalyst. If the gasification rate is greater than the formation rate, no carbon is formed. Therefore, in the above mentioned systems, hydrogen plays a key role in the control of the deactivation rate and TPH can provide useful insights into carbon reactivity and the regeneration of the catalyst. TPO is also a useful technique and is used extensively for the study of carbon on catalysts. An advantage is that the CO<sub>2</sub> which is generated

upon carbon gasification can be detected with a mass spectrometer, which can be calibrated, to give quantitative information. The disadvantage is that oxygen reacts much faster and the resolution between different carbon species in a TPO spectrum may be compromised. Nevertheless, TPO provides a useful way to study carbon phases that are resistant to hydrogen.

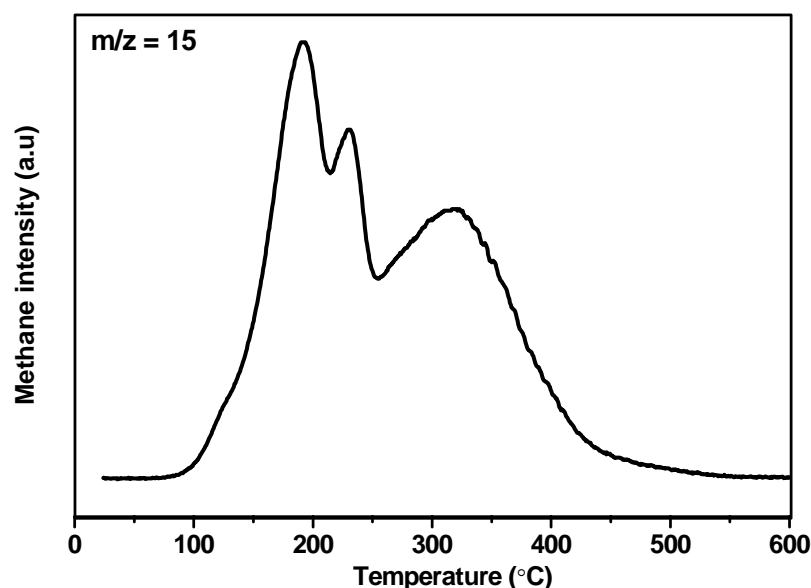


**Figure 2.7** *TPH methane profile of a 20 wt% Co/Al<sub>2</sub>O<sub>3</sub> catalyst after being exposed to model FTS conditions for 4h (230 °C, 1 bar, H<sub>2</sub>/CO = 0.5).*

## 2.5 Transmission electron microscopy (TEM)

The transmission electron microscope (TEM) operates on the same basic principles as the light microscope but uses electrons instead of light [2]. The resolution of a light microscope is limited by the wavelength of light. TEMs use electrons as the "light source" and their much lower wavelength (less than 1Å) makes it possible to get a resolution a thousand times better than with a light microscope. A number of phenomena can occur when a high energy (200 keV) electron source interacts with a solid sample (Figure 2.8). A portion of the electrons may pass through without suffering energy loss. These transmitted electrons form a two dimensional projection of the object. Electrons can be diffracted enabling one to obtain dark-field images as well as diffraction patterns. Electrons may also be backscattered. Electrons can lose

energy via electronic interaction with the solid (inelastic scattering). This energy loss is characteristic of the elements present. With the advent of 2-dimensional detectors, one is able to create energy filtered TEM (EFTEM) maps of different elements. This has important implications particularly in catalysis where the location of promoters or deactivating coke can be mapped [9, 10].

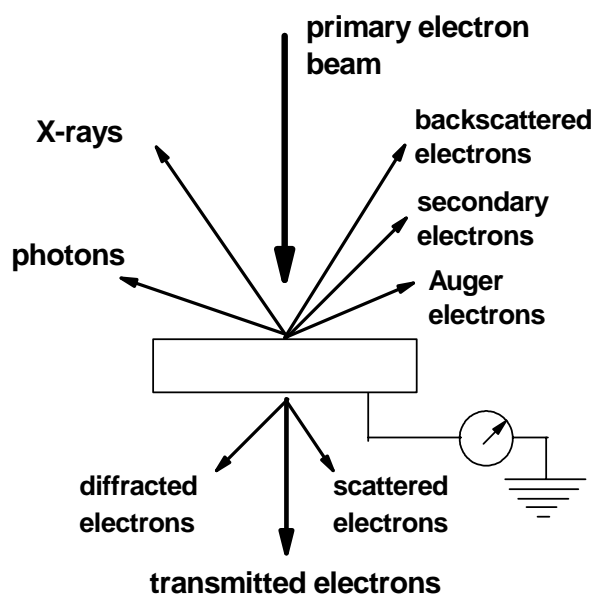


**Figure 2.8** *The interaction between the primary electron beam and the sample (adapted from [2]).*

### 2.5.1 *In-situ TEM*

In the majority of cases, electron microscopy studies of catalysts at the atomic-scale have been performed ex-situ after various gas treatments where the catalysts are removed from the reaction environments and studied under the high vacuum conditions in the microscope [9]. This approach undoubtedly has merit and has made a significant impact in understanding catalysts, however, it has been shown that the catalysts may respond dynamically to changes in the surrounding gas environment, and so, caution must be exercised to ensure that the observed structural details are representative of the catalyst in its working state [11].

In recent times the application of TEM to in-situ studies of catalysts during exposure to reactive gas environments has provided direct observation of such

dynamic changes in catalyst structure [12]. Such studies are by no means trivial due to the extremely small mean-free path of electrons in dense media (gases and solids), and significant instrumental modifications are needed in order to confine a high-pressure gas environment around the specimen area without affecting the microscope performance. This may be accomplished in two ways; by the application of advanced differential pumping systems and by using thin window cells [13]. These different approaches assist in minimizing the degradation of the electron beam as it passes through the gases by minimizing the gas volume.

Recent collaboration between Haldor Topsøe A/S and the FEI Company resulted in an in-situ high resolution TEM (HRTEM) facility capable of providing the first images with a resolution of 0.14 nm during exposure of the sample to reactive gases and elevated temperatures [12]. The in-situ experiments described in Chapter 7 were performed on an FEI CM 300 microscope at Haldor Topsøe, Lyngby equipped with the necessary gas lines ( $\text{CO}$ ,  $\text{H}_2$  and  $\text{H}_2\text{O}$ ) and an in-situ sample holder with a heating filament. The microscope is equipped with an FEG, a quadrupole mass spectrometer (QMS), a Gatan image filter (GIF), and a Tietz F144 CCD for data acquisition. Figure 2.9 nicely illustrates that atomic-scale resolution can be obtained for supported cobalt particles under reactive gas environments at elevated temperatures using this in-situ TEM.

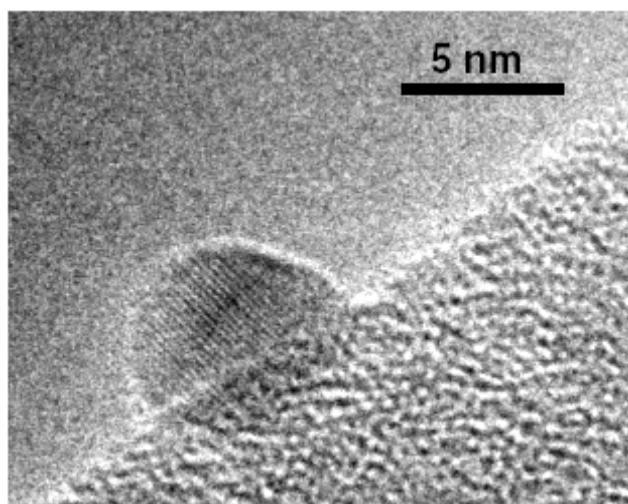


**Figure 2.9** *An in-situ HRTEM image (2 mbar  $\text{H}_2$ , 425 °C) of a 6 nm cobalt particle supported on a Stöber silica sphere. The lattice fringes observed correspond to fcc cobalt.*

## 2.6 Low energy ion scattering (LEIS)

In a low energy ion scattering (LEIS) experiment, a light noble gas ion with a known mass and energy is directed towards the surface that is studied [14]. At the surface, the ion collides with an atom in the outermost atomic layer and the ion is scattered back towards a detector. In the detector, the backscattered ions are sorted by their energy. The energy of the backscattered ion is determined by the classic laws of mechanics, the law of conservation of energy and the law of conservation of momentum. This means that ions that scatter from a heavy atom will scatter back with a higher energy than ions that scatter from a lighter atom. Thus, an analysis of the energy of the backscattered ions will yield a spectrum of the masses of the surface atoms. The information depth of LEIS is limited to one atomic layer, because of the high neutralisation probability of the noble gas ions.

Figure 2.10 shows LEIS spectra of a blank alumina support compared with a Co/Al<sub>2</sub>O<sub>3</sub> catalyst taken with an incident beam of <sup>4</sup>He<sup>+</sup> ions. For the supported cobalt catalyst, peaks due to Co, Al and O are seen. The spectra illustrates that ions lose more energy in collisions with light elements than with heavy elements. The Al signal for the cobalt catalyst is less than for the alumina support and the surface coverage of cobalt can be calculated based on comparison of such measurements. LEIS may also be applied to determine the location of poisons or carbon deposits on catalysts [15].

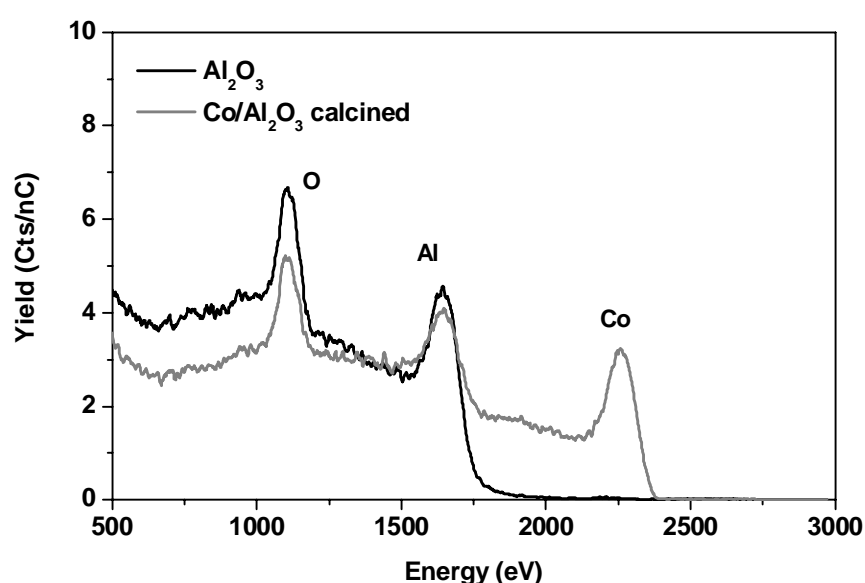


**Figure 2.10** *3 keV <sup>4</sup>He<sup>+</sup> spectra of oxygen treated alumina support and Co/Al<sub>2</sub>O<sub>3</sub> catalyst.*

## 2.7 References

- [1] D. C. Koningsberger, R. Prins (Eds.), *X-ray Absorption*, Wiley, New York, 1987.
- [2] J.W. Niemantsverdriet, *Spectroscopy in Catalysis*, 3rd ed., Wiley-VCH, Weinheim, 2007.
- [3] A.M. Saib, A. Borgna, J. van de Loosdrecht, P.J. van Berge, J.W. Niemantsverdriet, *Appl. Catal. A* 312 (2006) 12.
- [4] A.M. Moen, D.G. Nicholson, *Chem. Mater.* 9 (1997) 1241.
- [5] J.C.J. Bart, *Adv. Catal.* 34 (1986) 203.
- [6] G. Fierro, M.L. Jacono, M. Inversi, P. Porta, *Top. Catal.* 10 (2000) 39.
- [7] Z. Zsoldos, L. Gucci, *J. Phys. Chem.* 96 (1992) 9393.
- [8] S. Bhatia, J. Beltramini, D.D. Do, *Catal. Today* 7 (1990) 309.
- [9] A.K. Datye, In: *Handbook of Heterogeneous Catalysis*, Vol. 2, G. Ertl, H. Knözinger, J. Weitkamp, (Eds.), Wiley-VCH, New York (1997) 493.
- [10] M.D. Shannon, C.M. Lok, J.L. Casci, *J. Catal.* 249 (2007) 41.
- [11] P.L. Hansen, J.B. Wagner, S. Helveg, J.R. Rostrup-Nielsen, B.S. Clausen, H. Topsøe, *Science* 295 (2002) 2053.
- [12] S. Helveg, P.L. Hansen, *Catal. Today* 111 (2006) 68.
- [13] P.L. Hansen, S. Helveg, A.K. Datye, *Adv. Catal.* 50 (2006) 77.
- [14] H.H. Brongersma, M. Draxler, M. de Ridder, P. Bauer, *Surf. Sci. Reports* 62 (2007) 63.
- [15] J.M.A. Harmsen, W.P.A. Jansen, J.H.B.J. Hoebink, J.C. Schouten, H.H. Brongersma, *Catal. Lett.* 74 (2001) 133.





---

# Chapter 3

---

## **The impact of cobalt aluminate formation on the deactivation of cobalt-based Fischer-Tropsch synthesis catalysts**

---

*The aim of this study is to understand quantitatively, the role of cobalt aluminate formation on the deactivation behaviour of cobalt-based Fischer-Tropsch synthesis (FTS) catalysts. For this purpose, wax-coated samples were removed periodically from an extended demonstration reactor run operated at commercially relevant FTS conditions and analysed with X-ray Absorption Near Edge Spectroscopy (XANES). With XANES, wax protected spent samples could be analysed in a pseudo in-situ mode, i.e. without altering the oxidation state of cobalt that was present in the reactor prior to sampling. It is clear from our measurements that during commercially relevant FTS conditions the Co/Pt/Al<sub>2</sub>O<sub>3</sub> catalyst undergoes reduction and  $\leq 3$  wt% cobalt aluminate formation takes place. Based on the observation that the catalyst undergoes a relatively rapid reduction and a very gradual but slight cobalt aluminate formation it is proposed that this cobalt aluminate is formed from the residual cobalt oxide present in the catalyst following reduction. Additionally, the formation of aluminate was investigated with XANES and X-ray photoelectron spectroscopy (XPS) on catalysts taken from laboratory continuous stirred tank reactor (CSTR) runs, where the water partial pressure was varied between 1-10 bar. Even at high water partial pressures ( $P_{H_2O} = 10$  bar,  $P_{H_2O}/P_{H_2} = 2.2$ ) around 10 wt% cobalt aluminate is formed while the metallic fraction of cobalt remains constant.*

---

### 3.1 Introduction

In the next few decades natural gas is expected to become an important raw material as an alternative to crude oil for the production of liquid fuels [1]. The Fischer-Tropsch synthesis (FTS) is an integral part of gas-to-liquids (GTL) technology, which involves the conversion of synthesis gas ( $H_2/CO$ ), derived from natural gas, to liquid hydrocarbon fuels. These fuels have a low sulphur and aromatic content [2]. Cobalt-based catalysts are the preferred choice due to their high per pass conversion, selectivity towards linear hydrocarbons, and low selectivity towards  $CO_2$  [3, 4]. However, cobalt is an expensive metal and therefore high catalyst stability is desired. In order to optimise the usage of a cobalt catalyst for such processes, an understanding of the deactivation mechanisms at play is paramount.

The mentioned deactivation mechanisms in literature for cobalt-based catalysts include: poisoning of the cobalt surface by sulphur and nitrogen compounds [5,6]; oxidation of the metallic phase by product water to form an inactive oxidic fraction [7]; sintering of the active phase facilitated by the product water and the reaction conditions [8] reconstruction of cobalt surface due to the intrusive nature of CO [9,10]; solid state transformation involving the diffusion of cobalt into the support to form irreducible cobalt support compounds (e.g. aluminates and silicates) [11,12] and the formation of inert carbon phases which can block the cobalt active phase [13,14].

Due to the high costs of cobalt it is required that the catalyst has high dispersion and catalysts are thus designed with small cobalt nanoparticles (around 6nm) well dispersed over a high surface area carrier like silica, titania or  $\gamma$ -alumina [4].  $Co/Al_2O_3$  catalysts are usually prepared by: (a) impregnation of cobalt (II) nitrate (b) thermal treatment in air to decompose the nitrate precursor and oxidise the cobalt to  $Co_3O_4$  and finally (c) reduction of the  $Co_3O_4$  to metallic cobalt [15, 16]. In the case of thermal treatment in air at high temperatures ( $> 350\text{ }^\circ\text{C}$ ), it is possible for cobalt ions to diffuse into the support to produce cobalt support compounds which are only reducible at harsh conditions ( $> 800\text{ }^\circ\text{C}$  in  $H_2$ ) [7]. It is known that  $Co_3O_4$  and  $\gamma$ -alumina have isotopic crystal structures and this contributes to the ease of migration of ions from cobalt oxide into the support during these oxidative treatments [17].

Additionally the ionic radius of trivalent cobalt (0.063 nm) and aluminium (0.054 nm) are quite similar and during high temperature calcination it is possible that  $\text{Co}^{3+}$  ions from  $\text{Co}_3\text{O}_4$  are gradually replaced by  $\text{Al}^{3+}$  to produce a series of spinel compounds which may include  $\text{CoAl}_2\text{O}_4$  or  $\text{Co}_2\text{Al}_2\text{O}_4$  [18]. It was also shown that during the reduction of  $\text{Co}/\text{Al}_2\text{O}_3$  catalysts with hydrogen, water vapour is produced which results in the formation of a non-reducible cobalt aluminate-like spinel [19]. Considering all of the above it may be expected that fresh cobalt on alumina catalysts prepared via the above traditional route will contain a small amount of cobalt aluminate. For example, Wang and Chen [20] have shown by TPR that catalysts with 20 wt%  $\text{Co}/\text{Al}_2\text{O}_3$  do have the presence of a cobalt aluminate phase.

It is known from thermodynamic calculations by van Berge et al. [7] that bulk Co will not oxidise to  $\text{CoO}$  or  $\text{Co}_3\text{O}_4$  during standard FTS conditions, whereas the formation of support compounds during the reaction such as cobalt aluminate is favourable. It is argued that the latter does not take place to a significant extent seeing as the formation of cobalt aluminate is kinetically hindered. This is supported by work by Bolt [21] who showed that relatively severe hydrothermal treatment, i.e. steam at 500-800 °C, of  $\text{Co}/\text{Al}_2\text{O}_3$  is required for the further formation of cobalt aluminate.

Water is always present in the FTS due to the removal of adsorbed oxygen, which arises from the dissociation of CO on the metal surface, by hydrogen. The amount of water will vary depending on the choice of reactor, catalytic system and process conditions [22]. Commercially relevant FTS conditions (i.e. 230 °C, 20 bar,  $\text{H}_2$ +CO conversion between 50-70 %, feed gas composition of 50-60 vol. %  $\text{H}_2$  and 30-40 vol. % CO.) create water partial pressures in the range of 4-6 bar. In a slurry phase reactor at these conditions, high water concentrations and low reactant concentrations will exist throughout the entire reactor due to extensive back mixing [23]. The produced water will not be converted to  $\text{CO}_2$  due to the low water gas shift activity of cobalt [3].

Water has been shown to increase the rate of metal aluminate formation [21] on model catalyst consisting of cobalt evaporated onto polycrystalline  $\gamma$ -alumina. Various authors [11, 23, 24, 25] have also claimed that high water partial pressure

increases the formation of aluminate on cobalt-based catalysts either during FTS or at model conditions in mixtures of  $H_2/H_2O$ . Often the observed deactivation is ascribed to the formation of aluminate as it is proposed that the irreducible cobalt-support species is formed from/at the expense of active metallic cobalt.

Jacobs et al. [25] have showed using X-ray Absorption Near Edge Spectroscopy (XANES) that high levels of water which occur at high conversions (due to low space velocity employed) resulted in an irreversible deactivation of platinum promoted  $Co/Al_2O_3$  catalysts in the FTS due to the formation of a cobalt aluminate like species from small cobalt clusters. Hilmen et al. [26] also ascribed the deactivation observed under model conditions with their rhenium promoted  $Co/Al_2O_3$  catalysts to the formation of a cobalt aluminate phase. The authors showed, using XPS and TPR, that at 250 °C, and at  $P_{H_2O}/P_{H_2} = 10$ , cobalt aluminate formation was favoured [26].

Li and co-workers manipulated CO conversion by varying the space velocity over platinum promoted  $Co/Al_2O_3$  catalysts during FTS in a CSTR [11]. They found that at high conversions and hence higher water partial pressures that there was an irreversible deactivation of the catalyst. They also co-fed water and reported that increasing the amount of added water to provide a  $P_{H_2O} = 8.35$  bar and a ratio of  $P_{H_2O}/P_{H_2} = 0.59$  in the feed resulted in a permanent deactivation of the catalyst. These observations, along with increased  $CO_2$  selectivity led them to assume that either  $CoO$  or  $Co_2Al_2O_4$  had formed at these conditions. Similarly Tavasoli et al. [27] showed recently that alumina-supported cobalt catalysts deactivated at higher reaction rates due to the high partial pressure of water. Rapid deactivation was noted for  $P_{H_2O}/(P_{H_2}+P_{CO}) > 0.55$  and  $P_{H_2O}/P_{CO} > 1.5$ . They postulated that the water aided in the formation of irreducible cobalt aluminate which they detected by TPR.

Various techniques have been used to detect cobalt aluminate and these include XPS [26], XRD [19], Raman spectroscopy [19] and TPR [20, 26]. XRD fails to effectively differentiate between  $CoO$  and small amounts of cobalt aluminate while TPR, Raman spectroscopy and XPS are most useful for unused calcined catalysts. As an alternative, XANES is powerful technique that is able to differentiate between  $Co^0$ ,  $CoO$ ,  $Co_3O_4$  and  $CoAl_2O_4$  with a high sensitivity as compared to many other

techniques. It has been used previously for the characterisation of used wax-coated cobalt catalysts [25, 28]. The objectives of this study were to observe if cobalt aluminate will form during commercially relevant FTS conditions in an extended FTS run and to observe the effect of increasing water partial pressure on formation of cobalt aluminate and possibly relate this to the deactivation process.

## 3.2 Experimental

### 3.2.1 Catalyst preparation

A 20 wt% Co/Al<sub>2</sub>O<sub>3</sub> catalyst, promoted with 0.05 wt% platinum, was prepared by slurry impregnation of a  $\gamma$ -alumina support (Puralox 5/150 from Sasol Germany) with an aqueous cobalt nitrate solution, also containing the platinum promoter. After impregnation and drying, the catalyst intermediate was calcined at 250 °C in air and reduced in pure hydrogen at 425 °C. To achieve the required cobalt loading two impregnation and calcination steps were performed [29-34].

### 3.2.2 Characterisation of freshly reduced catalyst

The freshly reduced catalyst was previously analysed with transmission electron microscopy (TEM), hydrogen chemisorption, magnetic measurements and XANES [28,34]. Based on the results from these characterization techniques a model was obtained, describing the cobalt phases and crystallite size distribution for the freshly reduced catalyst prior to the FTS (Table 3.1).

**Table 3.1** *Cobalt phase and crystallite size distribution modeled with data from TEM, XANES, hydrogen chemisorption and magnetic measurements [28, 34]*

Crystallite size	<2–3 nm	6 nm	15 nm
Co <sup>0</sup> in crystallites (%)	-	45	20
CoO in crystallites (%)	24	7 <sup>a</sup>	4 <sup>a</sup>

<sup>a</sup> Unreduced cobalt due to close interaction with support, i.e. two layers of cobalt closest to the support. It is likely that the layer closest to the support is in the form of CoAl<sub>2</sub>O<sub>4</sub>. Mass % are shown.

### 3.2.3 Catalyst Testing

#### 3.2.3.1. Demonstration unit run

The Co/Pt/Al<sub>2</sub>O<sub>3</sub> catalyst was tested in a 100 bbl/day slurry bubble column reactor with a diameter of 0.9 m at commercially relevant FTS conditions, i.e. 230 °C, 20 bar, H<sub>2</sub>+CO conversion between 50-70 %, feed gas composition of 50-60 vol. % H<sub>2</sub> and 30-40 vol. % CO. Direct comparison of catalyst performance can only be done at exactly the same realistic test conditions. As this is difficult to achieve experimentally, a model was developed using the Satterfield [35, 36] equation,  $r_{FT} = (kP_{H_2}P_{CO})/(1+KP_{CO})^2$ , in which the observed catalytic performance can be recalculated to exactly the same test conditions. For this study the Relative Intrinsic (Fischer-Tropsch) Activity Factor (R.I.A.F.) was compared to an in-house baseline catalyst.

#### 3.2.3.2 Laboratory CSTR runs

Fischer–Tropsch synthesis tests were performed in a slurry-phase CSTR with a reactor volume of 670 ml. The catalyst samples (i.e. 10–30 g) were pre-reduced at 380 to 425 °C for 16 h, in pure hydrogen at 1 bar, at a heating rate of 1°C/min, and suspended, under an argon blanket, in 300 ml molten Fischer–Tropsch hydrogenated wax (Sasol H1 hard wax) inside the reactor. Realistic FTS conditions were employed, i.e., 230 °C, ~10-20 bar, commercial synthesis gas as feed of composition: 50 vol% H<sub>2</sub>, 25vol% CO and 25 vol% inerts. The  $P_{CO}$  was kept at (4.0±0.2 bar) and  $P_{H_2}$  at (4.5±0.2 bar) while the  $P_{H_2O}$  was varied from 1-10 bar by adjusting the synthesis gas conversion and the total pressure. The synthesis gas flows were regulated by Brooks mass-flow controllers, and use was made of the ampoule-sampling technique as the selected synthesis performance monitoring method [37].

#### 3.2.4 XANES sample preparation

The sample preparation was done as previously in a glove box (0.1 ppm H<sub>2</sub>O, 2 ppm O<sub>2</sub>) to prevent oxidation of the cobalt [28]. Catalyst samples in wax were removed from the demonstration reactor at varying times-on-stream and at the end of each

laboratory run and cooled down under nitrogen so as to maintain the integrity of the sample. XANES samples were prepared by pelletising 40-50 mg of wax-coated cobalt catalyst removed from the reactor into a 1.3 cm<sup>2</sup> disc. The samples were sealed in Kapton tape and removed from the glove box prior to measurement. Previous benchmarking experiments with in-situ and ex-situ reduced wax-protected samples showed that the sample preparation method does not introduce artificial oxidation [28].

### *3.2.5 XANES analyses of references and wax-coated catalysts*

XANES measurements on reference compounds and wax-coated samples were performed at the ELETTRA synchrotron facility (Trieste, Italy) using a beam line with energy of 2-2.4 GeV. A double crystal monochromator (Si (111) and Si (311)) was used for varying the energy between the desired range. Measurements were carried out at the K-edge of Co. Calibration was performed with a Co foil using the first point of inflection of Co i.e. 7709 eV [38]. All spectra were recorded at liquid nitrogen temperatures. The XANES spectra were extracted from raw data by a conventional procedure. The pre-edge background was subtracted by using power series curves. Subsequently, the spectra were normalized by dividing by the height of the absorption edge. Spectra were quantified by fitting the experimental data with a weighted linear combination of reference compounds (Co<sup>0</sup>, CoO, and CoAl<sub>2</sub>O<sub>4</sub>).

### *3.2.6 X-ray Photoelectron Spectroscopy analysis*

Samples of the spent catalysts tested at various water partial pressures, protected in a wax layer, were taken from the slurry-phase CSTR at the end of the reaction. The catalyst was allowed to congeal under an inert nitrogen environment. Due to the interference of this wax layer, prior to XPS analysis it was removed by an exhaustive reflux extraction with dry, deoxygenated tetrahydrofuran (THF, b.p. 66 °C) under an argon (99.999%) environment for around 3 h, using a P40 glass frit. After extraction the obtained catalyst particles were dried under vacuum at room temperature to remove the THF. The catalyst was then transferred under vacuum using Schlenk glassware into a glove box (2 ppm O<sub>2</sub>, 0.1 ppm H<sub>2</sub>O) for passivation. The samples



were prepared in the glove box by crushing the wax-extracted, FTS catalyst samples in a pestle and mortar. Afterwards, the powders were pressed into an indium layer on top of standard stainless steel XPS stubs and transferred via the glove box into the XPS prechamber.

The XPS measurements were carried out using a VG Escalab 200 MKII spectrometer. An aluminum anode ( $K_{\alpha} = 1486.6$  eV) was used to generate the X-ray radiation (240 W (20 mA; 12kV)). Measurements were carried out with a 0.1 s dwelling time; 0.1 eV step for the selected regions. To obtain sufficient signal-to-noise ratio the Co 2p region was scanned 80 – 120 times (i.e. making the total measurement approximately 3 hours). During measurement the pressure in the main chamber remained below  $10^{-8}$  mbar.

### 3.3 Results and discussion

#### 3.3.1 XANES analysis of reference compounds

Figure 3.1 shows XANES analyses of cobalt reference compounds CoO, Co<sub>3</sub>O<sub>4</sub>, CoAl<sub>2</sub>O<sub>4</sub>, and cobalt foil (Co<sup>0</sup>). The oxidic reference compounds display a strong absorption white line with unique spectral features due to the presence of cobalt atoms in different Co–O environments and oxidation states. The XANES spectra of the oxides also display a small pre-edge feature (ca. 7710 eV). This pre-edge feature arises from the 1s–3d absorption transition and appears most strongly for tetrahedral cobalt environments as compared to octahedral environments [39]. CoO consists of Co<sup>2+</sup> ions octahedrally coordinated to oxygen, whereas Co<sub>3</sub>O<sub>4</sub> has a spinel type structure with both tetrahedral Co<sup>2+</sup> and octahedral Co<sup>3+</sup> ions [39]. CoAl<sub>2</sub>O<sub>4</sub> is a normal spinel with Co<sup>2+</sup> ions in tetrahedral sites [40]. Hence, this pre-edge feature is most pronounced for CoAl<sub>2</sub>O<sub>4</sub> and Co<sub>3</sub>O<sub>4</sub>. It is clear from Figure 3.1 that using XANES it is easy to distinguish between Co<sup>0</sup>, CoO and Co<sub>3</sub>O<sub>4</sub> and to a lesser extent CoAl<sub>2</sub>O<sub>4</sub>. However if we use the derivative spectrum (Figure 3.2), it is clear that the CoO and CoAl<sub>2</sub>O<sub>4</sub> are clearly distinguishable.

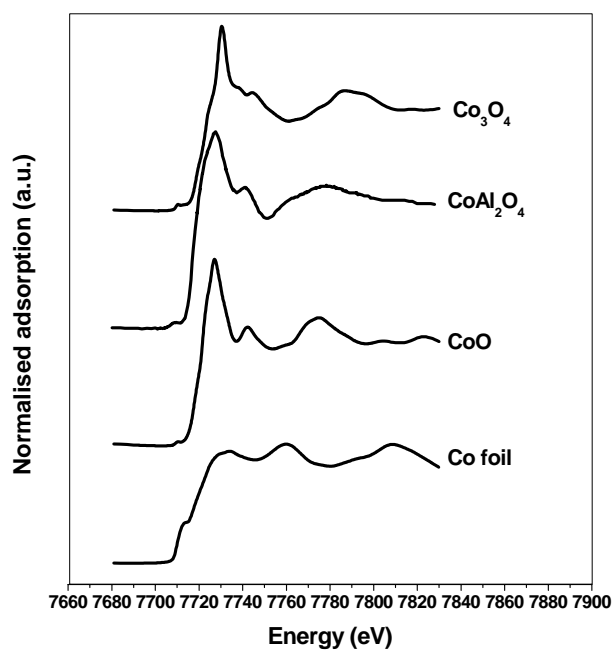


**Figure 3.1** XANES Co K-edge spectra of reference compounds  $\text{Co}_3\text{O}_4$ ,  $\text{CoAl}_2\text{O}_4$ ,  $\text{CoO}$  and cobalt foil ( $\text{Co}^0$ ).

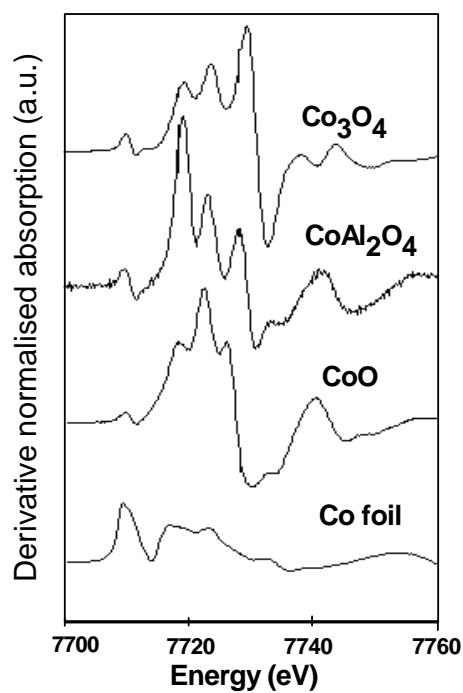


**Figure 3.2** XANES derivative spectra of reference compounds  $\text{Co}_3\text{O}_4$ ,  $\text{CoAl}_2\text{O}_4$ ,  $\text{CoO}$  and cobalt foil ( $\text{Co}^0$ ).

## 3.3.2 Extended demonstration unit FTS run

Figure 3.3 shows the activity data for an extended FTS run conducted with a Co/Pt/Al<sub>2</sub>O<sub>3</sub> catalyst in a 100 bbl/day slurry bubble column reactor [28]. The catalyst undergoes deactivation during the course of the run which starts to level off after 50 days. As mentioned earlier the presence of reaction water at partial pressures of 4-6 bar may be one of the factors that may lead to catalyst deactivation. XANES analysis of catalyst samples was done to observe if cobalt aluminate was formed. Figure 3.4 shows that during the course of the reaction the catalyst does not undergo any oxidation but is instead reduced as the XANES spectrum of samples closely resembles the spectrum of a Co foil. The observed behaviour for > 6 nm Co particles (at  $P_{H_2O}/P_{H_2} = 1-1.5$ ,  $P_{H_2O} = 4-6$  bar) is in line with previous work [28] and also supported by thermodynamic calculations [41]. Furthermore the derivative spectrum (Figure 3.5) shows that very little cobalt aluminate, i.e.  $\leq 3\%$ , is formed gradually. Hence, at these conditions, with water partial pressure of 4-6 bar, cobalt aluminate formation is not that significant (Table 3.2) and cannot account for the deactivation seen in Figure 3.3. Due to the strongly reducing environment during FTS the observed cobalt aluminate arises most likely from the reaction of the unreduced cobalt oxide with the alumina support and this should have no influence on the deactivation of the catalyst.

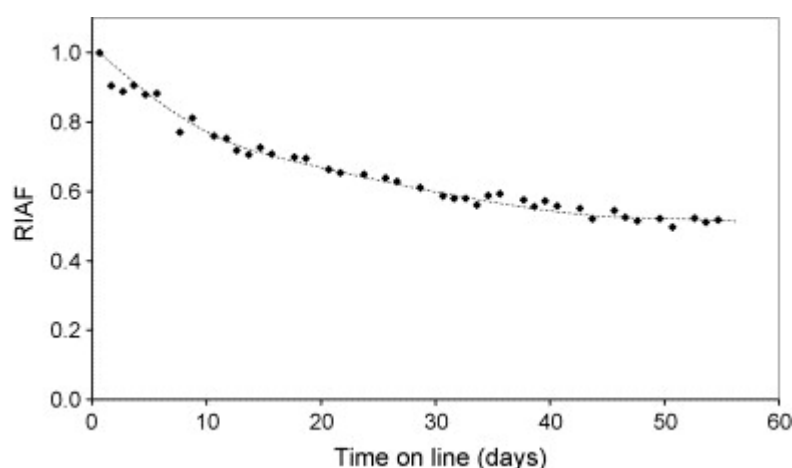


**Figure 3.3** *Relative intrinsic activity factor (RIAF) for a Co/Pt/Al<sub>2</sub>O<sub>3</sub> catalyst during realistic FTS, i.e. 230 °C, 20 bar, H<sub>2</sub> + CO conversion between 50-70 %, feed gas composition of 50-60 vol. % H<sub>2</sub> and 30-40 vol. % CO. (from [28]).*

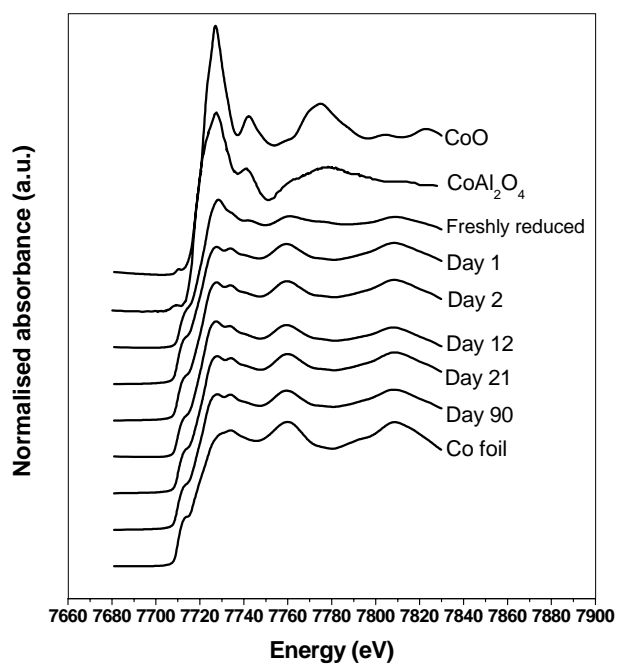


**Figure 3.4** *XANES Co K-edge spectra of Co/Pt/Al<sub>2</sub>O<sub>3</sub> catalyst taken at different intervals from an extended FTS and compared to reference compounds.*

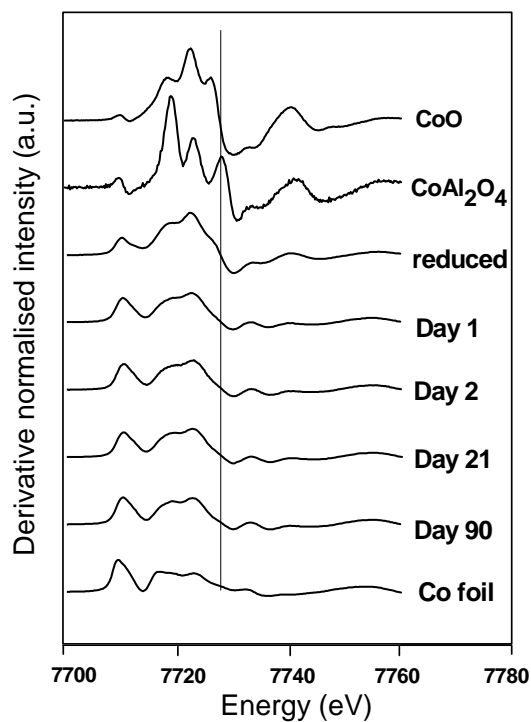


**Figure 3.5** *XANES derivative spectra of Co/Pt/Al<sub>2</sub>O<sub>3</sub> catalysts taken at different intervals from an extended FTS and compared to reference compounds.*

**Table 3.2** *Quantification of XANES analyses of a series of Co/Pt/Al<sub>2</sub>O<sub>3</sub> catalysts tested during realistic FTS in a 100 bbl/day slurry bubble column, using a linear combination of reference compounds. Error =  $\pm 1-2\%$ .*

Sample	Co <sup>0</sup> (%)	CoO (%)	CoAl <sub>2</sub> O <sub>4</sub> (%)
Freshly reduced	58	42	-
Day 1	84	16	-
Day 2	86	12	2
Day 21	86	11	3
Day 90	87	11	2

### 3.3.3 Runs with varying water partial pressure

#### 3.3.3.1 XANES analysis of samples tested at various water partial pressures

FTS runs were carried out in laboratory CSTR at 230 °C, 10-20 bar, where the water partial pressure was varied at 1-10 bar. This was done in order to observe if higher water partial pressures, will result in aluminate formation. The initial activities for the catalysts tested at the various water partial pressures were similar. Depending on the support, different results on the effect of water on catalyst activity have been reported [42]. For Co/Al<sub>2</sub>O<sub>3</sub> catalysts it is known that high water partial pressures result in decreased activity and this is ascribed to oxidation and aluminate formation [11, 25]. Under our conditions the oxidation of cobalt is not observed with XANES (Figure 3.6.). XANES analyses showed that at higher water partial pressures the catalyst still underwent reduction compared to the fresh catalyst, which is in line with thermodynamics. Interestingly at higher water partial pressures the amount of cobalt aluminate that was formed increased. From the quantification (Table 3.3) it can be seen that the cobalt aluminate is formed at the expense of the cobalt oxide and not the metal. Instead even at high water partial pressures ( $P_{\text{H}_2\text{O}} = 10$ ,  $P_{\text{H}_2\text{O}}/P_{\text{H}_2} = 2.2$ ), a reduction is observed when compared to a freshly reduced catalyst. Bulk thermodynamic data indicates that at these conditions the reduction of CoO to Co should be spontaneous at  $P_{\text{H}_2\text{O}}/P_{\text{H}_2}$  below 50. It must be stated that most of the CoO

exists as 2-3 nm crystallites (Table 3.1) and these small particles are expected to have a strong interaction with the support and may be difficult to reduce. The derivative spectrum (Figure 3.7) indicated that only small amounts of cobalt aluminate are formed ( $\leq 10$  wt%) even at higher water partial pressures.

**Table 3.3** *Quantification of XANES analyses of a series of Co/Pt/Al<sub>2</sub>O<sub>3</sub> catalysts exposed to varying water partial pressures during FTS (10-20 bar, 230°C) taken from a laboratory CTSR using a linear combination of reference compounds. Error =  $\pm 1-2\%$ .*

Sample	TOS (days)	H <sub>2</sub> O/H <sub>2</sub>	Co <sup>0</sup> (%)	CoO (%)	CoAl <sub>2</sub> O <sub>4</sub> (%)
Freshly reduced	-	-	58	42	-
1 bar	3	0.2	88	12	-
4.5 bar	7	1	74	23	3
7 bar	2	1.6	73	18	9
10 bar	10	2.2	72	18	10

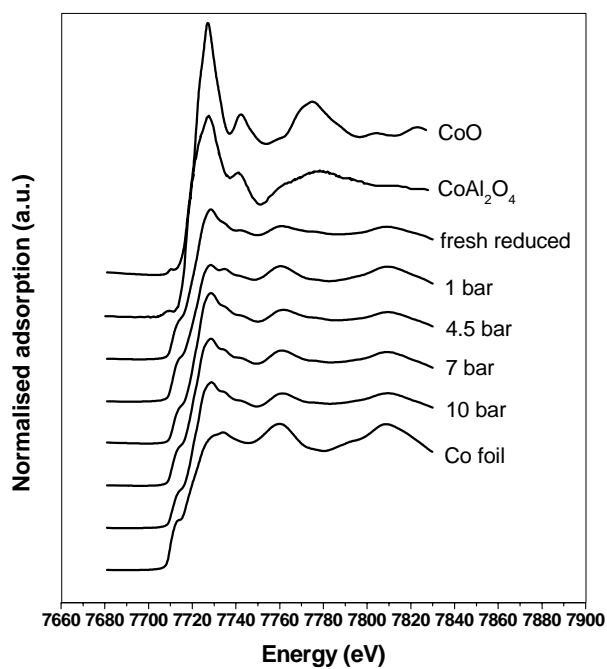


**Figure 3.6** *XANES Co K-edge spectra showing the influence of varying water partial pressures on Co/Pt/Al<sub>2</sub>O<sub>3</sub> catalysts.*

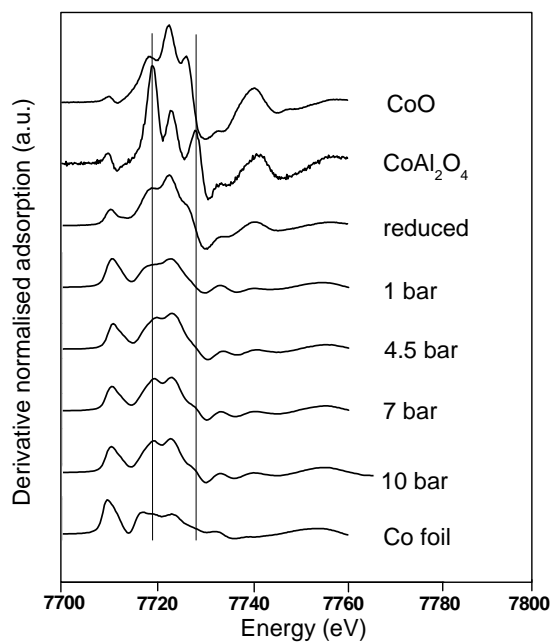


**Figure 3.7** *XANES derivative spectra of Co/Pt/Al<sub>2</sub>O<sub>3</sub> catalysts exposed to varying water partial pressures compared to reference compounds. The slight evolution of cobalt aluminate can be noted.*

### *3.3.3.2 XPS analysis of samples with varying water partial pressure*

Four catalyst samples were analyzed by XPS with the aim of observing changes in composition that may occur during FTS conducted with higher water partial pressures. The samples included a freshly reduced catalyst and catalysts treated at 4.5, 7 and 10 bar water partial pressures. The wax covered samples were first extracted with THF at mild extraction conditions ( $\sim 66\text{ }^{\circ}\text{C}$  in Ar) and this treatment is not expected to cause any change in the amount of cobalt aluminate in the catalysts. The catalysts were then passivated in a glove box. These were then transferred under a protective atmosphere into the XPS set-up.

When comparing the Co 2p region of the XPS spectra in Figure 3.8 along with data presented in Table 3.4 it can be seen that the Co  $2p_{3/2}$  peak positions for 10 bar sample seem to be shifted to higher binding energies compared to the reduced catalyst. The binding energy and doublet separation information (Table 3.4) combined with the fact that the spectra show strong shake-up features (about 5-6 eV from main peak) gives an indication that the samples contain cobalt compounds in high spin states e.g. CoO and  $\text{CoAl}_2\text{O}_4$  [43]. Unfortunately by using the Co 2p XPS region only, it is extremely difficult to differentiate between the CoO and cobalt aluminate for the extracted samples.

However, the Al 2p region of the XPS spectra can possibly provide information in support of XANES, with regards to cobalt aluminate formation. The Al 2p peak position of the reduced catalyst (Figure 3.8) corresponds more closely with  $\text{Al}_2\text{O}_3$ , which has a value of 74.4 eV [43]. This peak shifts to lower binding energies for samples exposed to higher water partial pressures. This decrease in the Al 2p binding energy possibly points to the formation of a cobalt aluminate support compound. The Al 2p position in a  $\text{CoAl}_2\text{O}_4$  reference sample was determined to be 74.1 eV. Although the amount of cobalt aluminate formed is small ( $\leq 10\text{ wt\%}$ ), there is considerable shift in the bind energies of the Al 2p peak. This may be explained by the premise that cobalt aluminate formation results in the flattening out of a particle over the support surface, resulting in an increased sensitivity in XPS.



**Table 3.4** *Co 2p<sub>3/2</sub> binding energy, doublet separation (DS) values for Co 2p<sub>3/2</sub> and Co 2p<sub>1/2</sub> components and Al 2p binding energy of reference compounds, freshly reduced catalyst and catalysts tested at various water partial pressures.*

Sample	Co 2p <sub>3/2</sub> (eV)	DS	Al 2p (eV)
Reduced	780.9	16.0	74.4
4.5 bar	781.1	15.7	74.3
7 bar	780.4	15.6	73.9
10 bar	781.0	15.5	74.1
CoO	780.5*	15.5	-
CoAl <sub>2</sub> O <sub>4</sub>	780.9*	15.5	74.1

\*Measured in-house

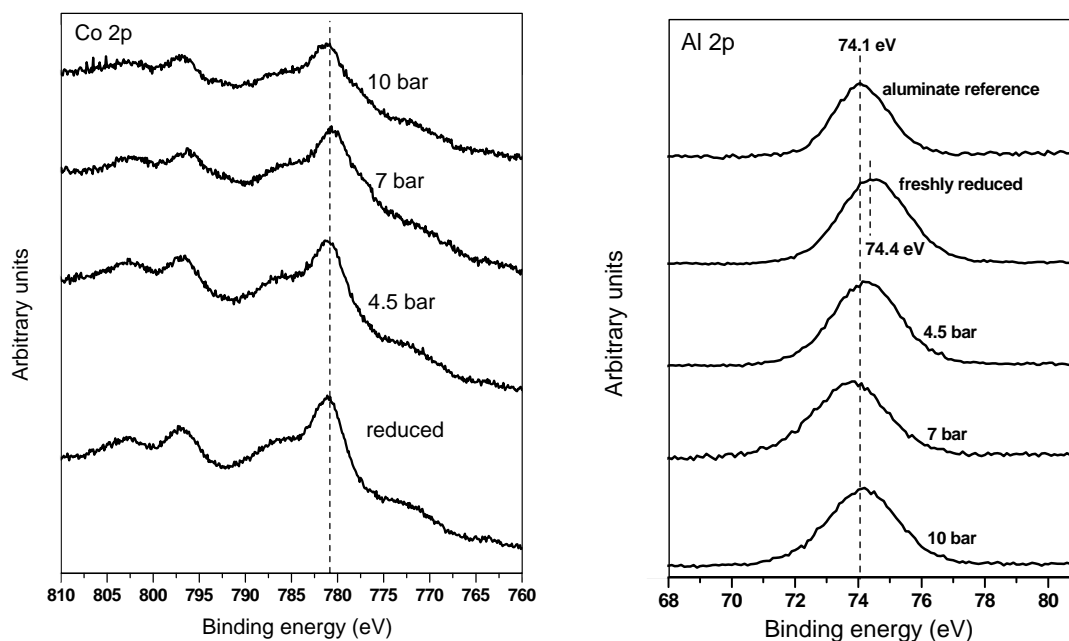
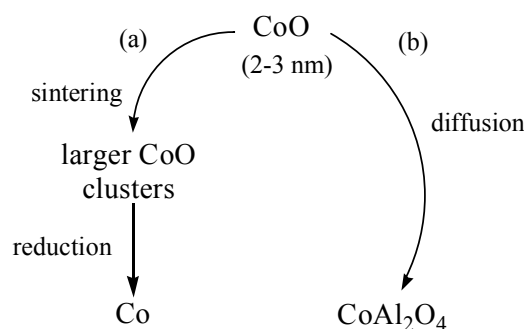


**Figure 3.8** *XPS Co 2p and Al 2p spectra of wax-extracted samples of freshly reduced catalyst and catalyst exposed to various water partial pressures. A reference cobalt aluminate sample is also included in the Al 2p region.*

### 3.4. Mechanism of reduction and aluminate formation

It is clear from the XANES measurements that CoO undergoes a reduction during the extended FTS run at commercially relevant conditions and aluminate formation is not observed to a great extent. This reduction behaviour was reported previously by Saib et al. [28] for cobalt catalysts tested in a slurry bubble column under similar conditions, which shows that strong reducing nature of the FT environment. Oosterbeek [44] also showed the strong reduction tendency of cobalt oxide under synthesis conditions. He observed the complete reduction of a highly oxidic Co(poly) crystal under FT conditions with XPS.

In the case of catalysts exposed to higher water partial pressures than what would exist under normal FTS conditions, we still observe a reduction compared to the fresh catalyst and cobalt aluminate formation in the order of 10 wt%. This is in line with thermodynamic expectations. Based on the quantification it is proposed that this aluminate is formed from existing 2-3 nm CoO clusters and not from metallic cobalt as an increase in the reduction extent is observed from the fresh catalyst. To explain this we propose two possibilities (Scheme 3.1): (a) sintering of small CoO crystallites to form larger clusters, with a relatively weakened interaction with the support, which are then reduced; and (b) a slower process involving the formation of cobalt aluminate from interaction of CoO with the support which could be enhanced by water.



**Scheme 3.1** Possible pathways for formation of metallic cobalt and cobalt aluminate from CoO. The hypothesis is that pathway (a) is favoured over (b)

As mentioned earlier, it is expected that the small CoO crystallites have a strong interaction with the support. However water is known to affect the interface energy between the support and crystallites and the dynamic gas environment that exists can drive the sintering process [45]. Once the CoO crystallites sinter to above 4-5 nm then it is thermodynamically [41] and possibly kinetically favourable for them to be transformed to Co in the highly reducing  $H_2/CO$  environment [46].

The formation of cobalt aluminate is known to proceed via CoO as an intermediate [7]. The presence of water can result in hydration of the alumina support as reported by Oukaci et al. [47]. The hydrated alumina appears to enhance the diffusion of small CoO particles in strong interaction with the support, during prolonged treatment resulting in the formation of non-reducible cobalt aluminate. This may explain why small amounts of aluminate are formed in the case of catalyst exposed to higher water partial pressures [47]. It is expected that this is a kinetically slow process as it involves diffusion into the support [48]. It is therefore believed that the sintering/reduction process (a) is favoured over the transformation of CoO into aluminate (b).

The observed deactivation in the demonstration unit can thus not be explained by oxidation or aluminate formation. The reduction to Co metal should have resulted in an increase in intrinsic catalyst activity however this was not the case. The deactivation is most likely due to a complex interplay of other deactivation mechanisms such as sintering (enhanced by water), surface reconstruction and carbon deposition which may overshadow the effect of CoO reduction.

### 3.5 Conclusions

During this study we showed that XANES can distinguish between CoO,  $CoAl_2O_4$  and  $Co^0$  in wax-coated cobalt on alumina FTS catalysts, taken from a 100 bbl/day slurry bubble column reactor, with reasonable sensitivity. We did not observe oxidation of  $> 6$  nm Co crystallites at  $P_{H_2O}/P_{H_2}$  ratios up to 2.2 but instead reduction of CoO was noted. The amount of cobalt aluminate formed was small and it appears that its formation is difficult during FTS (surface and bulk). Water does seem to enhance aluminate formation but even at high water partial pressure (10 bar) less than

10 wt% cobalt aluminate formed and a reduction was observed compared to a fresh catalyst. The cobalt aluminate that did form, resulted from existing CoO. This leads us to the conclusion that cobalt aluminate formation does not influence deactivation of cobalt catalysts during realistic FTS conditions. The observed deactivation is likely due to an interplay between other phenomena which may include, sintering, surface reconstruction and carbon deposition.

## Acknowledgements

The authors would like to thank Mr. Tiny Verhoeven and Dr. Ionel Ciobică for assistance during XANES measurements.

## 3.6 References

- [1] R. Zennaro, *Oil Gas* 2 (2007) 88.
- [2] A.P. Steynberg, M.E. Dry (Eds.), *Fischer-Tropsch Technology*, Studies in Surface Science and Catalysis, Vol. 152, Elsevier, 2004.
- [3] E. Iglesia, *Appl. Catal. A* 161 (1997) 59.
- [4] M. E. Dry, *Appl. Catal. A* 276 (2004) 1.
- [5] C.H. Bartholomew, R.M. Bowman, *Appl. Catal.* 15 (1985) 59.
- [6] J. Inga, P. Kennedy, S. Leviness, United States Patent Application 20050154069 A1 (2004) to Syntroleum.
- [7] P.J van Berge, J. van de Loosdrecht, S. Barradas, A.M. van der Kraan, *Catal. Today* 58 (2000) 321.
- [8] G.Z. Bian, N. Fujishita, T. Mochizuki, W.S. Ning, M. Yamada, *Appl. Catal. A* 252 (2003) 251.
- [9] G.L. Bezemer, J.H. Bitter, H.P.C.E. Kuipers, H. Oosterbeek, J.E. Holewijn, X. Xu, F. Kapteijn, A.J. van Dillen, K.P. de Jong, *J. Am. Chem. Soc.* 128 (2006) 3956.
- [10] J. Wilson, C. de Groot, *J. Phys. Chem.* 99 (1995) 7860.
- [11] J. Li, G. Jacobs, T. Das, B.H. Davis, *Appl. Catal. A* 228 (2002) 203.
- [12] G. Kiss, C. Kliever, G.J. DeMartin, C.C. Culross, J.E. Baumgartner, *J. Catal.* 217 (2003) 127.
- [13] V. Gruver, R. Young, J. Engman, H.J. Robota, *Prepr. Pap.-Am. Chem. Soc., Div. Pet. Chem.* 50 (2005) 164.
- [14] J.J.H.M. Font Freide, T.D. Gamlin, R.J. Hensman, B. Nay, C. Sharp, *J. Nat. Gas Chem.* 13 (2004) 1.
- [15] J. van de Loosdrecht, S. Barradas, E.A. Caricato, N.G. Ngwenya, P.S. Nkwanyana, M.A.S. Rawat, B.H. Sigwebela, P.J. van Berge, J.L. Visagie, *Top. Catal.* 26 (2003) 121.
- [16] R. Oukaci, A.H. Singleton, J.G. Goodwin Jr., *Appl. Catal. A* 186 (1999) 129.
- [17] F. Dumond, E. Marceau, M. Che, *J. Phys. Chem. C*, 111 (2007) 4780.
- [18] W. Chu, P.A. Chernavskii, L. Gengembre, G.A. Pankina, P. Fongarland, A.Y. Khodakov, *J. Catal.* 252 (2007) 215.
- [19] B. Jongsomjit, J. Panpranot, J.G. Goodwin Jr., *J. Catal.* 204 (2001) 98.
- [20] W.J. Wang, Y.W. Chen, *Appl. Catal.* 77 (1991) 223.
- [21] P.H. Bolt, "Transition metal-aluminate formation in alumina-supported model catalysts", PhD thesis, University of Utrecht, The Netherlands, 1994.
- [22] R.B. Anderson, in: P.H. Emmett (Ed.), *Catalysis*, Vol. 4, Reinhold, New York, 1956.
- [23] D. Schanke, A.M. Hilmen, E. Bergene, K. Kinnari, E. Rytter, E. Ådnanes, A. Holmen, *Catal. Lett.* 345 (1995) 269.

- [24] G. Jacobs, T.K. Das, P.M. Patterson, J. Li, L. Sanchez, B.H. Davis, *Appl. Catal. A* 247 (2003) 335.
- [25] G. Jacobs, P.M. Patterson, Y. Zhang, T. Das, J. Li, B. Davis, *Appl. Catal. A* 233 (2002) 215.
- [26] A.M. Hilmen, D. Schanke, K.F. Hanssen, A. Holmen, *Appl. Catal. A* 186 (1999) 169.
- [27] A. Tavasoli, A. Nakhaeipour, K. Sadaghiani, *Fuel Proc. Tech.* 88 (2007) 461.
- [28] A.M. Saib, A. Borgna, J. van de Loosdrecht, P.J. van Berge, J.W. Niemantsverdriet, *Appl. Catal. A* 312 (2006) 12.
- [29] P.J. van Berge, J. van de Loosdrecht, J.L. Visagie, United States Patent 6 806 226 (2004), to Sasol.
- [30] P.J. van Berge, J. van de Loosdrecht, E. Caricato, S. Barradas, B.H. Sigwebela, United States Patent 6 455 462 (2002), to Sasol.
- [31] P.J. van Berge, J. van de Loosdrecht, E. Caricato, S. Barradas, United States Patent 6 638 889 (2004), to Sasol.
- [32] R.L. Espinoza, J.L. Visagie, P.J. van Berge, F.H. Bolder, United States Patent 5 733 839 (1998), to Sasol.
- [33] P.J. van Berge, J. van de Loosdrecht, J.L. Visagie, T.J. van der Walt, H. Veltman, C. Sollié, European Patent 1 444 040 B1 (2003), to Sasol.
- [34] P.J. van Berge, J. van de Loosdrecht, J.L. Visagie, United States Patent 6 385 690 (2004), to Sasol.
- [35] C.A. Chanenchuk, I.C. Yates, C.N. Satterfield, *Energy Fuels* 5 (1991) 847.
- [36] I.C. Yates, C.N. Satterfield, *Energy Fuels* 5 (1991) 168.
- [37] H. Shultz, A. Geertsema, *Erdöl und Kohle* 20 (1985) 38.
- [38] [www.csrri.iit.edu/periodic-table.html](http://www.csrri.iit.edu/periodic-table.html).
- [39] D. Bazin, I. Kovacs, L. Guzzi, P. Parent, C. Laffon, F. de Groot, O. Ducreux, J. Lynch, *J. Catal.* 189 (2000) 456.
- [40] M. Zayat, D. Levy, *Chem. Mater.* 12 (2000) 2763.
- [41] E. van Steen, M. Claeys, M. Dry, E. Viljoen, J. van de Loosdrecht, J.L. Visagie, *J. Phys. Chem. B* 109 (2005) 3575.
- [42] Ø. Borg, S. Storsæter, S. Eri, H. Wigum, E. Rytter, A. Holmen, *Catal. Lett.* 107 (2006) 95.
- [43] N.S. McIntyre, M.G. Cook, *Anal. Chem.* 47 (1975) 2208.
- [44] H. Oosterbeek, *Phys. Chem. Chem. Phys.* 9 (2007) 3570.
- [45] P. Hansen, J.B. Wagner, S. Helveg, J.R. Rostrup-Nielsen, B.S. Clausen, H. Topsøe, *Science* 295 (2002) 2053.
- [46] A. M. Saib, "Towards a cobalt Fisher-Tropsch synthesis catalyst with enhanced stability: A combined approach", PhD thesis, Eindhoven University of Technology, The Netherlands, 2006.
- [47] A. Sirijaruphana, A. Horvath, J.G. Goodwin Jr., R. Oukaci, *Catal. Lett.* 91 (2003) 89.
- [48] P.H. Bolt, F.H.P.M. Habraken, J.W. Geus, *J. Solid State Chem.* 135 (1998) 59.

---

# Chapter 4

---

## **The formation and influence of carbon on cobalt-based Fischer-Tropsch synthesis catalysts: *A Review***

---

*Cobalt-based Fischer-Tropsch synthesis (FTS) catalysts are the systems of choice for use in gas-to-liquid (GTL) processes. As with most catalysts, cobalt systems partially lose their activity with increasing time-on-stream. There are various mechanisms that have been proposed for the deactivation of cobalt-based catalysts during realistic FTS conditions. These include poisoning, sintering, oxidation, metal support compound formation, restructuring of the active phase and carbon deposition. Most of the recent research activities on cobalt catalyst deactivation during the FTS have focused on loss of catalyst activity due to oxidation of the metal and support compound formation. Relatively few recent studies have been conducted on the topic of carbon deposition on cobalt-based FTS catalysts. The purpose of this review is to integrate the existing open and patent literature to provide a clearer understanding on the role of carbon as a deactivation mechanism.*

---

## 4.1 Introduction and scope

The Fischer-Tropsch synthesis (FTS) is a process that converts synthesis gas into mixtures of higher molecular weight hydrocarbons [1]. The FTS is at the heart of the gas-to-liquids (GTL) process which converts natural gas to “clean” synfuels [2]. This approach is attractive due to the rising oil price and the need to comply with more stringent legislation on the quality of liquid fuels [3].

The two catalytically active metals for FTS which are used in industry are iron (fused or precipitated) and cobalt (supported). Iron catalysts display higher water gas shift activities ( $\text{CO} + \text{H}_2\text{O} \rightarrow \text{CO}_2 + \text{H}_2$ ) and are more suitable for use with coal and biomass-derived synthesis gas feeds, which have lower hydrogen content [4]. Cobalt catalysts exhibit high per pass activities, have low water gas shift activity which leads to improved carbon utilization and are suitable for use on synthesis gas produced via reforming of natural gas [5]. Cobalt FTS catalysts yield mainly straight chain hydrocarbons. Since cobalt is much more expensive than iron, dispersing the ideal concentration and size of metal nanoparticles onto a support can help reduce catalyst costs while maximizing activity and durability. However, as with almost all catalysts, cobalt FTS catalysts also deactivate with time-on-stream.

Various mechanisms have been proposed for the deactivation of cobalt-based catalysts during realistic FTS conditions. These include:

*(a) Oxidation of the active phase and support compound formation*

The oxidation of cobalt metal to inactive cobalt oxide by product water has long been postulated to be a major cause of deactivation of supported cobalt FTS catalysts [6-10]. Recent work has shown that the oxidation of cobalt metal to the inactive cobalt oxide phase can be prevented by the correct tailoring of the ratio  $P_{\text{H}_2\text{O}}/P_{\text{H}_2}$  and the cobalt crystallite size [11]. Using a combination of model systems, industrial catalyst and thermodynamic calculations it was concluded that Co crystallites  $> 6$  nm will not undergo any oxidation during realistic FTS, i.e.  $P_{\text{H}_2\text{O}}/P_{\text{H}_2} = 1-1.5$  [11-14]. Deactivation may also result from the formation of inactive cobalt support compounds (e.g. aluminate). Cobalt aluminate formation which likely proceeds via the reaction of

CoO with the support is thermodynamically favourable but kinetically restricted under typical FTS conditions [6].

*(b) Poisoning by contaminants in the synthesis gas feed*

One of the causes of deactivation and selectivity changes is the strong chemisorption of poisons on the metallic cobalt phase. According to Bartholomew [15] poisons may (a) block active sites for the reaction (b) electronically modify the metals nearest neighbour affecting chemisorption and dissociation of CO and (c) cause reconstruction of the catalyst surface resulting in a more stable configuration. Sulphur [16], halides and  $\text{NH}_3/\text{HCN}$  [17-20] are generally the major poisons for cobalt catalysts during FTS. Poisoning is synthesis gas feed related and can therefore be minimised through synthesis gas purification steps, e.g. (1) ZnO guard beds reduce sulphur levels significantly [21] and (2) a synthesis gas washing step with an aqueous solution of alkaline ferrous sulphate promotes the absorption of the above-mentioned impurities [22].

*(c) Sintering of the cobalt active phase*

To prepare a good catalyst in terms of activity and cost, cobalt nanoparticles have to be well dispersed on a support which typically consists of alumina, silica or titania. Small metal particles have a high surface free energy and tend to minimise this either by changing shape or agglomerating together (sintering). Sintering results in deactivation via the loss of catalytic surface area and has previously been reported during FTS on cobalt catalysts [8, 23, and 24]. Sintering may occur via crystallite migration and coalescence or by atom migration/ Oswald ripening [15]. The Hüttig temperature of cobalt, at which atoms at defects become mobile, is 253 °C [25], close to temperatures employed for realistic FTS conditions, supporting the above evidence for sintering. It should also be noted that sintering of the active phase may be facilitated by reaction water [15] and the formation of mobile sub-carbonyl species [26].



(d) *Cobalt reconstruction*

It has been observed that cobalt may undergo large scale reconstruction under a synthesis gas environment [27]. Reconstruction is a thermodynamically driven process that results in the stabilization of less reactive surfaces. Recent molecular modeling calculations have shown that atomic carbon can induce the clock reconstruction of an fcc cobalt (100) surface [28] (see section 4.4 for further details). It has also been postulated and shown with in-situ X-ray adsorption spectroscopy (XAS) on cobalt supported on carbon nanofibres that small particles (< 6 nm) undergo a reconstruction during FTS which can result in decreased activity [29].

(e) *Fouling by product wax and deposition of carbon*

Although the FTS is considered a carbon in-sensitive reaction [30] deactivation of the cobalt active phase by carbon deposition during FTS has been widely postulated [31-38]. This mechanism, however, is hard to prove during realistic synthesis conditions due to the presence of heavy hydrocarbon wax product and the potential spillover and buildup of inert carbon on the catalyst support. Also, studies have been conducted on supported cobalt catalysts that suggest deactivation by pore plugging of narrow catalyst pores by the heavy ( $> C_{40}$ ) wax product [39, 40]. Very often regeneration treatments which remove these carbonaceous phases from the catalyst result in reactivation of the catalyst [32]. Many of the companies with experience in cobalt-based FTS research report that these catalysts are negatively influenced by carbon (Table 4.1).

The purpose of this review is to integrate the literature on this topic to provide a clearer understanding on the role of carbon as a deactivation mechanism. Characterization techniques that have been used as well as the minimization of carbon, regeneration of catalysts and some selectivity implications will also be briefly discussed.

**Table 4.1** *Carbon deactivation postulated for industrial cobalt catalysts*

<b>Company</b>	<b>Catalyst</b>	<b>Typical Conditions</b>	<b>Comments</b>	<b>Ref.</b>
BP	Co/ZnO	218 °C, 29 bar, H <sub>2</sub> /CO = 2	Deactivation due to the formation of small amounts of inert, deleterious carbon species on the cobalt active phase. Regeneration of the catalyst is required to maintain activity.	35
Conoco-Philips	Co/Al <sub>2</sub> O <sub>3</sub>	225 °C, 24 bar, H <sub>2</sub> /CO = 2	Regeneration process by steam needed due to coking of the catalyst caused by high support acidity or high temperatures in particles resulting from high initial conversions	38
ExxonMobil	Co/TiO <sub>2</sub>	225 °C, 20 bar, H <sub>2</sub> /CO = 2	Regeneration process that is necessary due to the deposition of carbon or coke on catalyst.	36
Shell	Co/Zr/SiO <sub>2</sub>	220 °C, 25 bar, H <sub>2</sub> /CO = 2	Regeneration process needed to remove heavy products and carbonaceous deposits that diminish activity.	37
Syntroleum	Co/Al <sub>2</sub> O <sub>3</sub>	220 °C, 20 bar, H <sub>2</sub> /CO = 2	Accumulation of unreactive polymeric carbon with time-on-stream resulting in deactivation.	34

## 4.2 Formation of carbon deposits on cobalt catalysts during FTS and implications for activity

Carbonaceous species on metal surfaces can be formed as a result of interaction of metals with carbon monoxide or hydrocarbons. In the FTS, where CO and H<sub>2</sub> are converted to various hydrocarbons, it is generally accepted that an elementary step in the reaction is the dissociation of CO to form surface carbidic carbon and oxygen [1]. The latter is removed from the surface through the formation of gaseous H<sub>2</sub>O and CO<sub>2</sub> (mostly in the case of Fe catalysts). The surface carbon if it remains in its carbidic form is an intermediate in the FTS and can be hydrogenated to form hydrocarbons. However, the surface carbidic carbon may also be converted to other less reactive forms of carbon, which may build up over time and influence the activity of the catalyst [15].

There are a number of ways that carbon may interact with a cobalt catalyst to affect its performance during FTS:

- (a) Carbon deposits or heavy hydrocarbons ( $> C_{100}$ ) may block the catalyst pores causing diffusion problems [39].
- (b) Carbon may adsorb on the metal surface irreversibly therefore acting as a poison [35]. This irreversibly bonded carbon could also affect the adsorption and dissociation of neighbouring species such as CO.
- (c) Carbon could also go subsurface and play a role in electronic inhibition of activity by affecting the adsorption and dissociation of CO [41].
- (d) Carbon may bind to a metal surface and induce a surface reconstruction whereby a more active metal plane is transformed to one with a lower activity [28].
- (e) At higher temperatures, out of the typical FT regime, carbon could encapsulate the active metal thereby blocking access to reactants. In extreme cases carbon filaments can also be formed which can result in the break up of catalyst particles [42].

### **4.3 Classification of carbon types on cobalt FTS catalysts**

Figure 4.1 summarises the different routes that can potentially lead to carbon deposition during FTS: (a) CO dissociation occurs on cobalt to form an adsorbed atomic carbon, which is also referred to as surface carbide, which can further react to produce the FT intermediates and products. The adsorbed atomic carbon may also form bulk carbide or a polymeric type of carbon. Carbon deposition may also result from the Boudouard reaction (b) and due to further reaction and dehydrogenation of FTS product (what is commonly called coke) (c), a reaction which should be limited at typical FT reaction conditions. Carbon formed on the surface of cobalt can also spill over or migrate to the support. This is reported to readily occur on Co/Al<sub>2</sub>O<sub>3</sub> catalysts [43]. The chemical nature of the carbonaceous deposits during FTS will depend on the conditions of temperature and pressure, the age of the catalyst, the chemical nature of the feed and the products formed.

It would be fitting at this stage to define in detail the various carbon species for this review as often different terms are used in the literature. A representation of the various carbon species is shown in Figure 4.2. Surface carbide or atomic carbon can be defined as isolated carbon atoms with only carbon-metal bonds, resulting from CO dissociation or disproportionation, the latter of which is not favoured on cobalt at normal FTS conditions. Recent theoretical and experimental work has indicated that the CO dissociation is preferred at the step sites so adsorbed surface carbide is expected to be located near these sites [44, 45, 46].

CH<sub>x</sub> and hydrocarbon wax are respectively, the active intermediates formed by the hydrogenation of surface carbide and products of FTS formed by chain growth and hydrogenation of CH<sub>x</sub> intermediates. The hydrocarbon wax can contain molecules with the number of carbon atoms in excess of 100. Bulk carbide refers to a crystalline Co<sub>x</sub>C structure formed by the diffusion of carbon into bulk metal. Subsurface carbon may be a precursor to these bulk species and is formed when surface carbon diffuses into an octahedral position under the first surface layer of cobalt atoms.

Polymeric carbon refers to chains of carbon monomers (surface carbide) that are connected by covalent bonds. It has been shown recently [47] that the barrier for

C-C coupling on flat surfaces (1.22 eV) is half that for a step site (2.43 eV) and may indicate that the growth of these polymeric species is favoured on terraces. Polymeric carbon may also refer to carbon chains that contain hydrogen. In the case of CO hydrogenation on ruthenium catalysts polymeric carbon has been identified as a less reactive carbon that forms from polymerisation of  $\text{CH}_x$  and has an alkyl group structure [48].

Graphene is a single layer of carbon atoms densely packed into a benzene-ring structure and may be considered a precursor to graphite. In graphite, each carbon atom is covalently bonded to three other surrounding carbon atoms. The flat sheets of carbon atoms are bonded into hexagonal structures, which are layered. These graphitic species (or free carbon as they are often called) have strong carbon-carbon bonds and weaker bonds to the metal surface. The Boudouard reaction ( $2\text{CO} \rightarrow \text{C} + \text{CO}_2$ ) at FTS temperatures (around 230 °C) has been reported on cobalt catalysts and also results in the deposition of atomic carbon and its transformation to polymeric or graphitic forms of carbon on the surface [49]. Typically at high temperature Boudouard carbon can diffuse in cobalt to form metastable bulk carbide species [50]. The decomposition of the bulk carbide results in the formation of filaments and other forms of carbon on the surface. Filaments consist of stacked cone-segment (frustum) shaped graphite basal plane sheets and grow with a catalyst particle at their tip and, as can be expected, lead to the break-up of the catalyst [50]. Another graphitic nanomaterial produced by carbon deposition is encapsulated metal nanoparticles [50]. These are roughly spherical formations, consisting of catalyst particles surrounded by graphitic carbon.

These different types of carbon tend to have different reactivities towards gases such as hydrogen, oxygen or steam. Hence, a relatively simple technique such as temperature programmed hydrogenation or oxidation can be used to classify them. Table 4.2 summarises different reactivities of carbon species towards hydrogen.

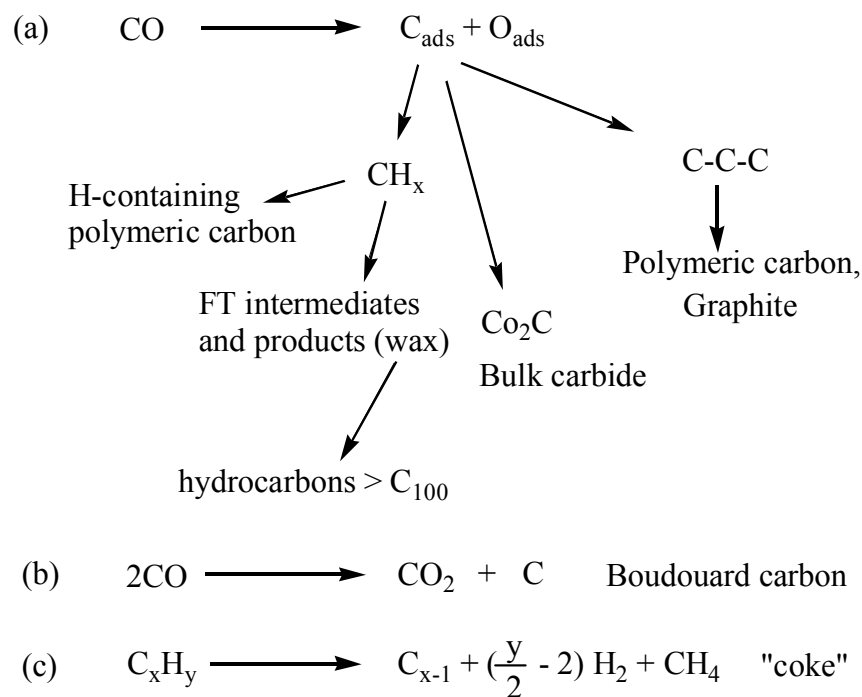


**Figure 4.1** Possible modes of carbon formation during FTS on cobalt catalysts

**Table 4.2** Examples of various carbon species on cobalt FTS catalysts along with their hydrogenation temperatures.

Carbon species	Catalyst	Reaction conditions in study			$T_{\text{hyd}} (^{\circ}\text{C})$	Ref.
		Temp ( $^{\circ}\text{C}$ )	$\text{H}_2/\text{CO}$	Pressure (bar)		
$\text{CH}_x$ fragments	Co (0001)	220	1	1	<100	51-52
Surface carbide	Co/ $\text{Al}_2\text{O}_3$	250	CO only*	1	180-200	31
Bulk carbide	Na-Co/ $\text{Al}_2\text{O}_3$	240	2	50	<250	53
Hydrocarbons, paraffinic wax	Co/ $\text{Al}_2\text{O}_3$	225	2	24	250-350	34
Polymeric carbon	Co/ $\text{Al}_2\text{O}_3$	225	2	24	>350	31,34
Graphite or graphene	Co/ $\text{SiO}_2$	200	2	1	>620	54,55

\* Surface carbide can be a product of both CO dissociation and disproportionation and can be formed from a mixture of  $\text{H}_2/\text{CO}$  as well

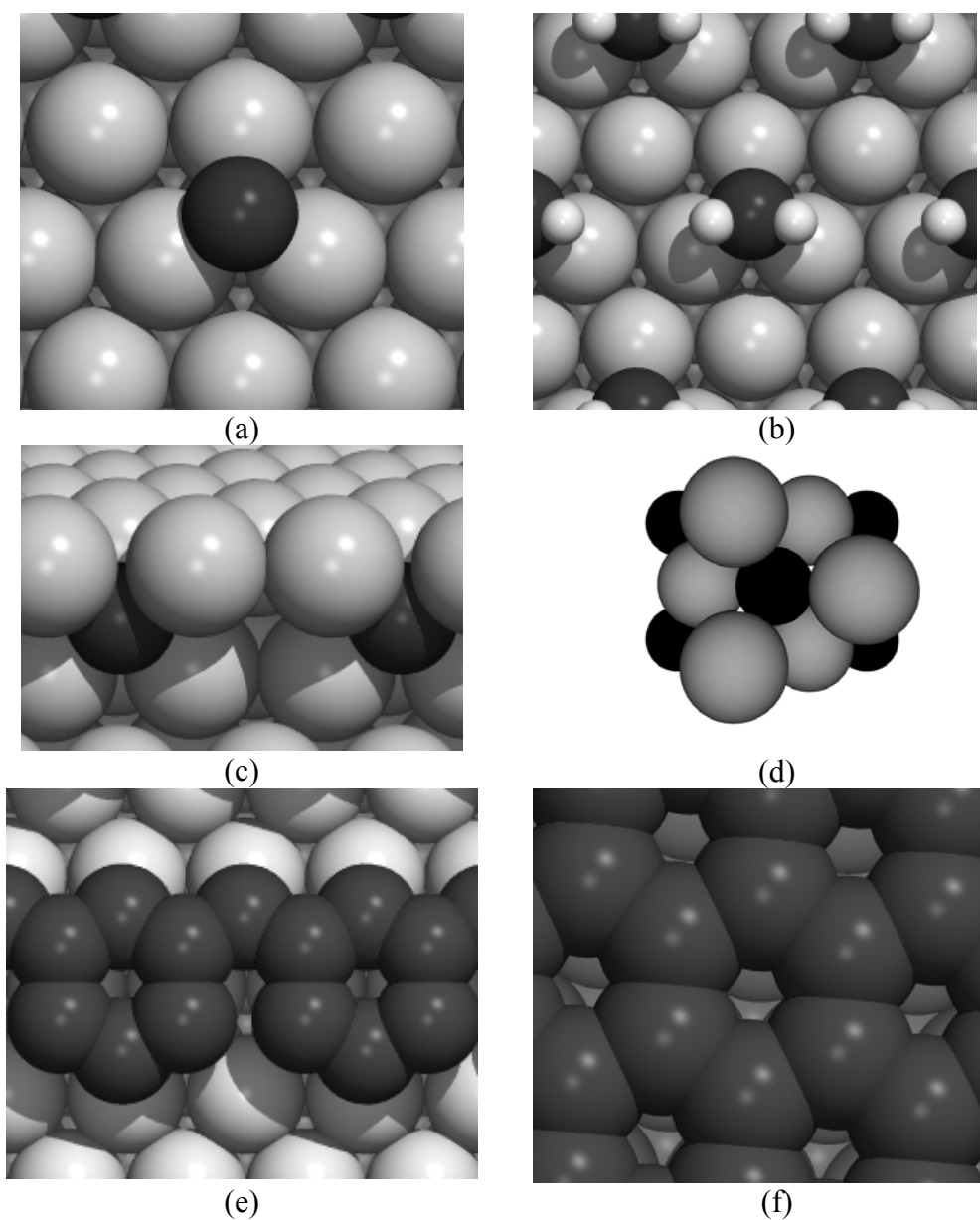


**Figure 4.2** *Representation of different carbon types on cobalt (a) Atomic carbon/surface carbide in a three-fold hollow site (b)  $\text{CH}_x$  species located in three-fold hollow sites (c) subsurface carbon lying in octahedral positions below the first layer of cobalt (d) Cobalt carbide ( $\text{Co}_2\text{C}$ ) with an orthorhombic structure (e) polymeric carbon on a cobalt surface (f) a sheet of graphene lying on a cobalt surface. The darker spheres represent carbon atoms in all the figures.*

#### **4.4 Factors that generally influence carbon deposition on catalysts for CO hydrogenation**

##### *a) Temperature and pressure*

Temperature plays an important role in determining the amount and type of the carbon deposit. Generally during FTS at higher temperatures the amount of carbon deposited will tend to increase [30, 31] but the case is often not so straightforward. An example of temperature dependence on the rate of carbon deposition and deactivation is the case of nickel CO hydrogenation catalysts, as studied by Bartholomew [56]. At temperatures below 325 °C the rate of surface carbidic carbon removal by hydrogenation exceeds that of its formation so no carbon is deposited. However above 325 °C, surface carbidic carbon accumulates on the surface since the rate of surface carbidic carbon formation is greater and exceeds that of its hydrogenation. As surface carbidic carbon accumulates (at 325-400 °C), it is converted to a polymeric type of carbon which deactivates the nickel catalyst; however, above 425 °C the rate of polymeric carbon hydrogenation exceeds that of formation and no deactivation occurs.

Higher temperatures will also aid in the transformation of surface carbon species into more stable species that will have decreased reactivity towards H<sub>2</sub>. Nakamura et al. [49] showed that at 230 °C, carburization of a Co/Al<sub>2</sub>O<sub>3</sub> catalyst by CO results in formation of mainly carbidic carbon. Such carbidic carbon converts to graphitic carbon if the temperature is raised to around 430 °C [49]. Increasing the exposure time to CO will also result in the formation of more stable carbon species [57]. If the catalyst is exposed to a too high a temperature during FTS, undesired carbonaceous phases will be formed, which may damage the structural integrity of the catalyst (for example, carbon fibres or filaments).

Carbon deposition is a strong function of partial pressures of CO and H<sub>2</sub> in the gas phase. Rostrup-Nielsen showed that the amount of carbon deposited on the catalyst uniformly increases with the combined hydrogen and carbon monoxide pressure [58]. Moeller and Bartholomew [59] showed that amount of carbon deposited on Ni catalysts was proportional to the partial pressure of CO. However,



greater conversion at higher temperatures results in a corresponding decrease in  $P_{\text{CO}}$  and  $P_{\text{H}_2}$ , and may therefore lead to smaller amounts of carbon on the catalyst [60]. Higher conversions also lead to high water partial pressures which can also influence carbon deposition. According to Dry the formation rate of Boudouard carbon is a function of pressure for Fe catalysts [61]. He showed that at higher total pressure and lower  $P_{\text{H}_2}/(P_{\text{CO}})^2$  ratio, the rate of carbon formation decreased.

*b) Size and crystallographic nature of cobalt*

Two studies [31, 58] have suggested that carbon deposition rates are greater on smaller metal particles. This is most likely due to the presence of a higher concentration of defects on the small particles which is known to enhance CO dissociation. Furthermore it was found in the case of Co/Al<sub>2</sub>O<sub>3</sub> catalysts that the carbon formation rate and subsequent deactivation was higher for smaller cobalt particles [31, 58]. The dissociation of adsorbed CO on a cobalt catalyst is also sensitive to the crystallographic structure of the surface and it is known that dissociation of CO occurs readily on more open surfaces. The dissociation of CO<sub>ads</sub> and formation of surface carbidic carbon occurs preferentially on Co (1012) and (1120) rather than on Co (0001) and (1010) planes [57, 62]. It is argued that CO adsorption at step sites (which are widely available on high index surfaces) weakens the C-O bond, which enables dissociation at lower temperatures. However, the carbon formed at these highly reactive cobalt sites may have enhanced stability (i.e. be strongly bound) and therefore, may act as a poison. Hence, the optimum cobalt site is one which dissociates CO rapidly without leading to irreversible bonding of carbon.

*c) Surface coverage of carbon*

As the surface coverage of carbon increases, the deposited carbon becomes less reactive as suggested by Koerts [52]. Using temperature programmed hydrogenation he showed that the formation of reactive surface carbidic carbon decreased from 70% to 10% as the surface coverage of carbon was increased towards 100%. Agrawal et al. [33] showed on Co/Al<sub>2</sub>O<sub>3</sub> that greater CO concentrations resulting in an increased surface carbon concentration led to more rapid bulk carburization and rapid deactivation. Hence, the balance between dissociation and hydrogenation must be

maintained. Molecular modelling work on fcc cobalt (100) by Ciobîcă et al. [28], shows that increased coverage of 50% atomic carbon will induce a clock type reconstruction (Figure 4.3) similar to that observed for Ni (100). The adsorption energy of the carbon is stabilized by 15 kJ/mol compared to the unreconstructed surface, resulting in a more stable surface [28]. The reconstruction results in a shorter distance between the carbon and cobalt but also an increase in co-ordination of the cobalt atoms and thus fewer broken bonds. The barrier for the carbon induced clock reconstruction was found to be very small (1 kJ/mol) which suggested that the process is not kinetically hindered.

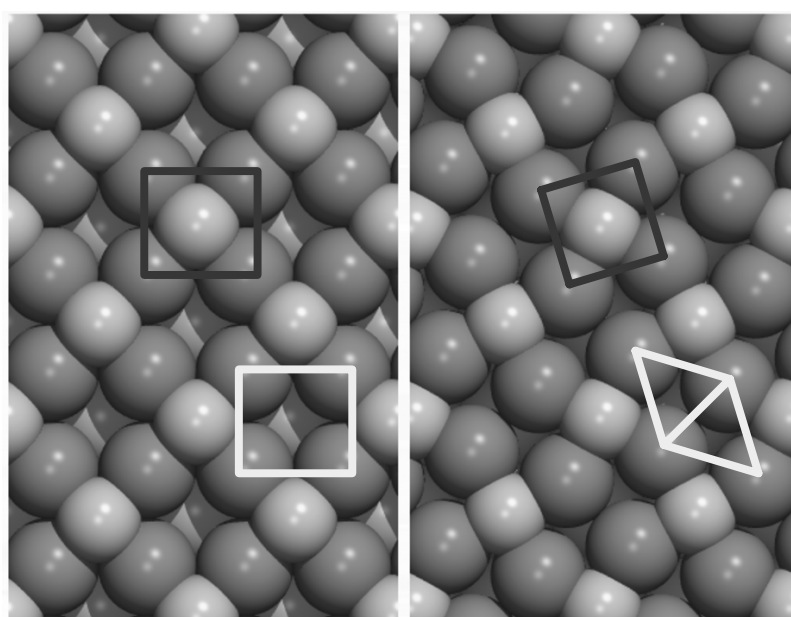


**Figure 4.3** *Left: the unreconstructed surface of 50% C/ fcc Co (100); Right: the clock reconstructed surface of 50% C/ fcc Co (100) (adapted from [28]). The darker spheres represent cobalt atoms and the lighter ones (in the four-fold hollow sites) represent carbon atoms.*

*d) Nature of gas feed*

The presence of a high concentration of  $H_2$ , i.e. high  $H_2/CO$  ratios during FTS will make the formation of carbon deposits less favourable since the rate of hydrogenation of carbonaceous intermediates will be increased. Poisons in the feed also play a role in the deposition of carbon. Low amounts (i.e. ppm levels) of sulphur in the feed

stream result in a decrease in carbon deposition on Co/Al<sub>2</sub>O<sub>3</sub> catalysts [63]. It has been shown that increased water concentrations result in a decreased formation of carbon on nickel methanation catalysts [64].

#### 4.5 Studies involving carbon formation on cobalt catalysts

##### (a) *Studies on model cobalt systems at model FT conditions (CO + syngas)*

Carbon deposition from CO on a cobalt catalyst at low pressures is known to be a structure sensitive process. CO is adsorbed molecularly on the low index surfaces (Co (0001)) but its dissociation occurs on the Co (1012), Co (1120) and polycrystalline surfaces [57, 62]. Deposition of carbon on Co (1012) and the probable formation of Co<sub>3</sub>C have been established by Auger electron spectroscopy (AES) and low energy electron diffraction (LEED) techniques [65].

Two forms of carbon (carbide and graphitic) have been observed by XPS on polycrystalline cobalt foil during the disproportionation of CO by Nakamura [57]. The dissociation of adsorbed CO occurred at temperatures higher than 60 °C, and carbide carbon and adsorbed oxygen were formed on the cobalt surface. After the surface is covered with adsorbed carbon and oxygen no further dissociation of adsorbed CO occurs. Contrary to the dissociation of adsorbed CO, the deposition of carbon by the concerted Boudouard reaction continues on the carbide carbon-deposited surface. The deposition of carbon increases with increasing exposure time and there is an increase in its transformation to graphitic carbon [57].

Johnson et al. [66] studied CO hydrogenation on bimetallic catalysts consisting of cobalt over layers on W (100) and (110) single crystals at 200 °C, 1 bar at a H<sub>2</sub>/CO ratio of 2. AES spectra showed the post-reaction Co/W surfaces to have high coverages of both carbon and oxygen, with carbon line shapes characteristic of bulk carbide carbon [66]. The catalytic activity apparently could not be correlated with surface carbon level [66].

Lahtinen et al. [67, 68] studied CO hydrogenation on polycrystalline cobalt foil at various temperatures at 1 bar and H<sub>2</sub>/CO ratio of 1.24. The cobalt surface was

then characterized by AES immediately after the reaction without any further sample treatment. The C/Co ratio was almost constant as temperature was increased to 252 °C. No significant deactivation for CO hydrogenation was observed on the foils at these conditions. At 297 °C the C/Co ratio was significantly higher. From the peak shape of the carbon KLL Auger lines it was deduced that carbon formed at 297 °C is in the graphitic form. Deactivation of the cobalt surface by carbon was observed at 276 °C. On these metal foils the hydrogenation of CO occurs in the presence of an active carbidic over layer. The transformation of this overlayer into graphite leads to a decrease in the catalytic activity of the metal surfaces.

The activity for CO hydrogenation was studied on Co (1120) and (1012) oriented single cobalt crystals by Geerlings et al. [51]. The height of cobalt Auger peak decreased while that of carbon increased due to the carbonaceous species on the surface. On the grooved Co (1120) surfaces long chain hydrocarbon fragments grow, however, on the stepped Co (1012) surface long chain fragments were not observed. The authors stated that under FTS conditions, the step sites, which are very reactive for CO dissociation under UHV conditions, are poisoned by carbon. As a result of very strong binding of carbon atoms to these sites efficient hydrogenation seems improbable. Hence, certain sites can aid carbon deposition and should be minimised. Beitel et al. [69] studied CO hydrogenation on Co (0001) at 250 °C, 1 bar at a H<sub>2</sub>/CO ratio of 2. They showed that the activity of a sputtered surface was greater than that of an annealed surface. However the activity of both the surfaces declined over time. They proposed that this could be due to the blocking of CO dissociation active sites by carbon deposition or by blocking of CO dissociation by hydrocarbons and water at defects. They conducted the experiments with clean syngas and sintering could be eliminated for the most compact surface and hence the observed deactivation could be due to carbon.

It has been shown that it is favourable for surface carbon to go into the first subsurface layer of cobalt [70]. Diffusion to octahedral sites of the first subsurface layer is thermodynamically preferred by 50-120 kJ/mol and the corresponding activation energy is low. Theoretical calculations on the conversion of surface carbidic to subsurface carbon on Co (0001) found that the electron withdrawing power and therefore the poisoning effect on potential CO adsorption is maximal for

subsurface carbon [41]. Metal  $d_{xz}$  orbitals are less likely to accept electrons from the CO  $5\sigma$  orbital and thus metal-CO bonding will weaken. The  $d_{xz}$  orbital will in turn be less able to back donate into the CO  $2\pi$  orbital resulting in additional metal-CO bond weakening as well as reduced C-O bond weakening. The net result is that the presence of subsurface carbon is likely to reduce both CO adsorption and dissociation processes on nearby atoms. Also the conversion of surface carbon may be self-catalyzing i.e., the more subsurface carbon, the greater electron withdrawing power thus more carbon atoms are driven into the surface. This electronic effect may be related to experimental work by Choi et al. [71] who investigated the surface properties of 5 wt% Co/Al<sub>2</sub>O<sub>3</sub> catalysts, exposed to CO at 250 °C, by employing Infra-red (IR) and temperature programmed desorption (TPD) techniques. They found that a carbon-deposited cobalt catalyst adsorbs CO more weakly as evidenced by a new IR band at 2073 cm<sup>-1</sup>.

*(b) Studies on supported catalysts at more realistic conditions*

Lee et al. deposited carbon by CO disproportionation on Co/Al<sub>2</sub>O<sub>3</sub> catalysts with different loadings (2-20 wt% Co) at different CO deposition temperatures (250-400 °C) [31]. Two forms of carbon were observed upon temperature programmed surface reaction with hydrogen: an atomic or surface carbide carbon (hydrogenated at ~190 °C) and polymeric carbon (hydrogenated at 430 °C). A fraction of the carbon was also resistant to hydrogenation at 600 °C. They found that with increasing temperature of deposition, the amount of carbon deposited increased and surface carbide carbon appears to be transformed into polymeric and graphitic carbon (Figure 4.4a). These catalysts where carbon was artificially deposited on, were tested in the FTS at 250-300 °C, H<sub>2</sub>/CO = 2 and 1 bar and exhibited lower activities when compared to the fresh catalyst (Figure 4.4b). The loss of activity was ascribed to the blockage of active sites by polymeric and or/graphitic carbon which is irreversibly bound to the metal surface. Bulk carbide was not observed by AES and as such the authors argued that the deactivation was not due to an electronic effect. This experiment clearly establishes that stable carbon species generated from CO can be a poison in FTS.

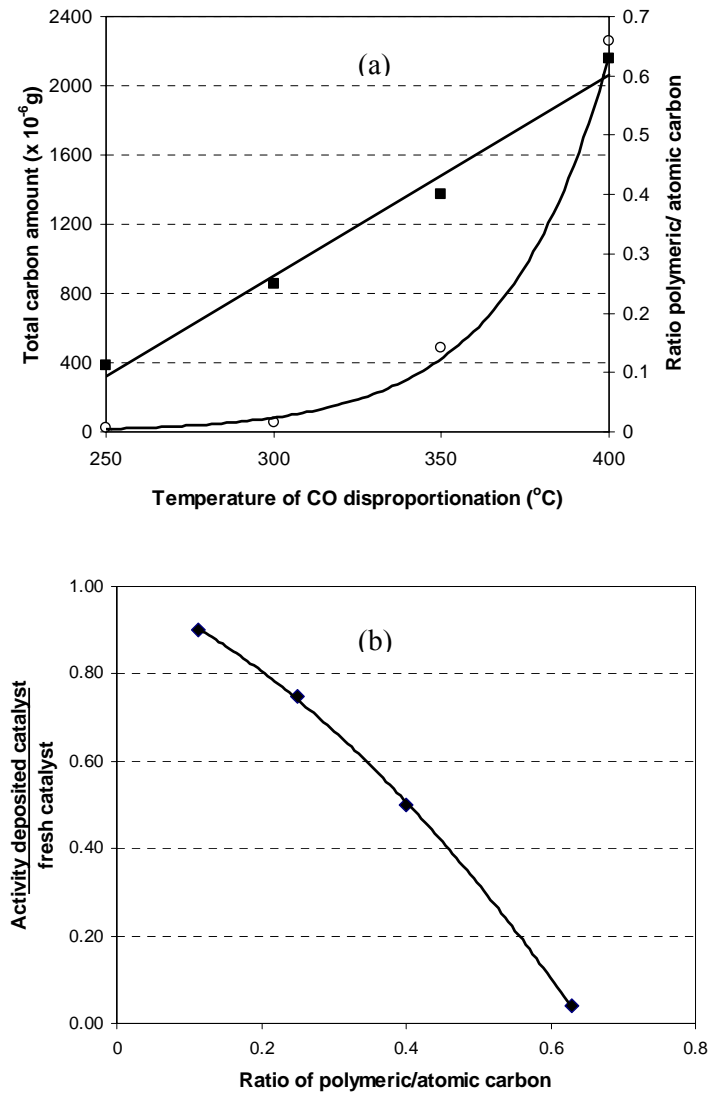


**Figure 4.4** (a) The total amount of carbon (■) and ratio of polymeric carbon to atomic carbon (○) deposited by the disproportionation of CO on Co/Al<sub>2</sub>O<sub>3</sub> catalysts at various temperatures. (b) A loss of FTS activity (250 °C, H<sub>2</sub>/CO = 2, 1 bar) activity compared to a fresh catalyst is noted with increasing amounts of polymeric carbon on Co/Al<sub>2</sub>O<sub>3</sub> catalysts (drawn from data in provided in [31])

Agrawal et al. [33] performed studies on Co/Al<sub>2</sub>O<sub>3</sub> methanation catalysts using sulphur-free feed synthesis gas and reported a slow continual deactivation of these catalysts at 300 °C due to carbon deposition. They postulated that the deactivation could occur by carburization of bulk cobalt and formation of graphite deposits on the Co surface which they observed by Auger spectroscopy.

Thermogravimetric techniques (TGA-MS) have been used to show that polymeric or graphitic carbon deposits may form on catalysts during realistic FTS (215-232 °C, 19-28 bar, H<sub>2</sub>/CO = 1.98-2.28) in a slurry bubble column reactor [34]. The deposits are resistant to hydrogenation at temperatures well above typical FT temperatures (350 °C). Gruver et al. [34] have shown that there is an increase in the

amount of carbon resistant to hydrogen on Co/Al<sub>2</sub>O<sub>3</sub> catalysts with an increase in time on-line (9 to 142 days) which could be related to catalyst activity as indicated in Figure 4.5a. The carbon formed was even resistant to a regeneration procedure under O<sub>2</sub>, indicating that it is quite stable. After 142 days the amount of hydrogen-resistant carbon formed on the catalyst was 1 wt% which was sufficient to block the available surface cobalt atoms. Chemisorption measurements showed a linear decrease in H<sub>2</sub> chemisorption capacity with an increase in amount of residual carbon remaining after a regeneration step (Figure 4.5b). The deposited polymeric carbon was proposed as one of the causes of deactivation in the FTS. The authors do not make mention of the effect on sintering and poisons on the chemisorption capacity nor did they determine whether the hydrogen resistant carbon was located on the support or on cobalt. No bulk cobalt carbide was detected by XRD. The slow accumulation of small amounts of deactivating stable carbon species on the cobalt active phase was also reported for Co/ZnO catalysts [35] tested in extended runs (218 °C, 29 bar, H<sub>2</sub>/CO = 2).

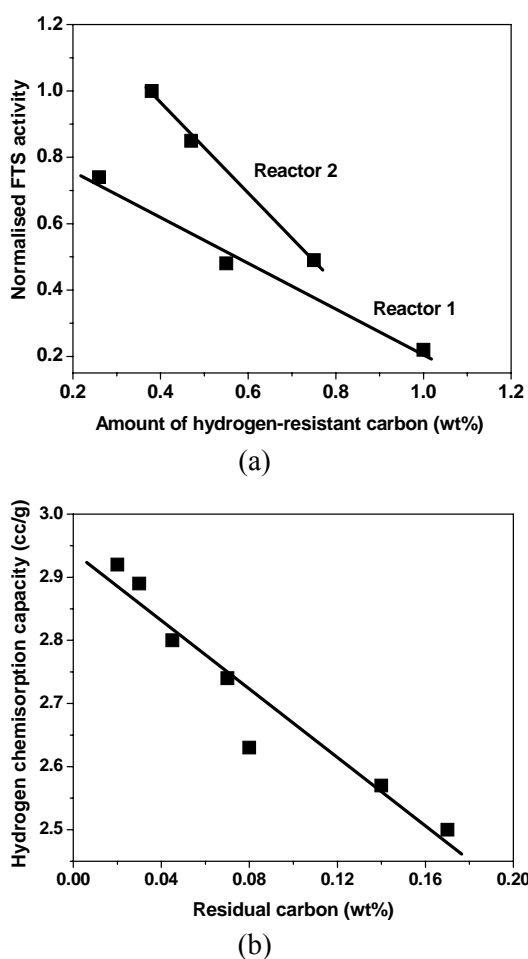


**Figure 4.5** (a) Correlation between the amount of H<sub>2</sub> resistant carbon and loss of FTS activity (215-232 °C, 19-28 bar, H<sub>2</sub>/CO = 1.98-2.28) in a two-stage slurry bubble column using a Co/Al<sub>2</sub>O<sub>3</sub> catalyst (b) Correlation between amounts of residual carbon after O<sub>2</sub> treatment and H<sub>2</sub> chemisorption capacity (drawn from data provided in [34]).

Barbier et al. [54] employed temperature-programmed hydrogenation (TPH) on the carbon species on used Co/SiO<sub>2</sub> FTS catalysts (200 °C, H<sub>2</sub>/CO = 2, 1 bar) and showed that the resulting methane evolution could be resolved into four peaks, representing different types of carbon, which vary in reactivity toward hydrogen. They showed that the formation of easily hydrogenated carbon decreased with increasing time-on-stream while the carbon that was hydrogenated at higher temperatures increased with time-on-stream. This observation points to the fact that during the course of the reaction the slow formation of carbon phases that are resistant to H<sub>2</sub> occurs. They postulated that the nature of this carbon may be polymeric or even graphitic.

Pore blockage by carbon or heavy products may cause a loss in activity over time. Niemela and Krause [39] reported a loss of turnover frequency for Co/SiO<sub>2</sub> FTS catalysts due to preferential blocking of the narrowest catalyst pores by carbon. Puskas [72] found unusually high amounts of wax in the pores on a Co/Mg/diatomaceous earth catalyst tested in the FTS at 190 °C, 1-2 bar, H<sub>2</sub>/CO = 2.55 for 125 days. In a separate study it was concluded that pore plugging by the waxy products resulted in a fast deactivation of such catalysts [73].

#### **4.6 Bulk cobalt carbide formation in the FTS?**

The formation and influence of bulk cobalt carbide during FTS has been a topic of interest for many research groups. [74, 75, 76, 77]. There is a general trend of decreasing bulk carbide stability as one goes from the left to the right of the periodic table through the transition metals. It has been shown that the activation energy for the diffusion of carbon into cobalt (145 kJ/mol) is much higher than that for iron (44-69 kJ/mol). This translated to a 10<sup>5</sup> times slower diffusion of carbon into cobalt than into iron [78]. Thus, it is reasonable to expect that cobalt will have a lesser tendency to form carbides than iron. Two forms of cobalt carbide are generally known for cobalt: Co<sub>2</sub>C which has an orthorhombic structure and Co<sub>3</sub>C which has structure similar to cementite.

The formation of bulk cobalt carbide is quite a slow process since it requires the diffusion of carbon into the cobalt bulk. It was reported that the full conversion of



unsupported and reduced Co to  $\text{Co}_2\text{C}$  only occurred after 500 h of exposure to pure CO at 230 °C. Increasing the reaction temperature resulted in a faster rate of carburization [79]. Bulk cobalt carbides are considered to be thermodynamically metastable species and therefore  $\text{Co}_2\text{C}$  will decompose to hcp cobalt and graphite while  $\text{Co}_3\text{C}$  will decompose to fcc cobalt and methane. Thermal decomposition of bulk carbides under an inert atmosphere is believed to occur under 400 °C [79]. Hydrogenation of the bulk carbides is believed to be a fast process and occurs around 200 °C [80, 81].

Early work at the Bureau of Mines on Co/ $\text{ThO}_2$ /kieselguhr catalysts showed that bulk carbide was not an intermediate in the FTS nor was it catalytically active [80]. Excessive amounts of carbides, produced by CO exposure prior to the reaction, were found to severely inhibit the FTS activity. Carbiding of Co/ $\text{ThO}_2$ /kieselguhr catalysts in CO at 208 °C had a dramatic effect on catalyst activity, decreasing conversion by 20% and increasing the formation of lighter hydrocarbons. The BET surface area of the catalysts remained constant, however, the CO chemisorption capacity decreased to 30% of the initial values before carbiding. In some cases, a four-fold increase in activity was noticed after the hydrogenation of the carbide at 150-194 °C. Also it should be noted that XRD still showed the presence of bulk cobalt carbide post reaction in the case of the pre-carbided catalysts exposed to synthesis gas. This indicates that while the bulk carbide can be readily hydrogenated in pure hydrogen it is stable for a considerable amount of time in synthesis gas mixtures at FTS conditions.

Recent work done by Xiong et al. [82] on Co/AC (activated carbon) catalysts showed that a  $\text{Co}_2\text{C}$  species formed during the catalyst reduction in hydrogen at 500 °C. Evidence for the carbide in the Co/AC catalysts was obtained by X-ray diffraction (XRD) and XPS measurements and the formation of this  $\text{Co}_2\text{C}$  species reduced the FTS activity over the Co-based catalysts. The presence of bulk carbide also seems to enhance alcohol selectivity [83].

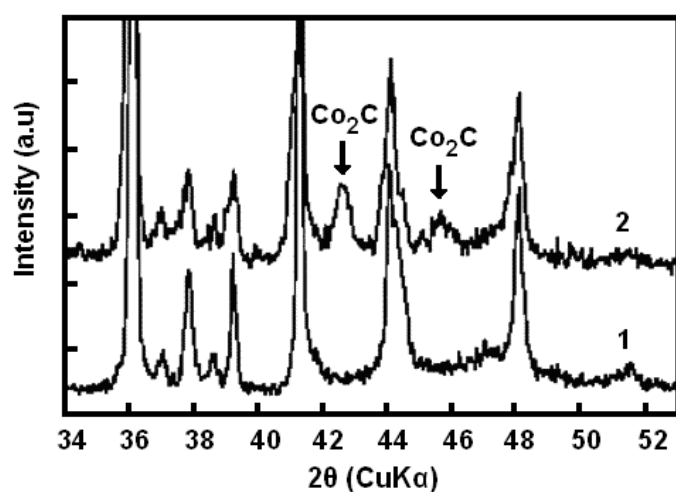
Several workers have reported that bulk carbide does not form readily during normal FTS conditions [74, 80]. Bureau of Mines work showed using laboratory XRD

measurements that detectable amounts of bulk carbide were not formed under synthesis conditions [80].

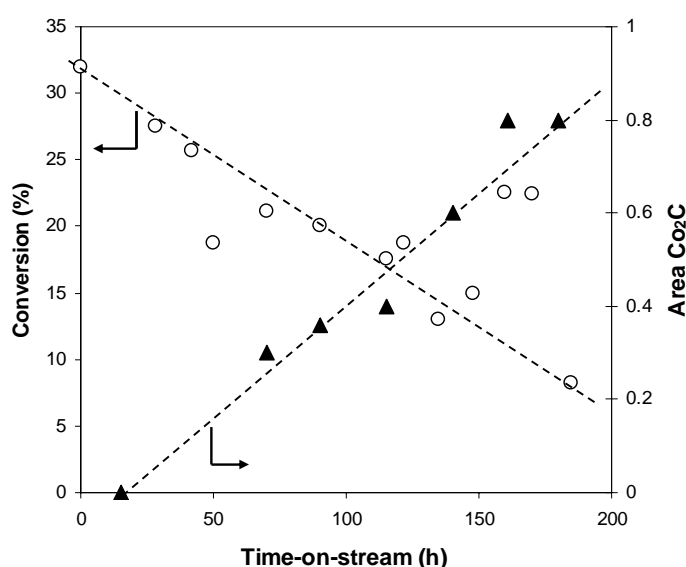
Work by Syntroleum on their Co/Al<sub>2</sub>O<sub>3</sub> proprietary catalyst showed that bulk carbide is formed during FTS in a continuously stirred tank reactor (CSTR) reactor (216 °C and 37 bar) in the presence of CO only for a period of 8 h (upset conditions) [74]. The performance of the catalyst was severely affected when standard H<sub>2</sub>/CO ratio (2) was reintroduced as the CO conversion dropped more than half and the methane selectivity doubled. An interesting observation was that the bulk carbide was hydrogenated to hexagonal cobalt at 225 °C by treatment in a pure hydrogen stream. In general small supported and reduced cobalt particles (< 40 nm) are cubic in nature [74, 83].

Pankina et al. [85] performed ex-situ post reaction TPH/magnetic studies on wax-extracted cobalt alumina catalysts tested in FTS and stated that methane evolution at 250 °C corresponds to an increase in magnetisation, which indicates the hydrogenation of cobalt carbide. The reduction of CoO was excluded as a cause of the increased magnetization. They argued that although cobalt carbide is said to be thermodynamically metastable during the FTS, it could be stable for small Co crystallites. This is due to the contribution of the surface free energy of small Co crystallites to the overall thermodynamic calculations.

Co<sub>2</sub>C is rarely observed in the FTS by ex situ techniques (see Table 4.3). Ducreux et al. [86] observed the formation of Co<sub>2</sub>C on Co/Al<sub>2</sub>O<sub>3</sub> and Co/Ru/TiO<sub>2</sub> FTS catalysts by in situ XRD techniques (Figure 4.6a) and related it with a deactivation process (Figure 4.6b) (230 °C; 3 bar; H<sub>2</sub>/CO = 9: no wax). Machocki [87] also showed the formation of Co<sub>2</sub>C on Co/SiO<sub>2</sub> catalysts after an initial 20 hour induction period in the FTS (275 °C; 1 bar; H<sub>2</sub>/CO = 1.1). This induction period is apparently needed to form a stable carbide nucleus. However he also noted that bulk carburization occurs more readily on iron catalysts due to the stronger Fe-C bond and that the hydrogenating ability of cobalt considerably decreases the amount of surface carbon that can migrate into bulk cobalt metal. Jacobs et al. [88] employing synchrotron XRD, detected a small amount of Co<sub>2</sub>C that may also have been formed during the synthesis (220 °C; 18 bar; H<sub>2</sub>/CO = 2).



(a)



(b)

**Figure 4.6** (a) Diffraction patterns of a Co/Ru/TiO<sub>2</sub> catalyst: (1) after reduction in hydrogen and (2) after 180 hours in synthesis gas (230 °C; 3 bar; H<sub>2</sub>/CO= 9) and (b) Syngas conversion and amount of Co<sub>2</sub>C as detected by in-situ XRD as a function of time-on-stream (adapted from [86]).

Pennline et al. [32] used bi-functional Co/ThO/ZSM-5 catalysts at 280 °C, 21 bar, H<sub>2</sub>/CO = 1 in the FTS. XRD of the used catalyst indicated that bulk cobalt carbide is present. They found that the relative amount of the bulk carbide species is larger on the used catalyst operated at 280 °C than on the used catalyst operated at 320 °C. They argued that this is because bulk cobalt carbide begins to decompose around 300 °C. Since this catalyst lacked high water gas shift activity, and a low feed gas ratio of H<sub>2</sub>/CO = 1 was used, the usage ratio of hydrogen to carbon monoxide was always greater than the feed ratio, and thus the catalyst was uniformly exposed to a low H<sub>2</sub>/CO ratio, which increases the chance for bulk carbide formation.

**Table 4.3** *An overview of reported claims of bulk cobalt carbide being observed after/when performing “Fischer-Tropsch synthesis” over supported cobalt-based catalysts.*

Catalyst	Reaction conditions			Technique	Effect on activity	Ref
	H <sub>2</sub> /CO ratio	Temp (°C)	Pressure (bar)			
Co/Pt/ Al <sub>2</sub> O <sub>3</sub>	2	220	18	Synchrotron XRD	n.s	88
Co/Al <sub>2</sub> O <sub>3</sub> and TiO <sub>2</sub>	9*	230	3	In-situ XRD	↓	86
Co/ThO <sub>2</sub> + ZSM-5 + Alumina	1	280	21	XRD	↓	32
Co/SiO <sub>2</sub>	1.1	275	1	XRD	↓	87
Co/Al <sub>2</sub> O <sub>3</sub>	2	220	1	TPH with magnetic measurements	n.s	85
Fe/Co metal/oxide composite	1	230	10	XRD, TEM and XPS	n.s	77
*Co/Al <sub>2</sub> O <sub>3</sub>	9	400	1	AES line shape	↓	33
Na-Co/Al <sub>2</sub> O <sub>3</sub>	2	240	50	TPH with magnetic measurements, XPS and XRD	n.s	53

\*Methanation conditions  
n.s.: not specified in study

#### 4.7 Experimental techniques used for the characterization of carbon on cobalt-based FTS catalysts

The major techniques used for the characterization of carbon on cobalt-based FTS catalysts are temperature programmed or gravimetric techniques, X-ray diffraction, transmission electron microscopy, X-ray photoelectron spectroscopy, Auger spectroscopy, magnetic measurements and secondary ion mass spectrometry (Table 4.4). Using a combination of these techniques, one may be able to determine the location, amount and morphology of the carbon species, although this is not a straightforward exercise. Carbon formation/deposition is probably the most difficult deactivation mechanism to characterise on cobalt-based FTS catalysts. This is due to the low quantities of carbon that are responsible for the deactivation (< 0.5 m%)

coupled with the presence of wax that is produced during FTS. Furthermore carbon is only detrimental to the FT performance if it is bound irreversibly to an active site or interacts electronically with it. Hence, not all carbon detected will be responsible for deactivation, especially if the carbon is located on the support. In order to circumvent the complexities that arise in the presence of wax, model conditions are often used. This section is aimed at discussing the key techniques that are used for characterising carbon on cobalt-based FTS catalyst along with their strengths and weaknesses.

*(a) Temperature programmed (TP) techniques*

Probably the most widely used technique of carbon determination on cobalt catalysts are the temperature programmed (TP) techniques as they are quite simple, relatively inexpensive and can be used for a wide variety of systems. In a typical TPH experiment, a sample of catalyst is heated in hydrogen with a linear ramp rate [54]. The carbon is reacted to form methane which is monitored by a mass spectrometer or GC (Figure 4.7). The reactivity of the carbon deposits towards various gases is determined and can be used as a criterion to classify them. Table 4.2 shows the different species of carbon that can be identified with this relatively simple technique. Quantitative analysis of carbon is also possible. Kinetic data on the reactivity of carbon deposits to various gases can be obtained which provide useful information in the design of regeneration processes. Reference compounds may also be useful in assigning the type of carbon formed. For example, it is known that bulk cobalt carbide is hydrogenated around 200 °C [80], polymeric carbon on cobalt at 430°C [31], while graphite on cobalt is hydrogenated around 600 °C [55]. A possible advantage of this technique is that it can be used for determining amounts of less reactive, deactivating carbon on wax covered catalysts [34]. A drawback of the technique is that thermal transformation (e.g. graphitization) may occur from one carbon form to the other [88]. In the case of spent samples taken from realistic FTS runs, there may also be an overlap of peaks due to pore size effects and the presence of hydrocarbon wax contamination [54, 85]. This would necessitate peak deconvolution.

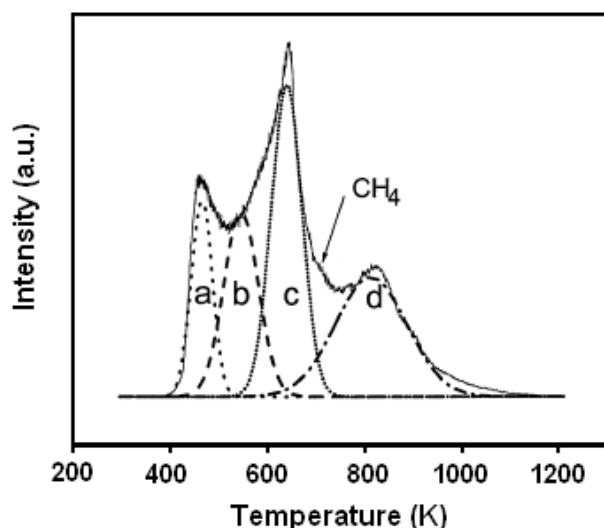


**Figure 4.7** A TPH profile of methane after 24 h of FTS on a 20 wt% Co/SiO<sub>2</sub> catalyst (200 °C, H<sub>2</sub>/CO = 2, 1 bar). The methane is deconvoluted into four different Gaussian peaks which represent different carbon species which vary in reactivity towards hydrogen. Specie d is believed to be polymeric or even graphitic in nature (from [54]).

*(b) X-ray diffraction (XRD)*

XRD can be used to determine crystalline phases of carbon on the catalyst. Bulk cobalt carbide (Figure 4.6a) and graphite were detected using XRD [79, 88]. In-situ XRD provides a powerful way to study the carbide phase in working catalysts [86]. Gruver et al. studied the formation of bulk cobalt carbide on a spent FTS catalyst in wax [74]. The sample was heated in dry nitrogen at 100 °C to melt the crystalline wax and remove the interference diffraction patterns [74]. Thus, XRD can be a powerful technique to study crystalline bulk carbides in a pseudo in-situ manner at elevated temperature where the product wax is rendered amorphous. The hydrogenation behaviour of the bulk carbide was also studied with in-situ-XRD. Decomposition or hydrogenation of bulk cobalt carbide results in selective transformation of cobalt from an fcc to hcp form [74, 76]. This phenomenon can possibly be used as a diagnostic test to determine if cobalt carbide has formed and been hydrogenated during the reaction. Synchrotron XRD was also used to detect small amounts of cobalt carbide in spent catalysts [88]. The benefit of using synchrotron radiation is that the higher intensity of the X-rays decreases the signal to noise ratio considerably, allowing for the analysis of small amounts of carbide species which would otherwise be below detectable limits. The general disadvantage of XRD is that it is unable to detect non-crystalline phases like amorphous polymeric carbon and small particles.

(c) *Transmission electron microscopy (TEM)*

High resolution TEM can be used to determine the lattice spacings of crystalline carbon phases present on the catalyst [89]. Tihay et al. [77] showed the presence of cobalt carbide in bimetallic catalysts after performing FTS, with TEM and micro diffraction. The lattice spacing of cobalt carbide ( $\text{Co}_2\text{C}$ ) was measured as 2.49 Å. It appears that isolated or encapsulated cobalt carbide appears as spherical particles in TEM [77]. Carbon filaments and fibres or poorly graphitized (ordered) carbon will also be clearly visible with TEM [90, 91]. The presence of wax necessitates extraction procedures or involves treating the sample prior to analysis which is a major disadvantage of using TEM to study carbon.

(d) *Auger Electron Spectroscopy (AES)*

Chemical bonding information can also be obtained using AES, when the Auger transition involves valence levels as with KVV Auger transitions of carbon [92]. The line shape of the C KVV transition can be used as a fingerprint of the state of carbon (See Figure 4.8). Carbodic carbon is characterized by an AES spectrum with two well-defined satellites at kinetic energies somewhat less than that of the main peak. These satellites are missing for graphitic carbon. Agrawal et al. [32] conducted Auger analysis on  $\text{Co}/\text{Al}_2\text{O}_3$  plates after the methanation reaction and detected graphite. The relative carbon concentration of cobalt particles may be estimated by Co to C ratio using standard AES sensitivity coefficients and was done for  $\text{Co}/\text{Al}_2\text{O}_3$  FTS catalysts [93]. Often AES gives the best results with model catalysts and conditions and the technique is compromised in the presence of layer of hydrocarbon wax.

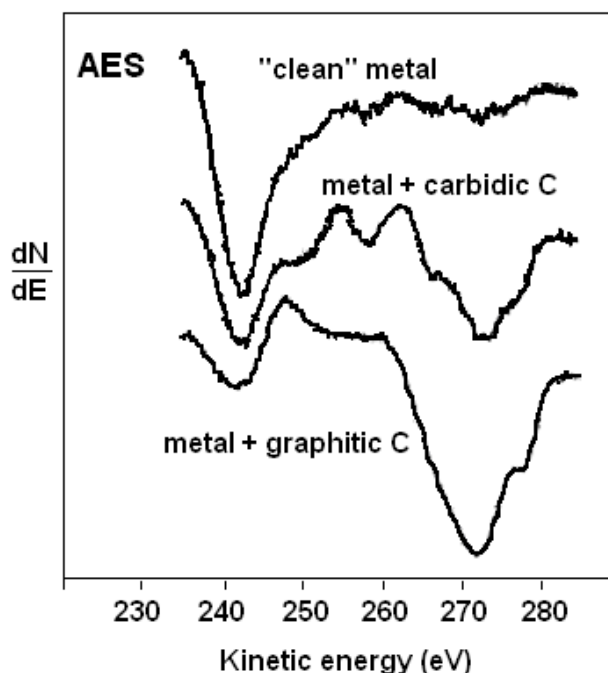


**Figure 4.8** *The Auger spectrum of carbon KVV Auger transitions can be used to fingerprint the state of carbon on a catalyst (adapted from [92]).*

*(e) X-ray photoelectron spectroscopy (XPS)*

XPS is a surface sensitive technique and probes the first few nanometres of the catalyst samples. For real FTS catalysts the wax would attenuate photoelectrons and should be extracted off in a controlled manner or the sample could be sputtered to expose underlying layers [77]. The nature of carbon i.e. graphitic or carbidic could be determined from chemical shifts in C 1s spectrum [49, 82]. If various forms of carbon are present, the C 1s signal is asymmetrical. A deconvolution of the peak could reveal the different forms of carbon (Figure 4.9). A peak at 283.6 eV can be attributed to carbidic carbon [57, 82]. The peak at 284.6 eV is attributed to that of carbon–carbon bonds [82]. Nakamura et al. [57] showed that graphite of cobalt foils has a binding energy of 284.8 eV. The relatively low resolution and presence of states that are close in binding energy limits the usefulness of XPS for this problem.



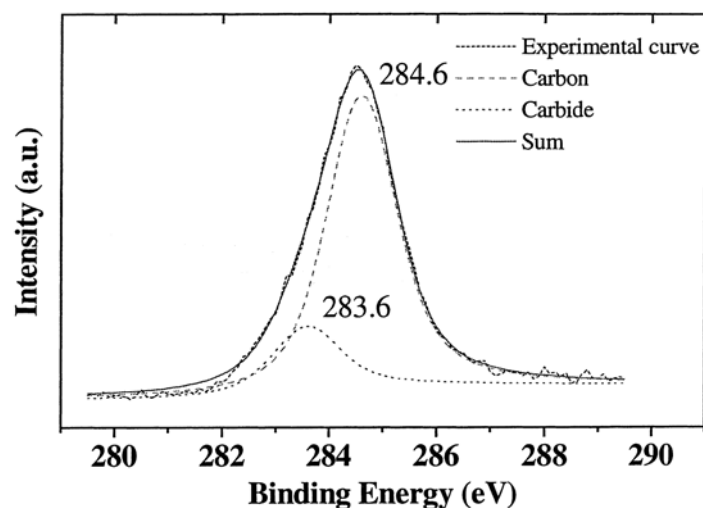


**Figure 4.9** Deconvolution of XPS spectra of C 1s region after a 5 min  $\text{Ar}^+$  bombardment of a used Fe-Co bimetallic catalyst showing the presence of carbide at 283.6 eV. The catalyst has been exposed to FTS for 60 h. ( $\text{H}_2/\text{CO} = 1$ , 230 °C, 10 bar) (from [77])

(f) *Magnetic measurements*

Cobalt carbides have a much lower magnetic susceptibility than cobalt metal [53, 75]. Hofer et al. [75] showed that the rate of decomposition of cobalt carbide can be measured by the change of the magnetic force experienced by a decomposing sample in a constant magnetic field of constant field gradient. As the carbide is decomposed an increase in magnetization is noted. Miradatos et al. [53] used results from magnetic measurements to propose that surface and bulk carbides, which are non-ferromagnetic phases, are the most likely phases formed during the FTS on Na-Co/ $\text{Al}_2\text{O}_3$  catalysts. They related the decrease of ferromagnetic cobalt to the formation of carbon deposits chemically interacting with the metallic cobalt phase. The advantage of this technique is that it could potentially be used on catalysts that contain hydrocarbon wax.

(g) *Secondary ion mass spectrometry (SIMS)*

SIMS can be used as a technique to identify individual carbon species in complex adlayers on cobalt catalysts [94]. Post reaction SIMS was conducted on Co/ $\text{SiO}_2$  FTS catalysts and revealed the presence of adsorbed  $\text{C}_x\text{H}_y$  species on the catalysts. The

method cannot be used quantitatively for the ion fragment intensities as sputter induced fragmentation of the carbon species is observed. In principle SIMS may also be able to detect carbidic species ( $\text{Co}_x\text{C}_y^+$ ) on spent FTS catalysts. Niemela and Krause used SIMS depth profiling to locate carbon on the outer surface of used Co/SiO<sub>2</sub> particles [39]. In the case of spent catalysts tested at realistic conditions a thick layer of hydrocarbon wax would interfere with SIMS analysis, so this necessitates extraction procedures.

**Table 4.4** *Experimental techniques previously used for the characterization of carbon on cobalt-based FTS catalysts and information obtained.*

Technique	Information on carbon species	Ref
TP	Amount, nature and location of carbon deposits. Reactivity of carbon to various gases.	34,54
XRD	Detection and quantification of crystalline carbon phases e.g. bulk cobalt carbides and graphite.	74,88
XPS	Detects carbidic, graphitic phases from changes in binding energy in C 1s regions. Amount of carbon from Co 2p/C 1s signal ratios.	77
AES	Chemical information from fine structure (graphite, bulk carbide). Amount of carbon from Co/C signal ratios.	31,33,93
Magnetic measurements	Formation and decomposition of bulk cobalt carbides.	53,75,85
TEM	Micro-diffraction can be used to study crystalline ordered carbons. Carbon filaments and fibres are clearly visible.	77
SIMS	Detects hydrocarbon fragments and possibly $\text{Co}_2\text{C}^+$ .	94
Gravimetry	Weight increase can be correlated to the amount of carbon deposits. Care should be take as various phenomena (e.g. water loss and oxidation) can lead to weight changes .	95

#### 4.8 Minimization of carbon deposits on cobalt FTS catalysts by promotion

Additives such as rare earth or noble metals are generally introduced into industrial cobalt FTS catalysts as structural or reduction promoters [96]. The addition of various promoters to cobalt catalysts has also been shown to decrease the amount of carbon produced during the FTS [82, 85, 97, 98]. Furthermore, the addition of promoter elements may decrease the temperature of regeneration, preventing the possible sintering of supported cobalt particles during such treatments [96].

In the case of cobalt foils it has been found that 0.1 monolayer of potassium coverage reduces the formation of graphite at high FTS temperatures (307 °C) [97]. It is not exactly clear how the potassium reduced the formation of graphitic carbon deposits in this study. It is known that alkali ad-atoms on a transition metal surface exist in a partially ionic state, resulting in a work function decrease [99]. Potassium promotion results in a weakening of the C-O bond and increase in the CO dissociation rate, resulting in increased coverage of active surface carbidic carbon [100]. Besides having an electronic effect, potassium could play a structural role in preventing graphite formation according to Wesner et al. [101]. They argued that the epitaxial growth of graphite was favoured on clean hexagonal cobalt and the promotion of the cobalt with potassium would disrupt the formation of epitaxial graphite islands by site blocking. However, already at the early stage of FT research it was shown that for supported cobalt catalyst potassium was a poison [102]. The mobility of potassium during FTS conditions could also result in it being distributed on the support.

It was shown that manganese added to cobalt on activated carbon catalysts resulted in a decrease in bulk carbide formation during reduction and a decrease in the subsequent deactivation rate [82]. Magnesium added to the support in alumina supported cobalt catalysts showed a lower extent of carburization due to decrease in Lewis acidity of the alumina surface in the presence of  $Mg^{2+}$  ions [85].

It has been also postulated using molecular modelling and proven experimentally using temperature programmed techniques that promotion with boron inhibits detrimental carbon formation [70]. Ab initio calculations indicate that boron behaves rather similar to carbon and prefers to adsorb in the octahedral sites of the

first subsurface layer of cobalt. The boron thus forces the carbon to remain on the surface in an active form. Additionally boron present in the first subsurface layer reduces the surface carbon binding energy, lowering the carbon coverage and may prevent the nucleation of graphene islands [70].

It is also known that the common reduction promoters (e.g. Pt and Ru) aid in carbon gasification. Iglesia et al. [98] showed using XPS that in the case of ruthenium promoted cobalt on titania catalysts, the promoter inhibits the deposition of carbon during FTS. Ruthenium may promote hydrogenolysis during the reaction and the intimate association of ruthenium with cobalt might allow carbon deposits on the catalyst to be gasified via hydrogenolysis at lower temperatures as opposed to carbon gasification via combustion with oxygen.

#### **4.9 Regeneration processes to remove carbon deposits**

Regeneration of cobalt-based Fischer-Tropsch synthesis (FTS) catalysts is a cost effective way to increase the life of the cobalt catalyst. In fact, BP reported that the only way to manage activity decline and ensure a 4-year catalyst life was to regenerate their catalyst in situ [35]. This is important due to the high cost of cobalt which can be a considerable proportion of the overall operating cost. In most cases the regeneration process relies on the effective removal of carbon [36, 37, 38]. The deleterious carbonaceous deposits can be removed by gasification with  $O_2$ ,  $H_2O$  and  $H_2$  [15] which makes regeneration feasible. The order of decreasing reaction rate of carbon is  $O_2 > H_2O > H_2$ , which can be generalized.

Already in the early stages of the industrial application of cobalt catalysts it was noted that to secure longer catalyst lifetime, regeneration with hydrogen was required [103]. Over the next few years new regeneration technologies were developed and improved for cobalt-based FTS catalysts. The regeneration can be performed in a few manners: (i) reductive regeneration, (ii) oxidative regeneration, and (iii) steam/water regeneration. All these regeneration procedures focus on the removal of deleterious carbon types, i.e. polymeric and graphitic.

Carbon deactivated FTS catalysts can be rejuvenated or regenerated by treatment in hydrogen [103, 104, and 105]. This can be done in both an in-situ [104] and ex-situ manner [105]. Non desorbing reaction products (heavy waxes) can be also be removed from catalysts by treatment with hydrogen, or gases or vapours containing hydrogen [106]. Often it is necessary to remove wax and hydrocarbons from a spent catalyst before exposing it to regenerating gas such as oxygen, in order to limit exotherms that may result in damage to catalyst integrity. Various patents and publications claim that carbon deactivated catalysts can best be regenerated by conventional wax removal, oxidation and re-reduction techniques [35, 36, 37, 107, 108]. Steam regeneration can also be used to remove carbon from deactivated catalysts. Steam reacts with the carbon on the catalyst surface and forms CO and H<sub>2</sub>, thus cleaning the surface [38]. The important message is that regeneration efforts focus largely on the removal of carbon.

#### **4.10 The effect of carbon on FTS selectivities**

Along with catalyst activity, product selectivity is a key issue in cobalt-based FTS [1]. For GTL processes the preferred product is long chain waxy hydrocarbons. It is well known that FT reaction conditions have an important effect on product selectivities. High temperatures and H<sub>2</sub>/CO ratios are associated with higher methane selectivity, lower probability of hydrocarbon chain growth, and lower olefinicity in the products [109].

The deposition of the different types of inactive carbon species during FTS may have different influences on the product selectivities. It has been shown with CO adsorption studies on cobalt and molecular modelling that the presence of carbon will affect the CO adsorption strength and therefore the CO dissociation rate [41, 71]. Consequently the surface coverage of active carbon may decrease leading to shorter chained hydrocarbons. Indeed Bertole et al. [110] showed using isotopic transient experiments that an increase in the amount of surface active carbon (surface carbide) will result in a higher chain growth probability and thus an increase in desired selectivity for Co/SiO<sub>2</sub> FTS catalysts. Furthermore, it has been shown that presence of bulk cobalt carbide results in a dramatic increase in methane selectivity during the FTS [74, 80, 82]. It is also plausible that as the carbon becomes more stable, i.e.

graphitic, the interaction with the metal would decrease and it would have a lesser effect on the product distribution.

Co/Al<sub>2</sub>O<sub>3</sub> catalysts that contain higher amounts of less reactive polymeric carbon not only exhibited enhanced deactivation when tested in FTS when compared to the fresh catalyst but also showed an increase in selectivity to olefinic products [31]. The authors postulated that this was probably due to the reduction in hydrogenation ability of the carbon deposited catalyst to convert primarily formed olefins into the corresponding paraffins.

Iglesia et al. showed that the pore diameter of the catalyst is an important parameter for tailoring selectivity [111]. Hence, carbon deposition leading to physical blocking of the pores could have an influence on the selectivity. Niemela et al. [39] reported that for a Co/SiO<sub>2</sub> catalyst the relative turnover number for the C<sub>2</sub><sup>+</sup> species may increase significantly during the initial phase of carbon deactivation due to preferential blocking of the narrowest catalyst pores. Puskas et al. [73] also showed a decrease in the hydrocarbon growth rate of Co/Mg/diatomaceous earth catalyst with increasing time online, which they ascribed to pore blocking.

#### **4.11 Conclusions**

It is clear that the FTS over cobalt catalysts occurs in the presence of an active surface carbidic over layer and in the presence of various hydrocarbon products. The conversion of this active surface carbidic carbon to other inactive forms (e.g. bulk carbide, polymeric carbon and graphene) over time can result in deactivation and selectivity loss of the catalyst. Additionally, it is also evident that non-desorbing, heavy hydrocarbon wax can lead to pore plugging and deactivation. However, most of the recent studies on deactivation have dealt with oxidation of cobalt. From the available literature and regeneration patents, it does seem that deactivation by carbon deposits is an important deactivation pathway for cobalt-based FTS catalysts under realistic conditions that warrants further study. There is a lot of a scope for the development of characterization techniques that are able to pin-point the location and determine the exact nature of deactivating carbon species.

## 4.12 References

- [1] A.P. Steynberg, M.E. Dry (Eds.), Fischer-Tropsch Technology, Studies in Surface Science and Catalysis, Vol. 152, Elsevier, 2004.
- [2] J. Eilers, S.A. Posthuma, S.T. Sie, Catal. Lett. 7 (1990) 253.
- [3] The Catalyst Review Newsletter, Gas-to-Liquids: Peering into the Crystal Ball, 2005, p. 4.
- [4] V.U.S. Rao, G.J. Stiegel, G.J. Cinquergrane, R.D. Srivastava, Fuel Process. Technol. 30 (1992) 83.
- [5] P.J. van Berge, S. Barradas, J. van de Loosdrecht, J.L. Visagie, Erdöl Kohle Erdgas P. 117 (2001) 138.
- [6] P.J. van Berge, J. van de Loosdrecht, S. Barradas, A.M. van der Kraan, Catal. Today 58 (2000) 321.
- [7] G. Jacobs, T.K. Das, P.M. Patterson, J. Li, L. Sanchez, B.H. Davis, Appl. Catal. A 247 (2003) 335.
- [8] G. Kiss, C.E. Klier, G.J. DeMartin, C.C. Culross, J.E. Baumgartner, J. Catal. 217 (2003) 127.
- [9] A.M. Hilmen, D. Schanke, K.F. Hanssen, A. Holmen, Appl. Catal. A 186 (1999) 169.
- [10] J. Li, X. Zhan, Y. Zhang, G. Jacobs, T. Das, B.H. Davis, Appl. Catal. A 228 (2002) 203.
- [11] A.M. Saib, A. Borgna, J. van de Loosdrecht, P.J. van Berge, J.W. Niemantsverdriet, Appl. Catal. A 312 (2006) 12.
- [12] J. van de Loosdrecht, B. Balzhinimaev, J.-A. Dalmon, J.W. Niemantsverdriet, S.V. Tsybulya, A.M. Saib, P.J. van Berge, J.L. Visagie, Catal. Today 123 (2007) 293.
- [13] A.M. Saib, A. Borgna, J. van de Loosdrecht, P. van Berge, J.W. Niemantsverdriet, J. Phys. Chem. B. 110 (2006) 8657.
- [14] A.M. Saib, A. Borgna, J. van de Loosdrecht, P.J. van Berge, J.W. Geus, J.W. Niemantsverdriet, J. Catal. 239 (2006) 326.
- [15] C.H. Bartholomew, Appl. Catal. A 212 (2001) 17.
- [16] P.J. van Berge, R.C. Everson, Stud. Surf. Sci. Catal. 107 (1997) 207.
- [17] P.R.F. Baumann, C.W. DeGeorge, S.C. Leviness, WO 98/50485 (1997), to Exxon.
- [18] W.C. Behrmann, S.C. Leviness, WO 98/50486 (1997), to Exxon.
- [19] S.C. Leviness, W.N. Mitchell, WO 98/50488 (1997), to Exxon.
- [20] M. Chang, J. Stephen, C.J. Mart, WO 98/50489 (1997), to Exxon.
- [21] J.R. Rostrup-Nielsen, in: J.R. Anderson, M. Boudart (Eds.), Catalysis Science and Technology, Springer-Verlag, Berlin, 1984.
- [22] S.A. Posthuma, J.D. de Graaf, Great Britain Patent 2 231 581 (1989), to Shell.
- [23] G.Z. Bian, N. Fujishita, T. Mochizuki, W.S. Ning, M. Yamada, Appl. Catal. A 252 (2003) 251.
- [24] M.J. Overett, B. Breedts, E. du Plessis, W. Erasmus, J. van de Loosdrecht, Prepr. Pap.-Am. Chem. Soc., Div. Pet. Chem. 53 (2008) 126.
- [25] J.A. Moulijn, A.E. van Diepen, F. Kapteijn, Appl. Catal. A 212 (2001) 3.
- [26] M. Agnelli, H. M. Swaan, C. Marquez-Alvarez, G. A. Martin and C. Mirodatos, J. Catal. 175 (1998) 117.
- [27] J. Wilson, C. de Groot, J. Phys. Chem. 99 (1995) 7860.
- [28] I.M. Ciobica, R.A. van Santen, P.J. van Berge, J. van de Loosdrecht, Surf. Sci. 602 (2008) 17.
- [29] G.L. Bezemer, J.H. Bitter, H.P.C.E. Kuipers, H. Oosterbeek, J.E. Holewijn, X. Xu, F. Kapteijn, A.J. van Dillen, K.P. de Jong, J. Am. Chem. Soc. 128 (2006) 3956.
- [30] P.G. Menon, J. Mol. Catal. 59 (1990) 207.
- [31] D.-K. Lee, J.-H. Lee, S.-K. Ihm, Appl. Catal. 36 (1988) 199.
- [32] H.W. Pennline, R.J. Gormley, R.R. Schehl, Ind. Eng. Chem. Prod. Res. Dev. 23 (1984) 388.
- [33] P.K. Agrawal, J.R. Katzer, W.H. Manogue, J. Catal. 69 (1981) 312.
- [34] V. Gruver, R. Young, J. Engman, H.J. Robota, Prepr. Pap.-Am. Chem. Soc., Div. Pet. Chem. 50 (2005) 164.
- [35] J.J.H.M. Font Freide, T.D. Gamlin, R.J. Hensman, B. Nay, C. Sharp, J. Nat. Gas Chem. 13 (2004) 1.
- [36] S.L. Soled, E. Iglesia, R. Fiato, G.B. Ansell, United States Patent 5 397 806 (1995), to Exxon.
- [37] M.J. van der Burgt, J. Ansorge, Great Britain Patent 2 222 531 (1988), to Shell.
- [38] H.A. Wright, United States Patent 6 486 220 (2002), to Conoco.
- [39] M.K. Niemela, A.O.I. Krause. Catal. Lett. 42 (1996) 161.
- [40] H.W. Pennline, S.S. Pollack. Ind. Eng. Chem. Prod. Res. Dev. 25 (1986) 11.
- [41] M.C. Zonneville, J.J.C. Geerlings, R.A. van Santen, Surf. Sci. 240 (1990) 253.

- [42] L. Borko, Z.E. Horvath, Z. Schay, L. Gucci, *Stud. Surf. Sci. Catal.* 167 (2007) 231.
- [43] G. Boskovic, K.J. Smith, *Catal. Today* 37 (1997) 25.
- [44] X.-Q. Gong, R. Raval, P. Hu, *J. Chem. Phys.* 122 (2005) 24711.
- [45] Q. Ge, M. Neurock, *J. Phys. Chem. B* 110 (2006) 15368.
- [46] J.J.C. Geerlings, M.C. Zonneville, C.P.M. de Groot, *Surf. Sci.* 241 (1991) 302.
- [47] J. Cheng, X-Q Gong, P. Hu, C.M. Lok, P. Ellis, S. French, *J. Catal.* 254 (2008) 285.
- [48] P. Winslow, A.T. Bell, *J. Catal.* 91 (1985) 142.
- [49] J. Nakamura, K. Tanaka, I. Toyoshima, *J. Catal.* 108 (1987) 55.
- [50] P.E. Nolan, D.C. Lynch, A.H. Cutler, *J. Phys. Chem. B* 102 (1998) 4165.
- [51] J.J.C. Geerlings, M.C. Zonneville, C.P.M. de Groot, *Catal. Lett.* 5 (1990) 309.
- [52] T. Koerts, "The reactivity of surface carbonaceous intermediates", PhD thesis, Eindhoven University of Technology, 1992.
- [53] C. Mirodatos, E. Brum Pereira, A. Gomez Cobo, J.A. Dalmon, G.A. Martin, *Top. Catal.* 2 (1995) 183.
- [54] A. Barbier, A. Tuel, I. Arcon, A. Kodre, G. A. Martin, *J. Catal.* 200 (2001) 106.
- [55] D. Potoczna-Petru, *Carbon* 29 (1991) 73.
- [56] C.H. Bartholomew, *Catal. Rev.-Sci. Eng.* 24 (1982) 67.
- [57] J. Nakamura, I. Toyoshima, K.-I. Tanaka, *Surf. Sci.* 201 (1988) 185.
- [58] J. R. Rostrup-Nielsen, *J. Catal.* 27 (1976) 225.
- [59] A.D. Moeller, C.H. Bartholomew, *Ind. Eng. Chem. Proc. Des. Dev.* 21 (1982) 390.
- [60] S. Mukkavilli, C.V. Wittmann, *Ind. Eng. Chem. Process Des. Dev.* 25 (1986) 487.
- [61] M. E. Dry, *Hydrocarb. Process.* 59 (1980) 52.
- [62] M. P. Hooker, J. T Grant, *Surf. Sci.*, 62 (1977) 21.
- [63] M.S. Kim, N.M. Rodriguez, R.T.K Baker, *J. Catal.* 143 (1993) 449.
- [64] D.C. Gardner, C.H. Bartholomew, *Ind. Eng. Chem. Prod. Res. Dev.* 20 (1981) 80.
- [65] K.A. Prior, K. Schwaha, R.M. Lambert, *Surf. Sci.* 77 (1978) 193.
- [66] B.G. Johnson, C.H. Bartholomew, D.W. Goodman, *J. Catal.* 128 (1991) 231.
- [67] J. Lahtinen, T. Anraku, G. A. Somorjai, *J. Catal.* 142 (1993) 206.
- [68] J. Lahtinen, T. Anraku, G.A. Somorjai, *Catal. Lett.* 25 (1994) 241
- [69] G.A. Beitel, C.P.M. de Groot, H. Oosterbeek, J.H. Wilson, *J. Phys. Chem. B* 101 (1997) 4035.
- [70] J. Xu, K.F. Tan, A. Borgna, M. Saeys, "First Principles Based Promoter Design for Heterogeneous Catalysis", Poster 476ae, AIChE Annual meeting, San Francisco, 15 November 2006 (<http://aiche.confex.com/aiche/2006/techprogram/S2113.HTM>).
- [71] J.G. Choi, H.K. Rhee, S.H. Moon, *Appl. Catal.* 13 (1985) 269.
- [72] I. Puskas, *Catal. Lett.* 22(1993) 283.
- [73] I. Puskas, B.L. Meyers, J.B. Hall, *Prepr. Pap.-Am. Chem. Soc., Div. Pet. Chem.* 28 (1993) 905.
- [74] V. Gruver, X. Zhan, J. Engman, H.J. Robota, *Prepr. Pap.-Am. Chem. Soc., Div. Pet. Chem.* 49 (2004) 192.
- [75] L.J.E. Hofer, E.M. Cohn, W.C. Peebles, *J. Phys. Chem.* 53 (1949) 661.
- [76] S. Weller, L.J.E. Hofer, R.B. Anderson, *J. Am. Chem. Soc.* 70 (1948) 799.
- [77] F. Tihay, G. Pourroy, M. Richard-Plouet, A.C. Roger, A. Kiennemann, *Appl. Catal. A* 206 (2001) 29.
- [78] J.W. Niemantsverdriet, A.M. van der Kraan, *J. Catal.* 72 (1981) 385.
- [79] L.J.E. Hofer, W.C. Peebles, *J. Am. Chem. Soc.* 69 (1947) 893.
- [80] United States Bureau of Mines Bulletin 578, "Synthetic liquid fuels from hydrogenation of carbon monoxide", Washington, US Government print office, 1948-1959, p 19 (<http://www.fischer-tropsch.org>).
- [81] S.E. Weller, *J. Am. Chem. Soc.* 69 (1947) 2432.
- [82] J. Xiong, Y. Ding, T. Wang, L. Yan, W. Chen, H. Zhu, Y Lu, *Catal. Lett.* 102 (2005) 265.
- [83] L. Leclercq, A. Almazouari, M. Dufour, G. Leclercq, in: S.T. Oyama (Ed.), *The Chemistry of Transition Metal Carbides and Nitrides*, Blackie, Glasgow, 1996, p. 345.
- [84] O. Kitakami, H. Sato, Y. Shimada, F. Sato, M. Tanaka, *Phys. Rev. B* 56 (1997) 13849.
- [85] G.V. Pankina, P.A. Chernavskii, A.S. Lermontov, V.V. Lunin, *Petrol. Chem.* 42 (2002) 217.
- [86] O. Ducreux, J. Lynch, B. Rebours, M. Roy, P. Chaumette, *Stud. Surf. Sci. Catal.* 119 (1998) 1258.
- [87] A. Machocki, *Appl. Catal.* 70 (1991) 237.
- [88] G. Jacobs, P.M. Patterson, Y. Zhang, T. Das, J. Li, B.H. Davis, *Appl. Catal. A* 233 (2002) 215.
- [89] P.G. Harrison, R. Kannengiesser, *J. Chem. Soc, Chem. Commun.* 20 (1995) 2065.



- [90] T. Nemes, A. Chambers, R.T.K. Baker *J. Phys. Chem. B* 102 (1998) 6323.
- [91] J. Llorca, N. Homs, J. Sales, J-L.G. Fierro, P. Ramírez de la Piscina, *J. Catal.* 222 (2004) 470.
- [92] J.W. Niemantsverdriet, *Spectroscopy in Catalysis*, Third ed., Wiley-VCH, Weinheim, 2007.
- [93] S-K. Ihm, D.K. Lee, *Stud. Surf. Sci. Catal.* 68 (1991) 219.
- [94] C. Sellmer, S. Decker, N. Kruse, *Catal. Lett.* 52 (1988) 131.
- [95] G. R. Fredriksen, E. A. Blekkan, D. Shanke, A. Holmen, *Chem. Eng. Technol.* 18 (1995) 125.
- [96] F. Morales, B.M. Weckhuysen, *Catalysis* 19 (2006) 1.
- [97] J. Lahtinen, G.A. Samorjai, *J. Mol. Catal. A* 130 (1998) 255.
- [98] E. Iglesia, S.L. Soled, R.A. Fiato, G.H. Via, *J. Catal.* 143 (1993) 345.
- [99] C.T. Campbell, D.W. Goodman, *Surf. Sci.* 123 (1982) 413.
- [100] J.W. Snoek, G.F. Froment, *Ind. Eng. Chem. Res.* 41 (2002) 3548.
- [101] D.A. Wesner, G. Linden, H.P. Bonzel, *Appl. Surf. Sci.* 26 (1986) 335.
- [102] H. Pichler, *Adv. Catal.* 4 (1952) 271.
- [103] K.B. Arcuri, S.C. Leviness, The Regeneration of Hydrocarbon Synthesis Catalyst, A Partial Review of the Related Art Published during 1930 to 1952, AIChE Spring National Meeting, New Orleans, LA, April 2, 2003 ([www.fischer-tropsch.org](http://www.fischer-tropsch.org)).
- [104] O. Roelen, H. Heckel, F. Hanisch, United States Patent 2 289 731 (1942), to Hydrocarbon Synthesis Corporation.
- [105] E. Iglesia, S.L. Soled, R. Fiato, United States Patent 4 738 948 (1988), to Exxon)
- [106] W. Feisst, O. Roelen. United States Patent 2 369 956 (1945), to Hydrocarbon Synthesis Corporation.
- [107] R. Huang, K.L. Agee, B.A. Arcuri, P.F. Schubert, United States Patent 6 812 179 (2002), to Syntroleum Corporation.
- [108] X. Zhan, K. Arcuri, R. Huang, K. Agee, J. Engman, H. Robota, *Prep. Pap.-Am. Chem. Soc., Div. Pet. Chem.* 49 (2004) 179.
- [109] R.L. Espinoza, A.P. Steynberg, B. Jager, A.C. Vosloo, *Appl. Catal. A* 186 (1999) 13.
- [110] C.J. Bertole, G. Kiss, C.A. Mims, *J. Catal.* 223 (2004) 309.
- [111] E. Iglesia, S.L. Soled, J.E. Baumgartner, S.C. Reyes, *J. Catal.* 153 (1995) 108.

---

# Chapter 5

---

## **Carbon deposition as a deactivation mechanism of cobalt-based Fischer-Tropsch synthesis catalysts under realistic conditions**

---

*Deactivation of cobalt-based Fischer-Tropsch synthesis (FTS) catalysts by carbonaceous species has been previously postulated. This mechanism, however, is hard to prove due to the presence of heavy hydrocarbon wax product and the potential build-up of inert carbon on the catalyst support. Furthermore, the slow build-up of low quantities of inactive carbon with time on stream necessitates the use of data from extended FTS runs. In this study, the formation of carbon deposits on samples of a Co/Pt/Al<sub>2</sub>O<sub>3</sub> catalyst, taken from a 100 bbl/day slurry bubble column reactor operated over a period of 6 months at commercially relevant FTS conditions is reported. The spent catalysts were wax extracted in an inert environment and the amount, nature and location of carbon deposits were then studied using temperature programmed hydrogenation and oxidation (TPH/TPO), energy-filtered transmission electron microscopy (EFTEM), high sensitivity low energy ion scattering (HS-LEIS) and hydrogen chemisorption. TPH/TPO showed that there is an increase in polymeric carbon with time on stream which may account for a part of the catalyst deactivation. Carbon maps from EFTEM as well as HS-LEIS data show that the polymeric carbon is located both on the alumina support and cobalt. The polymeric carbon on the metal correlates with the catalyst deactivation in cobalt catalyzed FTS.*

---

## 5.1 Introduction

The Fischer-Tropsch synthesis (FTS) is at the heart of the gas-to-liquid (GTL) process, which involves the conversion of synthesis gas derived from natural gas to clean environmentally friendly diesel [1], i.e. low in sulphur and aromatics. Cobalt-based catalysts supported on oxidic carriers are preferred to iron for this industrial process due to their high per pass FT activity, low oxygenate and CO<sub>2</sub> selectivity [2]. However, cobalt-based FT catalysts are more expensive compared to iron-based catalysts and therefore a long catalyst lifetime is needed to ensure that the process is economically feasible [3]. On a commercial scale, Shell is operating a supported cobalt catalyst in a fixed bed reactor, as part of their Shell Middle Distillate Synthesis (SMDS) process in Bintulu, Malaysia. Sasol has a 34 000 bbl/day GTL plant in operation in Ras Laffan, Qatar, which is based on the Sasol Slurry Phase Distillate<sup>TM</sup> (Sasol SPD<sup>TM</sup>) process, using a supported cobalt catalyst in a slurry bed.

Cobalt-based catalysts tested under realistic conditions (Figure 5.1) exhibit deactivation with time on stream [4, 5]. In order to maximize the lifetime of a cobalt catalyst for such processes, an understanding of the deactivation mechanisms at play is important. A lot of attention has focused on investigating the role of oxidation of metallic cobalt on catalyst deactivation [4, 6-10]. However, recent work on an industrial Co/Al<sub>2</sub>O<sub>3</sub> catalyst using XANES, XRD and magnetic measurements has shown that oxidation is not a deactivation mechanism during realistic FTS [4, 11]. Other postulated deactivation mechanisms include cobalt support compound formation, poisoning, sintering, cobalt reconstruction and the formation of inert carbonaceous phases [12].

This study focuses on the role of carbon deposition. Menon [13] has classified the Fischer-Tropsch synthesis as a carbon insensitive reaction as there is apparently sufficient hydrogen on the catalyst surface and the strong hydrogenation activity of the catalyst keeps the surface relatively clean and active even when appreciable quantities of carbon are already present on the surface. It is also known that cobalt has a lesser tendency to produce carbon than iron [14]. Even so, a close inspection of the open and patent literature published especially by companies investing in GTL technologies suggests that cobalt-based FTS catalysts are negatively influenced by

carbon [15-19]. Syntroleum has reported the slow build-up of polymeric or graphitic carbon with increasing time on stream [15]. Small amounts of the carbon (1 wt%) as determined by TGA-MS, were sufficient to cause blocking of the cobalt active phase after 140 days online. BP also ascribed deactivation on a Co/ZnO catalyst to small amounts of what they termed a refractory carbon phase, that was present on cobalt [16]. Various regeneration patents also suggested that carbonaceous phases that form during FTS will deactivate the catalyst and need to be removed [17-19]. Also, deactivation of the cobalt active phase by carbonaceous species during laboratory scale CO hydrogenation has been postulated in a few studies [20-22]. This mechanism, however, is hard to prove in FT synthesis due to the presence of heavy hydrocarbon wax product and the potential spill over and build up of inert carbon on the catalyst support. It is also possible that deleterious carbon deposition is kinetically slow during realistic FTS conditions and its effect on activity is only seen during extended runs. Studies have also been conducted on supported cobalt catalysts that suggest deactivation by pore plugging by the heavy wax product [23, 24].

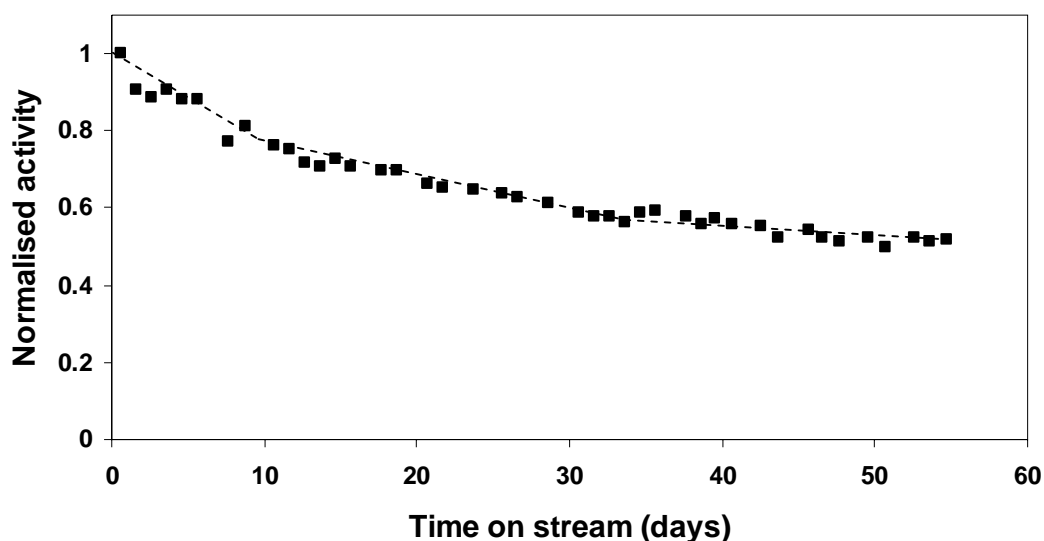


**Figure 5.1** *Normalized activity for a Co/Pt/Al<sub>2</sub>O<sub>3</sub> catalyst during realistic Fischer–Tropsch synthesis, i.e. 230 °C, 20 bar, (H<sub>2</sub> + CO) conversion between 50 and 70%, feed gas composition of 50-60 vol.% H<sub>2</sub> and 30-40 vol.% CO,  $P_{H_2O}/P_{H_2}=1-1.5$ ,  $P_{H_2O}=4-6$  bar (adapted from [4]).*

There are a number of ways that carbon may interact with a supported cobalt catalyst to affect its activity. The carbon deposits may block the catalyst pores resulting in diffusion limitations, poison the metal surface by binding irreversibly or even encapsulate metal particles [25]. Subsurface carbon may also play a role in electronic inhibition of activity [26]. It has also been shown that carbon bound to a metal surface can induce a surface reconstruction which will affect the activity [27]. The diffusion of carbon into cobalt can also result in the formation of bulk cobalt carbide [28]. Bulk cobalt carbide is not considered FT active and results in both activity and selectivity loss, presumably through electronic inhibition that affects the dissociation of CO [29, 30]. It has been shown that bulk carbide can form during conditions where hydrogen is depleted [31]. It has been reported that bulk carbides are thermodynamically unstable during the synthesis (200-240 °C) however they have been previously observed on cobalt FTS catalysts using in situ [32] and synchrotron XRD [33].

In this study we report on the formation of carbon deposits as a deactivation mechanism on Co/Pt/Al<sub>2</sub>O<sub>3</sub> catalyst samples taken from a demonstration run performed at realistic FTS conditions. The spent catalysts were wax extracted in an inert environment and were then characterized. The accumulation, location and nature of the carbon deposits was investigated using XPS, temperature programmed (TPO/TPH) techniques, hydrogen chemisorption, energy-filtered transmission electron microscopy (EFTEM) and high sensitivity low energy ion scattering (HS-LEIS).

## 5.2 Experimental

### 5.2.1. Catalyst preparation

A 20 wt% Co/Al<sub>2</sub>O<sub>3</sub> catalyst, promoted with 0.05 wt% platinum, was prepared by slurry impregnation of a  $\gamma$ -alumina support (Puralox 5/150 from Sasol Germany) with an aqueous cobalt nitrate solution, also containing the platinum precursor (ammonium platinum nitrate). After impregnation and drying, the catalyst intermediate was calcined at 250 °C in air and reduced in pure hydrogen at 425 °C. To achieve the

required cobalt loading two impregnation and calcination steps were performed [34-38].

#### *5.2.2 Extended catalyst testing in demonstration unit run*

The Co/Pt/Al<sub>2</sub>O<sub>3</sub> catalyst was tested in a 100 bbl/day slurry bubble column reactor with a diameter of 0.9 m at commercially relevant FTS conditions, i.e. 230 °C, 20 bar, H<sub>2</sub>+CO conversion between 50-70 %, feed gas composition of 50-60 vol. % H<sub>2</sub> and 30-40 vol. % CO. The reactor was well-mixed ensuring that representative samples were taken each time.

#### *5.2.3 Wax extraction procedure*

Samples of spent catalyst, protected in a wax layer, were taken from the reactor at various time intervals under an inert nitrogen environment and allowed to congeal. Due to the interference of this wax during the follow-up analyses, it was removed by an exhaustive reflux extraction with dry, deoxygenated tetrahydrofuran (THF, b.p. 66 °C) under an argon (99.999%) environment for around 3 h, using a P40 glass frit. After extraction the obtained catalyst particles were dried under vacuum at room temperature to remove the THF. The catalyst was then transferred under vacuum using Schlenk glassware into a glove box (4 ppm O<sub>2</sub>, 1 ppm H<sub>2</sub>O). The total carbon level for the catalysts after extraction was on average about 4 wt% as determined by LECO elemental analysis.

#### *5.2.4 X-ray Photoelectron Spectroscopy (XPS) analysis of wax-extracted samples*

The samples were prepared in the glove box by crushing the wax-extracted, FTS catalyst samples in a pestle and mortar. Afterwards, the powders were pressed into an indium layer on top of standard stainless steel XPS stubs and transferred via a glove box into the XPS prechamber. The XPS measurements were carried out using a VG Escalab 200 MKII spectrometer. An aluminum anode ( $K_{\alpha} = 1486.6$  eV) was used to generate the X-ray radiation (240 W (20 mA; 12kV)). Measurements were carried out with a 0.1 s dwell time and 0.1 eV step for the selected regions. To obtain sufficient signal-to-noise ratio the Co 2p region was scanned 80 – 120 times (i.e. making the

total measurement approximately 3 hours). During measurement the pressure in the main chamber remained below  $10^{-8}$  mbar. Peak deconvolution was carried out with CasaXPS software.

#### 5.2.5. *Temperature Programmed hydrogenation/oxidation (TPH/TPO) coupled with mass spectroscopic (MS) measurements*

In each TP-MS experiment a 100 mg sample of the passivated wax –extracted catalyst was loaded into a quartz reactor (4 mm internal diameter) followed by purging in helium for 30 min. In the case of TPH-MS experiments, the reactor was subsequently heated under a pure  $H_2$  flow of 20 ml/min while the temperature was ramped to 600 °C at 5 °C/min. The evolution of methane was monitored during the treatment with a Balzers QMA 400 mass spectrometer ( $m/z$  of 15, instead of 16 to avoid interference from ionized oxygen from water vapour). In coupled TPH/TPO experiments, the wax-extracted catalysts were first treated in flowing He for 30 min before ramping the temperature in a 50% He/ $H_2$  mixture (20 ml/min) to 350 °C at 10 °C/min and holding there for 1 h. The reactor was then cooled to room temperature, flushed with He for 30 min and then heated to 900 °C at 10 °C/min in 10%  $O_2$ /He flow of 20 ml/min and held there for 1 h. The evolution of  $CO_2$  ( $m/z = 44$ ) as a gasification product of carbon ( $C + O_2 \rightarrow CO_2$ ) was monitored. The  $CO_2$  area under the TPO curves was integrated using Microcal Origin 7.5 software. Under these conditions, the formation of significant amounts of CO from incomplete carbon gasification can be excluded. The mass percentage of carbon on the catalysts was determined from the area of the  $CO_2$  peaks which were calibrated from the stoichiometric decomposition of  $NaHCO_3$  (Analysis grade).

#### 5.2.6. *Hydrogen chemisorption experiments*

Samples of catalysts were taken from the slurry bubble column reactor at various intervals and wax-extracted in a similar manner as described above. After passivation of the catalyst over dry ice, chemisorption analysis was performed using an ASAP 2010 (Micromeritics) instrument. Approximately 0.25 g of sample was activated by reduction under a flow of hydrogen (UHP). The reduction procedure employed was 2°C/min to 350 °C (or 500 °C), hold for 240 minutes.

### *5.2.7 Transmission Electron Microscopy (TEM) and Energy Filtered TEM*

Thin samples for TEM were prepared by crushing the passivated catalyst with a mortar and pestle. Then an appropriate amount of sample was placed onto a holey carbon microscope grid covered with carbon windows. EFTEM analysis was done on a JEOL 2010F microscope operated at 200 keV, using a Gatan energy loss spectroscopy system.

### *5.2.8 High sensitivity low energy ion scattering (HS-LEIS) experiments*

HS-LEIS is a very surface specific technique. It can selectively analyze the outermost atomic layer of a sample [39]. The HS-LEIS experiments were performed at Calipso BV and the set-up used for the experiments is described in detail elsewhere [40]. A sample of wax extracted sample was first subjected to TPH and held at 350 °C for 1 hr and then passivated at room temperature in a dilute 0.1 % O<sub>2</sub>/He mixture. This sample was placed in a small sample container, mildly compacted and measured. The samples were analyzed with 3 keV<sup>4</sup>He<sup>+</sup> with typical ion currents of 0.3 – 2 nA. The ion beam is rastered over a certain area to obtain a homogeneous ion dose on the sample and to minimize the ion impact induced damage. Typically about 1 atomic % of the outer atomic layer was removed during the recording of a spectrum. Thereafter the sample was treated with atomic oxygen in the preparation chamber and then transferred to the analysis chamber. The oxygen atoms are generated by oxygen plasma and filtered (removal of energetic particles, ions and electrons) before they reach the sample. In this way any residual carbon on the sample is removed by the very reactive O-atoms, without damaging the surface by bombardment. Typically, the sample is clean after a 10 minute treatment.

## **5.3. Results**

The following methodology was used to characterize the carbon phases on the Co/Pt/Al<sub>2</sub>O<sub>3</sub> catalyst. Catalyst samples were removed from the 100-barrel/day slurry bubble column reactor operated over a period of 6 months. The catalyst samples (~1 cm<sup>3</sup>) were wax extracted with the THF and transferred into a glove box in a



protected environment. To gain information on the surface properties of the extracted catalysts XPS was performed. In order to follow the accumulation and reactivity of the carbon a combination of TPH and TPH/TPO were used. The nature of the carbon was investigated with TPH using carbon references. Finally, EFTEM, HS-LEIS and hydrogen chemisorption were used as tools to shed light on the location of carbon.

### 5.3.1 XPS following wax extraction

The Co 2p region of XPS spectra for selected wax extracted catalysts is shown in Figure 5.2. The typical probing depth for XPS varies between 1.5-6 nm [41] and the fact that a cobalt signal is visible implies that the wax has been extracted down to low levels. The spectra were deconvoluted using Gaussian peaks, based on reference cobalt compounds. As the catalyst has been passivated in the glove box, some oxidic cobalt is expected. It should also be noted that previous XANES analysis of catalysts containing a protective wax-layer taken from different stages of a FTS demonstration run showed the presence of both metallic cobalt and significant amounts (10-30 %) of CoO [11].

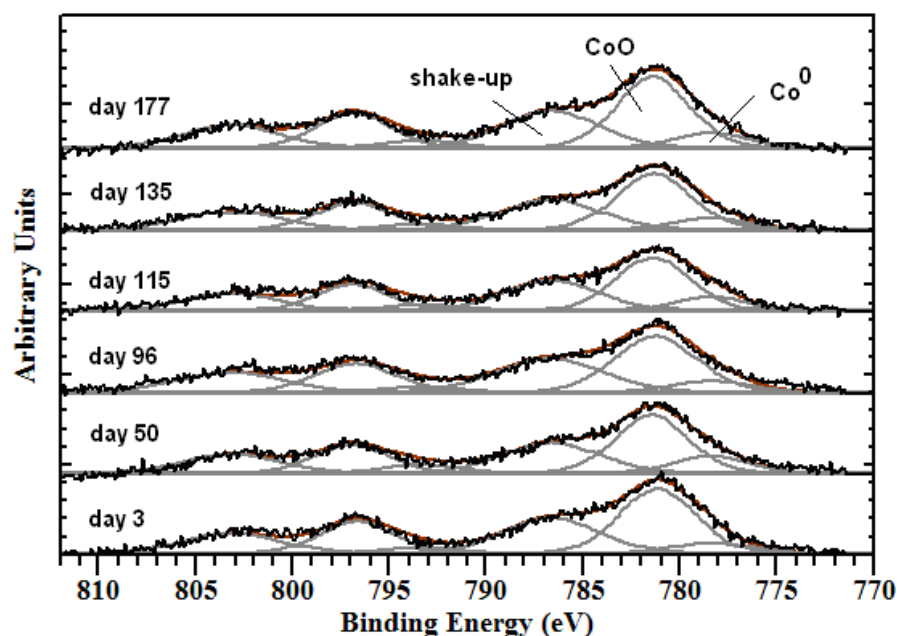


**Figure 5.2** Co 2p region of XPS spectrum for a series of wax extracted catalysts taken from a FTS run in the slurry bubble column.

The Co 2p core level spectrum is characterized by two components appearing due to spin-orbital splitting; Co 2p<sub>3/2</sub> and Co 2p<sub>1/2</sub>, and shake-up satellites. The presence of strong shake-up satellites about 5-6 eV from the main photoline, along with peak position and doublet separation of around 15.5 eV, indicate the presence of CoO [42, 43]. No Co<sub>3</sub>O<sub>4</sub> is expected in the catalysts [11], and indeed if it were present this would result in weaker shake-up satellites about 10–11 eV higher than the main peak, which is characteristic of the low spin Co<sup>3+</sup> compounds [43, 44]. The presence of metallic cobalt is also noted at 778.1 eV [45]. From this it can be inferred that the surface of these wax-extracted catalysts consists of passivated oxide but also cobalt still in the metallic state.

### *5.3.2 Temperature programmed hydrogenation (TPH) of carbonaceous species on wax-extracted catalysts*

TPH-MS experiments were conducted on a series of spent catalysts that were wax extracted. A blank sample comprising a freshly reduced sample coated in wax and then wax-extracted using the same procedure described above was also analyzed. The methane evolution profiles for a series of the catalysts are shown in Figure 5.3. It is evident that there are at least three major types of carbonaceous species based on their reactivity to H<sub>2</sub>. A closer inspection of one of the profiles (Figure 5.4) indicates carbon species that are hydrogenated at around 250, 330 and 445 °C. The methane peaks are compared to literature TPH values in an attempt to assign them to different types of carbon species (Table 5.1). A part of the first peak corresponds to atomic or surface carbidic carbon which is hydrogenated at around 197±20 °C according to Lee et al. [20].

The question arises whether bulk cobalt carbide hydrogenation contributes to the TPH profile. It has been reported that cobalt carbide is hydrogenated at around 250 °C [31]. Pankina et al [49] extracted spent Co/Al<sub>2</sub>O<sub>3</sub> FTS catalysts with hexane and performed the TPH along with magnetic measurements on the catalyst. They stated that the peak that evolves at around 230-250 °C in the TPH profile corresponds with an increase in magnetization to a maximum and therefore occurs as a result of the hydrogenation of bulk cobalt carbide. Furthermore they argued that this low temperature does not result in the reduction of cobalt oxides, so this was excluded as a

cause of the observed increased magnetization. We however could not detect bulk crystalline cobalt carbide by XRD. Bulk carbide is thought to be metastable and is rarely observed by ex-situ techniques [50].

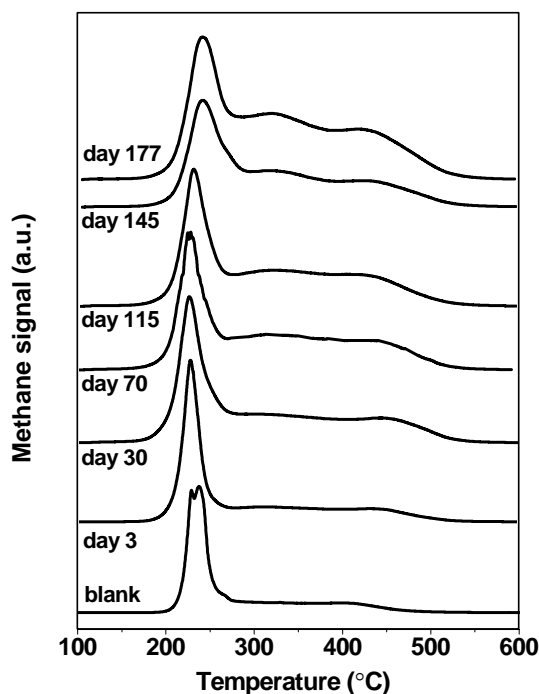


**Figure 5.3** *Methane ( $m/z = 15$ ) TPH profiles for a selected series of wax-extracted samples taken from the FTS run in the slurry bubble column.*

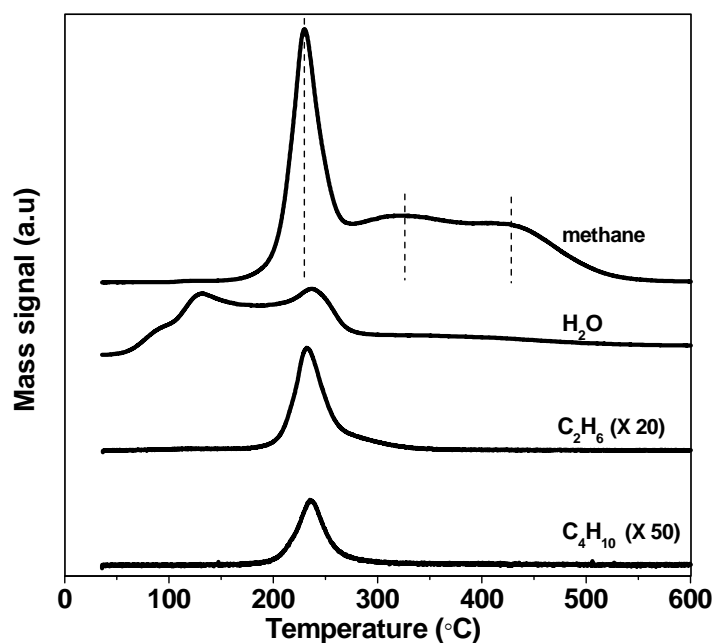


**Figure 5.4** *Water ( $m/z = 18$ ),  $C_2H_6$  ( $m/z = 30$ ),  $C_4H_{10}$  ( $m/z = 58$ ) and methane ( $m/z = 15$ ) TPH profiles for a typical wax-extracted sample from the FTS run in the slurry bubble column.*

The TPH of the blank sample (being a freshly reduced catalyst stored in wax and then wax- extracted) also contains a peak around 250 °C and the only source of carbon on this sample could be from residual hydrocarbon wax. It has been reported that wax is hydrogenated at around 250 °C [15]. Trace amounts of ethane and butane are also formed with the first methane peak as shown in Figure 5.4. This indicates that there must be a small amount of residual hydrocarbons still present after the wax extraction that undergo hydrogenolysis at around 230 °C or are carried into the mass spectrometer and undergo fragmentation. This provides strong evidence that a large part of the first peak corresponds to hydrogenation of waxy hydrocarbons. Additionally the observed water peak in Figure 5.4, at around 250 °C could be due to the reduction of CoO to Co metal.

The high temperature peak (450 °C, peak 3) corresponds to a polymeric type of carbon species [20], which could be located on the cobalt or on the support. It is proposed that the intermediate species (330 °C, peak 2) could be smaller chains of polymeric carbon species or hard –to-remove wax present in the narrowest of catalyst pores [15]. The blank sample also contains small amounts of carbon species in the 330-450°C range and this may correspond to transformed carbon that occurs during hydrocracking of the residual wax.

**Table 5.1** *Possible species observed in the TPH profile of the wax-extracted catalysts in Figures 5.3 and 5.4, based on literature values reported for TPH of cobalt-based FTS catalysts*

Peak	T <sub>Hyd</sub> (°C)	Possible carbon species based on T <sub>hyd</sub>	Ref
1	250	Surface carbidic species (atomic carbon)	20
		Residual wax/hydrocarbons	15
		Bulk cobalt carbide	31, 49
2	330	Residual wax (probably contained in small pores)	15
3	445	Polymeric (amorphous) carbon on cobalt or the support	20

The methane TPH profile was deconvoluted using Gaussian peaks (Figure 5.5) in a similar approach that was used by Xu and Bartholomew [51] for spent iron FTS catalysts and Barbier et al [52] for spent Co/SiO<sub>2</sub> catalysts. From the areas under peak it is observed that the more reactive species (Peak 1) diminishes slightly over time while more stable carbon species (Peaks 2 and 3) gradually increase with time (Figure 5.6). The evolution of more stable carbon species with increasing reaction time was previously observed over Co/SiO<sub>2</sub> catalysts by Barbier et al. [52] although in that study the on-stream time was much shorter (1 day). The deconvolution methodology is not ideal as it can be argued that a broad, symmetrical Gaussian curve results in considerable bias towards peak 2. It is believed that that due to its low reactivity towards hydrogen, the stable carbon species (Peak 3) is deleterious for catalyst activity. In order to gain more information on the amount of this difficult to remove species and other possible hydrogen-resistant carbon species, another set of experiments was designed to give quantitative information more directly.

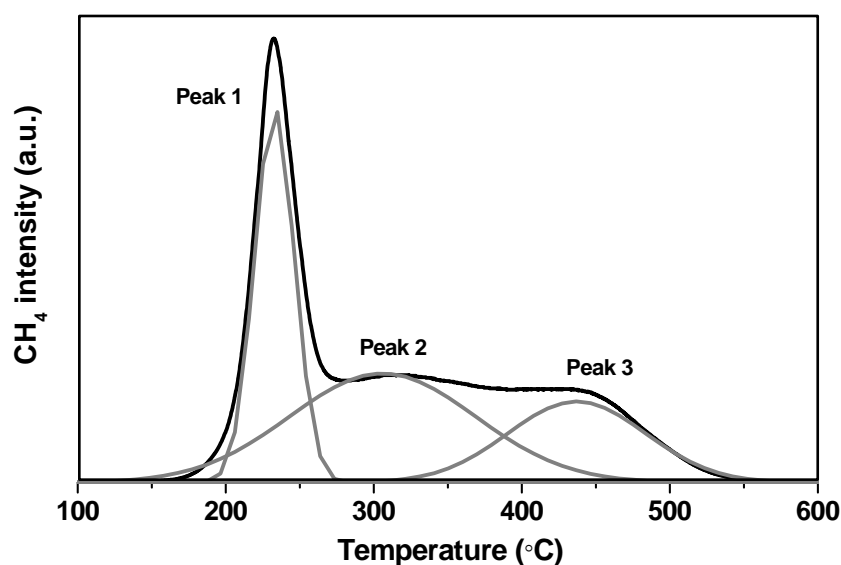


**Figure 5.5** *Peak deconvolution of a methane profile for TPH of a wax-extracted catalyst from the FTS run in the slurry bubble column*

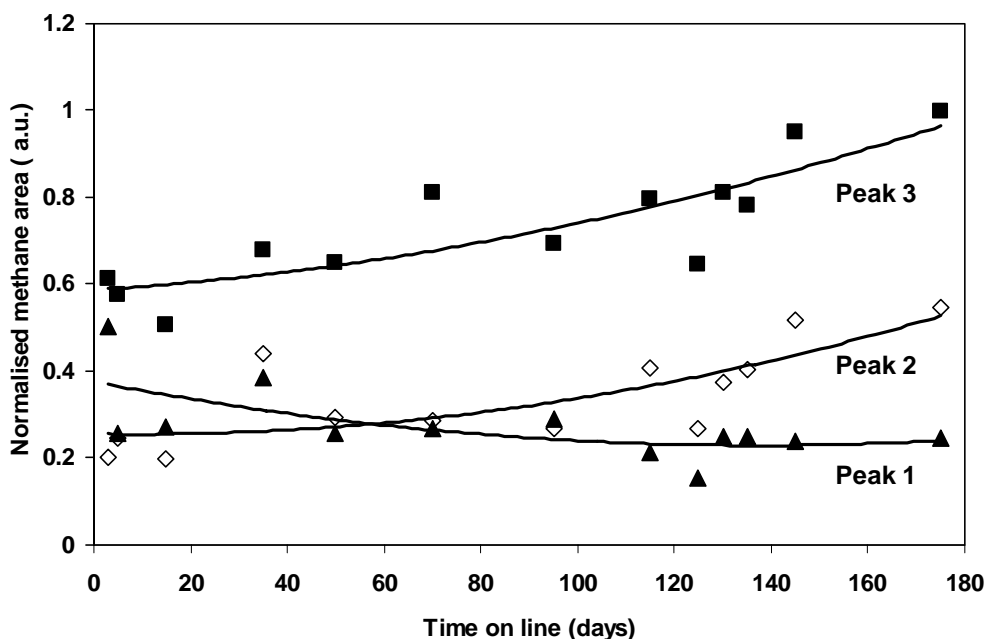


**Figure 5.6** The amount of the three carbon species, determined by deconvolution of the methane signal, with increasing time on stream

### 5.3.3 Determination of the nature and location of carbon using TPH and carbon references compounds

Various sets of carbon references were made in order to gain information on the location and nature of carbon deposits on Co/Al<sub>2</sub>O<sub>3</sub> catalysts. A fresh sample of the Co/Pt/Al<sub>2</sub>O<sub>3</sub> catalyst was reduced and deposited with carbon via CO disproportionation at 250 °C to produce a catalyst containing carbon without the presence of wax. Such treatment of a reduced cobalt alumina catalyst is known to produce both atomic and polymeric carbon [20]. Additionally a CoO powder was reduced and carburized at the same conditions to produce a sample containing carbon located on cobalt only. A sample of Co/Pt/Al<sub>2</sub>O<sub>3</sub> catalyst was reduced and deposited with carbon via CO disproportionation at 350 °C to produce a catalyst containing graphite. The presence of graphitic carbon in this sample was confirmed by TEM. The TPH profiles are shown in Figure 5.7.

The carbon deposited by CO disproportionation at 250 °C results in atomic and polymeric carbon (425 °C) (Figure 5.7a). The reduced CoO (Figure 5.7c) sample also seems to have a stable carbon species present around 425 °C, which may be

assigned to polymeric carbon on cobalt. On the basis of these reference samples the carbon we observe in these TPH experiments at high temperature ( $> 425\text{ }^{\circ}\text{C}$ ) present on the wax-extracted demonstration unit samples (Figure 5.7b), can be assigned to polymeric carbon in association with the metal and /or the support. The catalyst treated with CO at  $350\text{ }^{\circ}\text{C}$  which contains graphitic carbon has a TPH methane maximum at  $550\text{ }^{\circ}\text{C}$ . This indicates that the stable carbon species on the wax-extracted sample is likely not graphitic in nature.

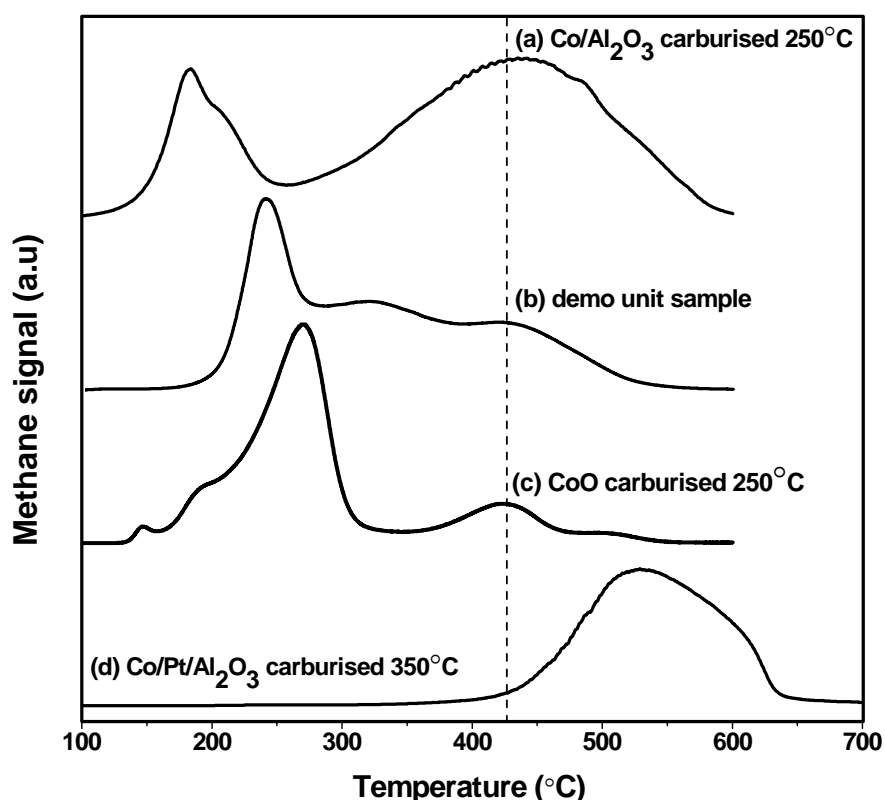


**Figure 5.7** *TPH of various carbon references compared with a wax extracted sample from the FTS run in the slurry bubble column. (a) TPH of a Co/Pt/Al<sub>2</sub>O<sub>3</sub> catalyst that was reduced and deposited with carbon via CO disproportionation at  $250\text{ }^{\circ}\text{C}$  (b) TPH of a wax extracted demonstration unit Co/Pt/Al<sub>2</sub>O<sub>3</sub> sample. (c) TPH of CoO powder reduced and deposited with carbon via CO disproportionation at  $250\text{ }^{\circ}\text{C}$  (d) TPH of a Co/Pt/Al<sub>2</sub>O<sub>3</sub> catalyst was reduced and deposited with carbon via CO disproportionation at  $350\text{ }^{\circ}\text{C}$*

### 5.3.4 Coupled TPO/TPH experiments to determine the amount of hydrogen-resistant carbon

The series of wax-extracted catalysts was first subjected to a hydrogenation step at 350 °C (Figure 5.8a), cooled to room temperature in a helium flow and then subjected to a TPO to oxidize the remaining carbon (i.e. the more stable Peak 3 carbon around 425 °C). The evolution of CO<sub>2</sub> ( $m/z = 44$ ) was monitored. This TPO treatment gives information about less reactive carbon types that do not undergo the methane formation process at 350 °C under H<sub>2</sub>. Most of the carbon is removed at around 450 °C in the TPO but there are trace amounts that are only removed above 900 °C (Figure 5.8b). The high temperature peak around 900 °C may be a fraction of carbon that is configurationally transformed (to graphitic or support carbon) during the TPH treatment. This behaviour i.e. increased stability of carbon deposits in TPO after treatment in H<sub>2</sub> has been reported for Co/Al<sub>2</sub>O<sub>3</sub> catalysts [53].

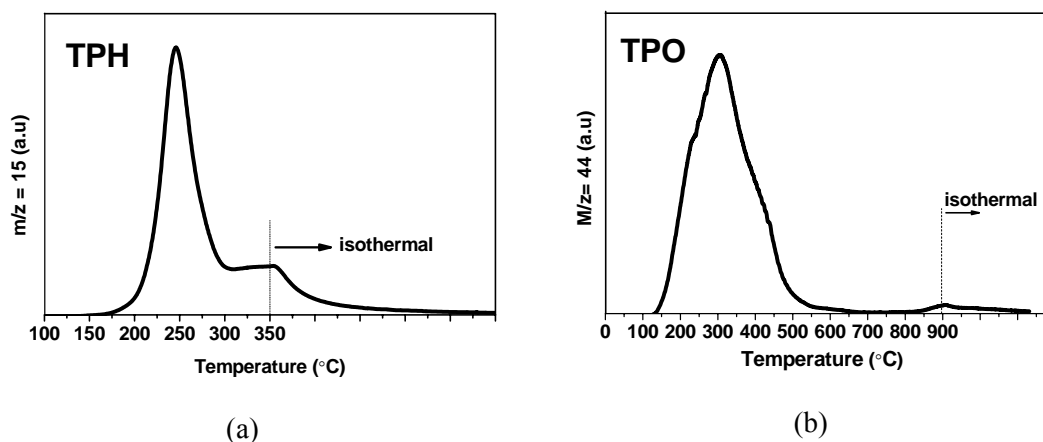


**Figure 5.8** TPH (a) till 350 °C and subsequent TPO (b) of a typical wax-extracted catalyst taken from the FTS run

The hydrogen-resistant carbon (at 350 °C) is plotted as a function of time on stream (Figure 5.9). There is an increase in this hard-to-remove carbon with catalyst age. Figure 5.9 thus, represents the amount of carbon which is resistant to hydrogen at temperatures in excess (> 100 °C) of realistic FTS temperatures. If one considers that the dispersion of the fresh Co/Pt/Al<sub>2</sub>O<sub>3</sub> catalyst is 16% [11] then the amount of carbon



(2.0 wt% when referenced to the blank sample) present on the end of run sample translates to the equivalent of 4 carbon atoms per surface cobalt atom. Even if a small portion of the carbon lies on the active metal phase then there is a strong probability that deactivation due to active site blocking will take place. The carbon amounts are therefore significant enough to cause a deactivation by a pure geometric active site blocking effect.

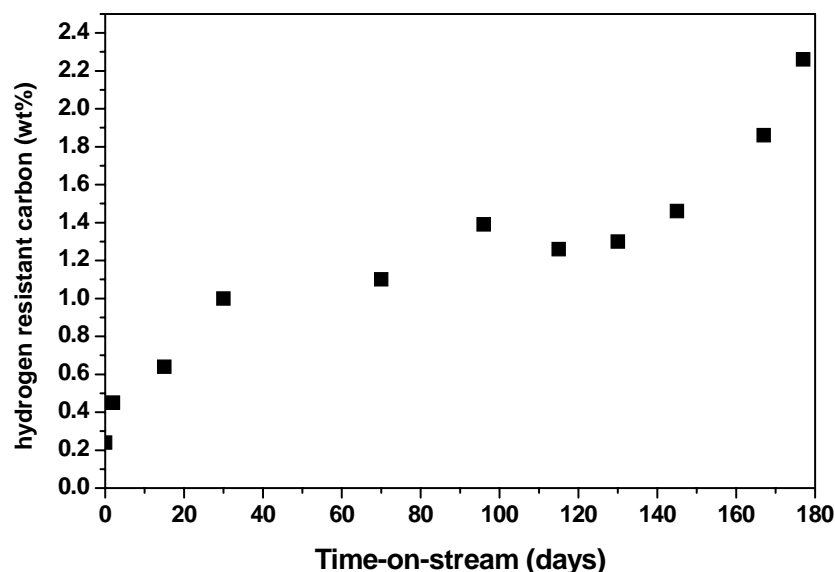


**Figure 5.9** Carbon amounts obtained from TPO experiments following TPH which represents carbon resistant to hydrogen at 350 °C

### 5.3.5 Location of carbon by using Energy Filtered Transmission Electron Microscopy (EFTEM) carbon maps

To provide a clearer answer on the location of the hard to remove carbon on the samples we performed energy filtered TEM on a catalyst sample from the end of the FTS run. EFTEM is a powerful tool, which has been used previously for carbon mapping on coked catalysts, enabling one to locate the regions of carbon lay down [54]. The cobalt catalyst sample was first subjected to a TPH step at 350 °C to remove the reactive carbon species, leaving behind the polymeric species and subsequently passivated at room temperature in a 1%O<sub>2</sub>/He mixture, before being analyzed by TEM. EELS analysis on cobalt particles revealed the presence of carbon, however EELS analysis on regions of the alumina support also showed a considerable amount

of carbon. Cobalt and carbon maps (Figure 5.10) show that carbon is distributed inhomogeneously over the sample with a large part of the carbon on the alumina support. The cobalt particles also have hydrogen resistant carbon present on them. Conventional HRTEM images also indicated that the carbon was amorphous in nature and not graphitic.

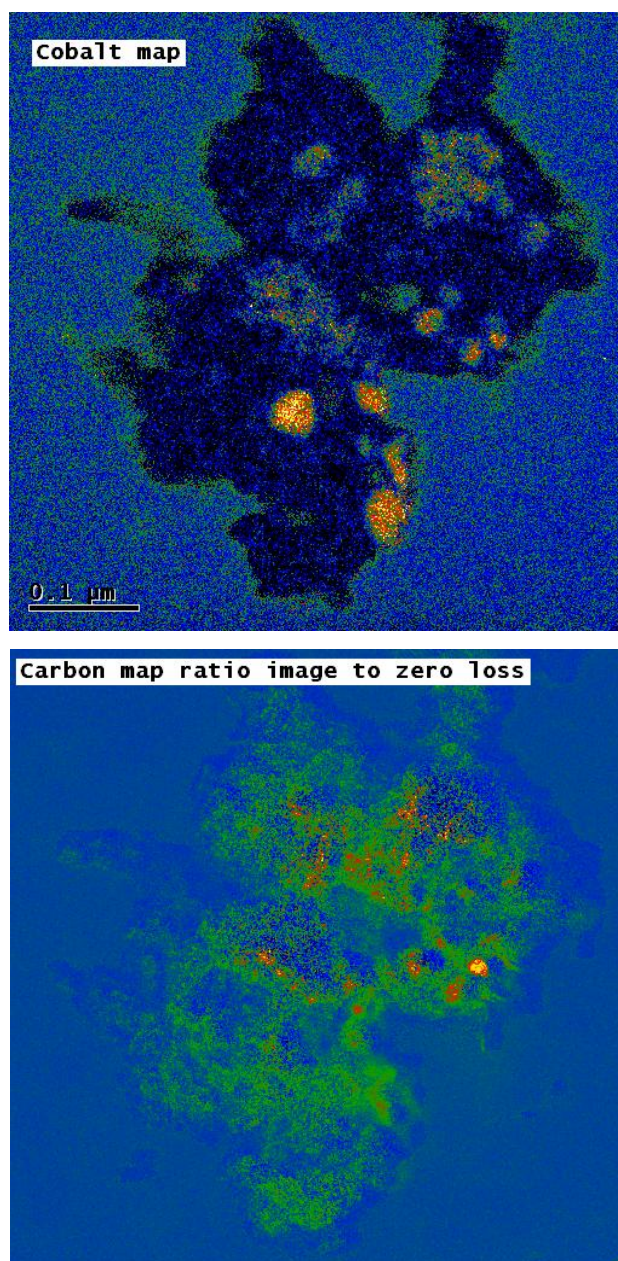


**Figure 5.10** *EFTEM cobalt (top) and carbon (bottom) maps of an end of run catalyst sample after a TPH treatment at 350 °C and passivation. The areas with the highest concentration of cobalt and carbon appear with the brightest intensity in the respective maps.*

### 5.3.6 High sensitivity low energy ion scattering (HS-LEIS) experiments to determine location of hydrogen resistant carbon at 350°C.

A catalyst sample taken from the FTS reactor at the end of the FTS run was given a hydrogenation treatment at 350 °C to remove the reactive carbon species. HS-LEIS was then used to determine where the remaining hydrogen resistant or polymeric carbon was located. No poisons were detected in the sample. Figure 5.11 shows the 3 keV  $^4\text{He}^+$  spectra for the sample after the hydrogenation treatment and after treatment with atomic oxygen. This atomic oxygen is very reactive and it has been demonstrated that at room temperature it can fully remove the hard carbon or coke [40]. The Co signal (onset at 2343 eV) is clearly visible in the hydrogenated sample. Since LEIS only probes the outermost atomic layer of the sample, if there was monolayer coverage of carbon on the surface of cobalt or if indeed all the hydrogen resistant carbon was located on the cobalt then no cobalt signal will be seen. As can be seen from Figure 5.11, the carbon peak (onset at 846 eV) disappears upon the atomic oxygen treatment, while the Al (onset at 1742 eV) and Co signals increase. From these increases it is derived that a part of the alumina surface but also the cobalt surface is covered with hydrogen resistant carbon. It seems that there is no significant preferential adsorption of the hydrogen resistant carbon on either the cobalt or the alumina surface.

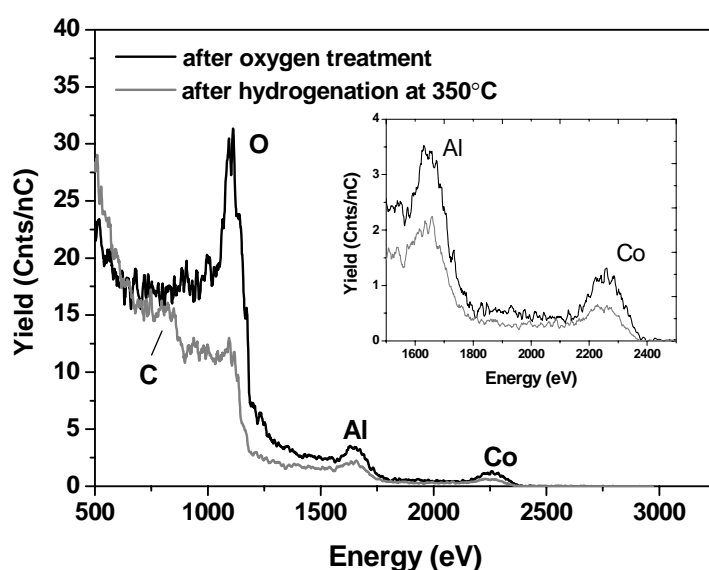


**Figure 5.11** 3 keV  $^4\text{He}^+$  HS-LEIS spectrum of a wax-extracted catalyst after hydrogenation at 350 °C to remove reactive carbon only (bottom) and after an oxygen treatment to remove the polymeric type of carbon (top). Inset: A magnification the Al and Co regions of spectrum.

### *5.3.7 Hydrogen chemisorption measurements*

The metallic surface area of the catalysts is plotted as a function of the amount of hard to remove carbon (Figure 5.12). It can be noted that the hydrogen chemisorption capacity of the catalyst decreases with increasing amount of hydrogen resistant carbon. It is well known that other phenomena like sintering and poisoning also will diminish the hydrogen chemisorption capacity of the metal. Sintering has been reported previously but is limited to the first 20 days on stream based on TEM, chemisorption, XRD and magnetic measurements [55] and levels off thereafter. Also analysis of the catalysts by XPS and a LECO elemental analyzer did not reveal any significant amounts or increase in catalyst poisons like nitrogen and sulphur. Therefore it is postulated that the observed decrease in chemisorption capacity after day 20 is due to the interaction of deleterious, polymeric carbon with metallic cobalt. Further evidence of the interaction of polymeric carbon with cobalt was obtained by comparing chemisorption measurements after reduction at 350 °C with that after reduction at 500 °C (Figure 5.13). At higher time on-stream (after the period where sintering levels off) large differences in the metallic surface areas are observed. The observed increase in the chemisorption capacity, after reduction at 500 °C is due to the removal of the polymeric carbon species interacting with cobalt. Previous TPH work (Figure 5.5) shows that a large amount of this carbon species should be removed in hydrogen at 500 °C. The difference in chemisorption capacity is not likely due to differences in the extent of reduction at 350 °C and 500 °C as the chemisorption capacity is similar for samples with shorter TOS (less than 20 days).

### *5.3.8 Regeneration of catalyst and testing in FTS*

Figure 5.14 shows the TPO profiles of a catalyst hydrogenated at 350 °C which has polymeric carbon remaining on it compared to a catalyst previously oxidized at 300 °C. As can be seen the amount of polymeric carbon species has significantly been lowered (believed to be due to the gasification of carbon on the cobalt) after the oxidation procedure. The oxidized catalyst when tested in FTS (after re-reduction) shows a 90% gain in activity. There is no gain in activity for catalyst where the carbon has been hydrogenated at 350 °C.

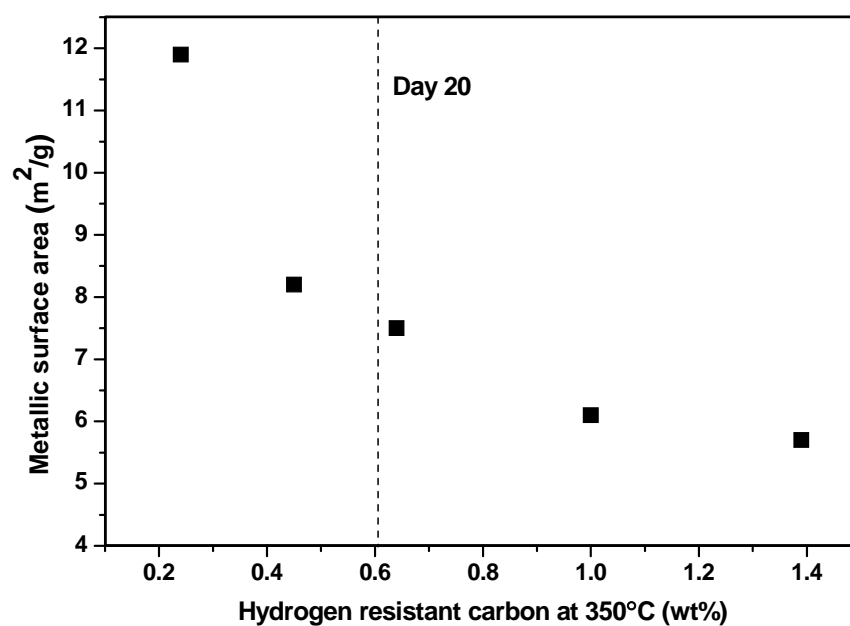


**Figure 5.12** *Metallic surface areas as a function of the hydrogen resistant polymeric carbon for a selected number of samples from the slurry bubble column. Sintering levels off around 20 days*

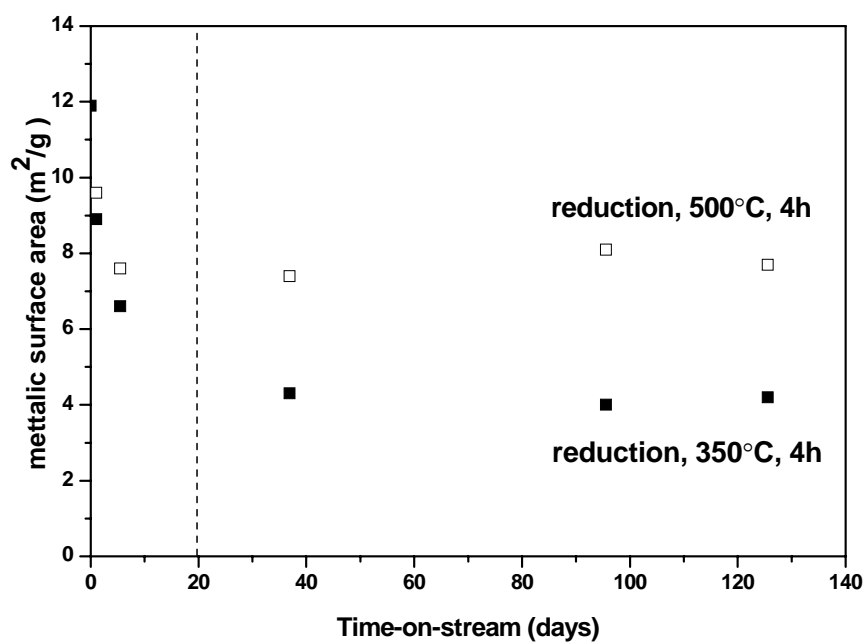


**Figure 5.13** *Metallic surface areas as a function of time on stream for a selected number of samples from the slurry bubble column after reduction at 350 °C (■) and 500 °C (□).*

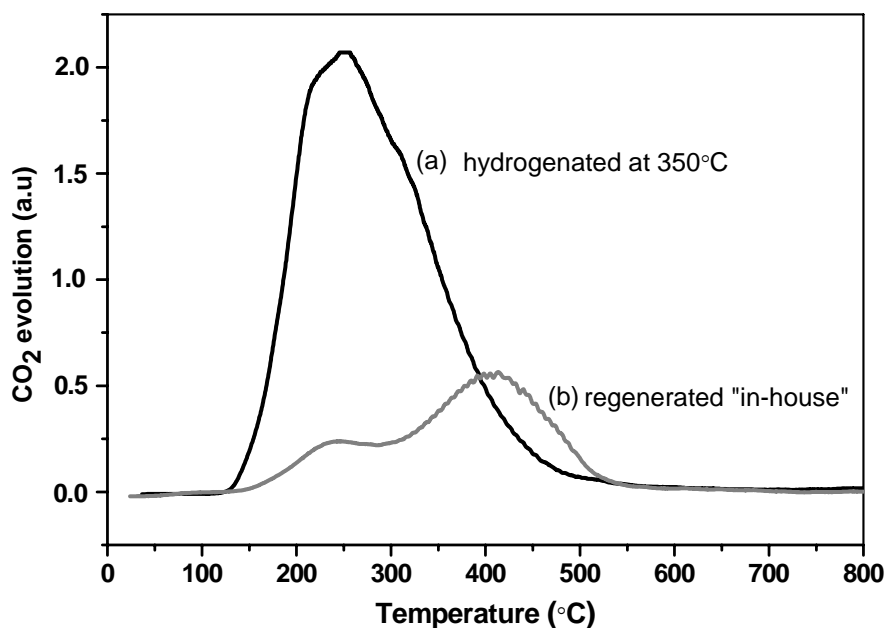


**Figure 5.14** TPO profiles of (a) a wax-extracted sample that has been hydrogenated at 350 °C compared to (b) a sample oxidized at 300 °C where part of the polymeric carbon has been removed.

#### 5.4. Discussion

During this study we have shown that:

- There is an increase in hydrogen resistant carbon with increasing time on-stream for wax-extracted cobalt catalysts tested at realistic FTS conditions in a large scale demonstration unit.
- The hydrogen resistant carbon has similar reactivity to polymeric carbon.
- This polymeric carbon is located on the support and on cobalt as evidenced by EFTEM, HS-LEIS and hydrogen chemisorption.
- Removal of the polymeric carbon results in a dramatic increase in FTS activity.

It is known that an elementary step in the Fischer-Tropsch reaction is the dissociation of CO to form surface carbidic carbon and adsorbed atomic oxygen [56]. The latter is removed from the surface through the formation of gaseous H<sub>2</sub>O and CO<sub>2</sub>

(mostly in the case of Fe catalysts). The surface carbon, if it remains in its carbidic form on the surface of the metal is a starting block in the FT synthesis and can be readily hydrogenated to form hydrocarbons. However this surface carbidic carbon may also be converted to other less reactive forms, i.e. polymeric or graphitic carbon, which may build up over time and possibly have a negative influence on catalyst activity [57]. The term polymeric carbon in the case of CO dissociation and disproportionation generally refers to chains of carbon monomers connected by covalent bonds. In the case of FTS on ruthenium catalysts polymeric carbon has been identified as a less reactive carbon that forms from polymerization of  $\text{CH}_x$  and has an alkyl group structure [58].

The three carbon peaks observed in this study during TPH experiments on spent cobalt catalyst samples were assigned to surface carbide, wax, and polymeric carbon (Table 5.2), which is in agreement with most of the literature on this topic.

**Table 5.2** *Assignment of the carbon species observed in this study with a comparison to literature.*

Peak	T <sub>Hyd</sub> (°C)	Carbon species	This study (Section)	Ref
1	250	Surface carbidic species		20
		Residual wax/hydrocarbons	Blank (5.3.2)	15
2	330	Residual wax (probably contained in small pores)		15
3	445	Polymeric carbon on cobalt	Reference samples (5.3.3)	20
			H <sub>2</sub> chemisorption (5.3.7)	
		Polymeric carbon on support	EFTEM (5.3.5) HS-LEIS (5.3.6)	

In this study we also showed the very gradual build up of a hydrogen resistant (at 350 °C) polymeric type of carbon species with time on stream. The amount of this polymeric carbon present after the hydrogenation step at 350 °C exceeds the monolayer coverage of the exposed metal surface. If we take into account the

sintering that occurs and use a 10% dispersion and a 2M coverage (maximum coverage of carbon on cobalt surface), then 2 wt% carbon on the catalyst is 2.5 times the amount which can be deposited maximum. It is thus unlikely that the hard to remove carbon is located exclusively on the metal as this will result in total deactivation of the catalyst by blocking, which is not observed. The EFTEM and HS-LEIS results show that carbon is located both on alumina and on cobalt. We believe that the carbon is most likely nucleated on cobalt sites and then migrates to the support. It has been reported previously that spill over of carbon may readily occur on alumina-supported cobalt catalysts [59].

The hydrogen chemisorption data even when considering other effects like poisoning and sintering also suggests that this polymeric carbon affects the available metallic surface area of the cobalt and hence the activity. It is believed that the accumulation of polymeric carbon on the cobalt surface will play a part in the deactivation of the catalyst. The link between the polymeric carbon and activity was then checked by monitoring the behaviour of the catalyst after removal of this carbon. A catalyst that has been regenerated to remove a large part of the polymeric carbon species exhibits a marked improvement in activity and an increase in metallic surface area. This fact along with other supporting characterization data provides strong evidence that polymeric carbon interacting with the metal plays a part in the catalyst deactivation.

## **5.5 Conclusions**

A wax-extraction procedure was developed to study Co/Pt/Al<sub>2</sub>O<sub>3</sub> FTS catalysts, covered in a wax layer, taken from a 100 bbl/day slurry bubble column reactor operated at commercially relevant FTS conditions. The wax was extracted down to low levels enabling characterization of the catalyst by both surface (XPS) and bulk techniques (TEM and TP). The carbon deposits on the wax extracted catalysts were studied using TP techniques and it was found that there is a slow accumulation of a polymeric type of carbon species on the catalyst during the extended FTS run. This carbon is resistant to hydrogen treatments at temperatures well above that used in realistic FTS. HS-LEIS and EFTEM analysis of samples containing this resistant polymeric carbon showed that it is dispersed largely over the support as well as on the



cobalt phase. A large part of the activity of the catalyst can be recovered by removal these polymeric carbon deposits and it is thus postulated that these play a role in deactivation of cobalt-based FTS catalysts in extended runs.

## Acknowledgments

We would like to thank Sanne Wijnans for her work in developing the wax-extraction procedure and the initial XPS fitting models. Prof. H.H. Brongersma and Niel Kuijpers (Calipso BV) and Dr. T. Grehl (IONTOF GmbH) are acknowledged for the HS-LEIS analysis. Sasol Technology's Materials Characterization group is thanked for the chemisorption measurements.

## 5.6 References

- [1] A.P. Steynberg, M.E. Dry (Eds.), Fischer-Tropsch Technology, Studies in Surface Science and Catalysis, Vol. 152, Elsevier, 2004.
- [2] E. Iglesia, Appl. Catal. A 161 (1997) 59.
- [3] M.E. Dry, Catal. Today 71 (2002) 227.
- [4] J. van de Loosdrecht, B. Balzhinimaev, J.-A. Dalmon, J.W. Niemantsverdriet, S.V. Tsybulya, A.M. Saib, P.J. van Berge, J.L. Visagie, Catal. Today 123 (2007) 293.
- [5] Fischer Tropsch Catalyst Test on Coal-Derived Synthesis Gas, Syntroleum Corporation, November 2007 accessed on <http://www.syntroleum.com>.
- [6] P.J. van Berge, J. van de Loosdrecht, S. Barradas, A.M. van der Kraan, Catal. Today 58 (2000) 321.
- [7] G. Jacobs, T.K. Das, P.M. Patterson, J. Li, L. Sanchez, B.H. Davis, Appl. Catal. A 247 (2003) 335.
- [8] G. Kiss, C.E. Kliewer, G.J. DeMartin, C.C. Culross, J.E. Baumgartner, J. Catal. 217 (2003) 127.
- [9] A.M. Hilmen, D. Schanke, K.F. Hanssen, A. Holmen, Appl. Catal. A 186 (1999) 169.
- [10] J. Li, X. Zhan, Y. Zhang, G. Jacobs, T. Das, B.H. Davis, Appl. Catal. A 228 (2002) 203.
- [11] A.M. Saib, A. Borgna, J. van de Loosdrecht, P.J. van Berge, J.W. Niemantsverdriet, Appl. Catal. A 312 (2006) 12.
- [12] A.M. Saib "Towards a cobalt FTS catalyst with enhanced stability: a combined approach" Phd Thesis, Eindhoven University of Technology, 2006.
- [13] P.G. Menon, J. Mol. Catal. 59 (1990) 207.
- [14] A.A. Adesina, R.R. Hudgins, P.L. Silveston, Catal. Today 25 (1995) 127.
- [15] V. Gruver, R. Young, J. Engman, H.J. Robota, Prepr. Pap.-Am. Chem. Soc., Div. Pet. Chem. 50 (2005) 164.
- [16] J.J.H.M. Font Freide, T.D. Gamlin, R.J. Hensman, B. Nay, C. Sharp, J. Nat. Gas Chem. 13 (2004) 1.
- [17] S.L. Soled, E. Iglesia, R. Fiato, G.B. Ansell, United States Patent 5 397 806 (1995), to Exxon.
- [18] M.J. van der Burgt, J. Ansorge, Great Britain Patent 2 222 531 (1988), to Shell.
- [19] H.A. Wright, United States Patent 6 486 220 B1 (2002), to Conoco.
- [20] D.-K. Lee, J.-H. Lee, S.-K. Ihm, Appl. Catal. 36 (1988) 199.
- [21] H.W. Pennline, R.J. Gormley, R.R. Schehl, Ind. Eng. Chem. Prod. Res. Dev. 23 (1984) 388.
- [22] P.K. Agrawal, J.R. Katzer, W.H. Manogue, J. Catal. 69 (1981) 312.
- [23] M.K. Niemela, A.O.I. Krause. Catal. Lett. 42 (1996) 161.
- [24] H.W. Pennline, S.S. Pollack, Ind. Eng. Chem. Prod. Res. Dev. 25 (1986) 11.
- [25] C.H. Bartholomew, Appl. Catal. A 212 (2001) 17.
- [26] M.C. Zonneville, J.J.C. Geerlings, R.A. van Santen, Surf. Sci. 240 (1990) 253.

- [27] I.M. Ciobica, R.A. van Santen, P.J. van Berge, J. van de Loosdrecht, *Surf. Sci.* 602 (2008) 17.
- [28] L.J.E. Hofer, W.C. Peebles, *J. Am. Chem. Soc.* 69 (1947) 893.
- [29] S. Weller, L.J.E. Hofer, R.B. Anderson, *J. Am. Chem. Soc.* 70 (1948) 799.
- [30] J. Xiong, Y. Ding, T. Wang, L. Yan, W. Chen, H. Zhu, Y. Lu, *Catal. Lett.* 102 (2005) 265.
- [31] V. Gruver, X. Zhan, J. Engman, H.J. Robota, *Prepr. Pap.-Am. Chem. Soc., Div. Pet. Chem.* 49 (2004) 192.
- [32] O. Ducreux, J. Lynch, B. Rebours, M. Roy, P. Chaumette, *Stud. Surf. Sci. Catal.* 119 (1998) 1258.
- [33] G. Jacobs, P.M. Patterson, Y. Zhang, T. Das, J. Li, B.H. Davis, *Appl. Catal. A* 233 (2002) 215.
- [34] P.J. van Berge, J. van de Loosdrecht, J.L. Visagie, United States Patent 6 806 226 (2004), to Sasol.
- [35] P.J. van Berge, J. van de Loosdrecht, E. Caricato, S. Barradas, B.H. Sigwebela, United States Patent 6 455 462 (2002), to Sasol.
- [36] P.J. van Berge, J. van de Loosdrecht, E. Caricato, S. Barradas, United States Patent 6 638 889 (2004), to Sasol.
- [37] R.L. Espinoza, J.L. Visagie, P.J. van Berge, F.H. Bolder, United States Patent 5 733 839 (1998), to Sasol.
- [38] P.J. van Berge, J. van de Loosdrecht, J.L. Visagie, T.J. van der Walt, H. Veltman, C. Sollie, European Patent 1 444 040 B1 (2003), to Sasol.
- [39] H.H. Brongersma, M. Daxler, M. de Ridder, P. Bauer, *Surf. Sci. Rep.* 62 (2007) 63.
- [40] J.M.A. Harmsen, W.P.A. Jansen, J.H.B.J. Hoebink, J.C. Schouten, H.H. Brongersma, *Catal. Lett.* 74 (2001) 133.
- [41] J.W. Niemantsverdriet, *Spectroscopy in Catalysis*, 3rd ed., Wiley-VCH, Weinheim, 2007.
- [42] G. Fierro, M.L. Jacono, M. Inversi, P. Porta, *Top. Catal.* 10 (2000) 39.
- [43] Z. Zsoldos, L. Guzzi, *J. Phys. Chem.* 96 (1992) 9393.
- [44] B. Ernst, L. Hilaire, A. Kiennemann, *Catal. Today* 50 (1999) 413.
- [45] A.M. Saib, A. Borgna, J. van de Loosdrecht, P. van Berge, J.W. Niemantsverdriet, *J. Phys. Chem. B.* 110 (2006) 8657.
- [49] G.V. Pankina, P.A. Chernavskii, A.S. Lermontov, V.V. Lunin, *Petrol. Chem.* 42 (2002) 217.
- [50] F. Tihay, G. Pourroy, M. Richard-Plouet, A.C. Roger, A. Kiennemann, *Appl. Catal. A* 206 (2001) 29.
- [51] J. Xu, C.H. Bartholomew, *J. Phys. Chem. B* 109 (2005) 2392.
- [52] A. Barbier, A. Tuel, I. Arcon, A. Kodre, G.A. Martin, *J. Catal.* 200 (2001) 106.
- [53] J. Goralski, J. Grams, T. Paryjczak, I. Rzeźnicka, *Carbon* 40 (2002) 2025.
- [54] D.J. Moodley, C. van Schalkwyk, A. Spamer, J.M. Botha, A.K. Datye, *Appl. Catal. A* 318 (2007) 155.
- [55] M.J. Overett, B. Breedts, E. du Plessis, W. Erasmus, J. van de Loosdrecht, *Prepr. Pap.-Am. Chem. Soc., Div. Pet. Chem.* 53 (2008) 126.
- [56] B.H. Davis, *Fuel Proc. Tech.* 71 (2001) 157.
- [57] D.W. Goodman, R.D. Kelley, T.E. Madey, J.T. Yates Jr., *J. Catal.* 63 (1980) 226.
- [58] P. Winslow, A.T. Bell, *J. Catal.* 91 (1985) 142.
- [59] G. Boskovic, K.J. Smith, *Catal. Today* 37 (1997) 25.



---

# Chapter 6

---

## Factors that influence carbon formation on Co/Al<sub>2</sub>O<sub>3</sub> catalysts

---

*Cobalt-based Fischer-Tropsch synthesis (FTS) catalysts are the preferred systems for use in gas-to-liquids processes. However, the activity of these catalysts typically declines with time-on-stream due to catalyst deactivation. In Chapter 5, carbon deposition has been put forward as a plausible deactivation mechanism for cobalt catalysts under realistic conditions. Understanding the factors that contribute toward carbon deposition will be an important step in trying to extend the lifespan of cobalt-based FTS catalysts. In this study, we report on the impact of temperature and H<sub>2</sub>/CO ratio on the build-up of carbonaceous species on Co/Pt/Al<sub>2</sub>O<sub>3</sub> catalysts using both model (1 bar) and realistic (20 bar) FTS tests. The influence of upset conditions on carbon deposition and its subsequent effect on catalyst structure was also investigated. Temperature programmed hydrogenation and oxidation (TPH/O), X-ray diffraction (XRD), X-ray photoelectron spectroscopy (XPS) and transmission electron microscopy (TEM) were used to characterise the carbonaceous phases. It was found that both temperature and gas composition play important roles in determining the amount and reactivity of carbon deposits on Co/Pt/Al<sub>2</sub>O<sub>3</sub> catalysts. Upset conditions, even if they occur over short periods result in the production of carbon phases that can be detrimental to catalyst activity.*

---

## 6.1 Introduction

Fischer–Tropsch synthesis (FTS) is a promising way to convert coal, biomass and natural gas to clean fuels and chemicals via syngas. Cobalt-based catalysts attract most of the current attention for the conversion of natural gas-derived syngas in FTS because of their high activity, high selectivity for long chain paraffins, and low water gas shift activity [1]. As cobalt is a relatively expensive metal, high stabilised lifetimes are required for commercial application [2].

One of the factors that may impact on the activity of cobalt catalysts is the accumulation of carbon deposits. Although cobalt-based FTS is in general viewed as a carbon-insensitive reaction [3], a few research groups have shown that deleterious carbon can form on cobalt catalysts [4-8]. Font Freide et al. [4] mentioned that the extremely low levels of carbonaceous species deposit on the cobalt active sites, which led to the deactivation of Co/ZnO catalysts during extended runs. Deactivation of a Co/Al<sub>2</sub>O<sub>3</sub> catalyst due to geometric blocking by polymeric or graphitic carbon was also reported by Gruver et al. [5]. Furthermore, upset conditions during FTS may result in temperature excursions or unfavourable gas compositions that result in accelerated deposition of unwanted carbonaceous species, which may affect catalyst structure and activity [9, 10].

Reaction temperature and H<sub>2</sub>/CO ratio are believed to be important parameters that will influence carbon deposition on FT catalysts. The formation temperature plays an important role in determining the amount and type of carbon deposit. Generally, at higher temperatures the amount of carbon will increase as the rate of CO dissociation will be higher [11]. However, as shown for a Ru/Al<sub>2</sub>O<sub>3</sub> catalyst, carbon deposition varies as a function of partial pressures of CO and H<sub>2</sub> in the gas phase [12]. It was stated that the higher conversion at higher temperatures results in a corresponding decrease in  $P_{\text{CO}}$  and  $P_{\text{H}_2}$ , and may therefore lead to smaller amounts of carbon on the catalyst [12]. Thus the rate of carbon formation and its subsequent hydrogenation can lead to a complex relationship between the amount of carbon and the reaction temperature. At high reaction temperatures shorter hydrocarbon chains will be formed and rapidly desorbed [13]. However, higher temperatures will also aid

in the transformation of surface carbon species into more stable species that will have decreased reactivity towards H<sub>2</sub> [12, 14].

Lahtinen et al. [15, 16] investigated the effect of varying reaction temperature on polycrystalline cobalt foil at 1 bar and H<sub>2</sub>/CO ratio of 1.24. The cobalt surface was then characterized by Auger electron spectroscopy (AES) after the reaction without any further sample treatment. They found that the carbon/cobalt ratio was almost constant as temperature was increased to 252 °C. No significant deactivation for CO hydrogenation was observed on the foils at these conditions. Deactivation of the cobalt surface by graphitic carbon was observed at 276 °C. At 297 °C the carbon/cobalt ratio was significantly higher. From the peak shape of the carbon KLL Auger lines it was deduced that carbon formed at 297 °C was graphitic.

The literature on the effect of H<sub>2</sub>/CO ratios on carbon deposition on cobalt-based FTS catalysts is scarce. A few studies have been conducted on Ni/Al<sub>2</sub>O<sub>3</sub> [17, 18] and Fe/Al<sub>2</sub>O<sub>3</sub> [19, 20]. The general view is that small amounts of H<sub>2</sub> enhance carbon deposition from CO. Bianchi and Bennet [19] reported that the rate of carbon deposition (compared to deposition with pure CO) was enhanced on Fe/Al<sub>2</sub>O<sub>3</sub> at H<sub>2</sub>/CO = 0.1. This was attributed to the hydrogen-assisted dissociation of CO. Presumably, small amounts of hydrogen remove oxygen from the surface creating sites for further CO dissociation. The low hydrogen amount is insufficient to hydrogenate off the carbon formed on the surface. Excess hydrogen, on the other hand acts to keep the metal surface free from carbonaceous species by reacting them away to form methane or hydrocarbons. Investigations on Ni/Al<sub>2</sub>O<sub>3</sub> showed that the rate of carbon deposition is lower at higher H<sub>2</sub>/CO ratios [17, 18]. Ideally, to prevent deactivation by carbon there should be higher rate of hydrogenation of the surface carbon than of its conversion to polymeric carbon and other stable carbon species.

A few studies have been conducted recently on the influence of H<sub>2</sub>/CO ratio on activity and product selectivity of cobalt FTS catalysts but these do not report on the impact on carbon deposition. Tristantini et al. [21] showed with a Co/Al<sub>2</sub>O<sub>3</sub> catalyst that CO conversion increases with increasing H<sub>2</sub>/CO ratio in the feed. Low ratios resulted in a slight increase in the water gas shift activity (more CO<sub>2</sub>) and increase in C<sub>5+</sub> selectivity. Calleja et al. [22] and Schulz [11] also showed that lower

H<sub>2</sub>/CO ratios favoured longer chain products. It was also claimed that higher H<sub>2</sub>/CO ratios caused catalyst deactivation through the formation of silicates on Co/SiO<sub>2</sub> catalysts [23].

In this study we report on the impact of temperature and H<sub>2</sub>/CO on the build-up of carbonaceous species on Co/Al<sub>2</sub>O<sub>3</sub> using both model (1 bar) and realistic (20 bar) FTS tests. We also focus some attention on the influence of upset conditions on carbon deposition and its subsequent effect on catalyst structure. Temperature programmed hydrogenation and oxidation (TPH/O), X-ray diffraction (XRD), X-ray photoelectron spectroscopy (XPS) and transmission electron microscopy (TEM) were used to characterise the carbonaceous phases.

## 6.2 Experimental

### 6.2.1 Catalyst preparation

A 20 wt% Co/Al<sub>2</sub>O<sub>3</sub> catalyst, promoted with 0.05 wt% platinum, was prepared by slurry impregnation of a  $\gamma$ -alumina support (Puralox 5/150 from Sasol Germany) with an aqueous cobalt nitrate solution, also containing the platinum promoter. After impregnation and drying, the catalyst intermediate was calcined at 250 °C in air and reduced in pure hydrogen at 425 °C. To achieve the required cobalt loading, two impregnation and calcination steps were applied [24-28]. A 15 wt% Co/Al<sub>2</sub>O<sub>3</sub> catalyst, promoted with 0.04 wt% platinum was also prepared in a similar way with a single impregnation step of Pural SB alumina (Sasol Germany), which was calcined at 700 °C for 4h.

### 6.2.2 Model FTS experiments with varying temperature and H<sub>2</sub>/CO ratio

To investigate the effect of temperature in the FTS range, in-situ reduction/FTS/TPH experiments were performed in a TP-MS unit at atmospheric pressure. A 100 mg sample of 20 wt% Co/Pt/Al<sub>2</sub>O<sub>3</sub> was reduced by ramping under pure H<sub>2</sub> (10ml/min) to 450 °C at a rate of 5 °C/min and held at this temperature for 1h. The reduction seems to be complete at this stage as the evolution of water is complete as observed in a typical water profile for the TPR. Peaks are observed at 225 °C corresponding to the reduction of Co<sub>3</sub>O<sub>4</sub> to CoO and 370 °C corresponding to the reduction of CoO to metallic cobalt [29]. Thereafter the reactor was cooled under H<sub>2</sub> to the desired

reaction temperature (200-260 °C) and FTS was performed using a flow of CO (~5 ml/min) and H<sub>2</sub> (~ 4 ml/min) in helium (6 ml/min) at a H<sub>2</sub>/CO ratio of 0.75. The conversion level in this set of experiments was not kept constant, since the flow rate of the synthesis gas mixture was kept constant. The reactor was then cooled in helium to RT and then a TPH was performed by heating to 800 °C (10 °C/min) using a 50% H<sub>2</sub>/He flow (20 ml/min).

For experiments with varying H<sub>2</sub>/CO ratios the same amount of catalyst was reduced as above. The catalyst is then cooled to 230 °C in H<sub>2</sub>, before switching to the desired H<sub>2</sub>/CO ratio for a period of 3h. The flow of CO (5 ml/min, P<sub>CO</sub> = 0.33 bar) as well as the total flow (15 ml/min, SV = 9000 ml/g<sub>cat</sub>/h) is kept constant by addition of He, while the flow of hydrogen is varied between 2.5-10 ml/min (P<sub>H<sub>2</sub></sub> = 0.17-0.66 bar). This was done to ensure that effects seen are not due to the variation in the amount of CO exposed or residence time. During this time water, methane and other hydrocarbons are evolved as the expected products of the FTS. The reactor was then cooled in helium to RT and then a TPH was performed as described above.

### *6.2.3 FTS runs in a CSTR at varying temperature*

Fischer–Tropsch synthesis tests were performed in a slurry-phase CSTR with a reactor volume of 670 ml. The catalyst samples (i.e. 10–30 g) were pre-reduced at 380 to 425 °C for 16 h, in pure hydrogen at 1 bar, at a heating rate of 1°C/min, and suspended, under an argon blanket, in 300 ml molten Fischer–Tropsch hydrogenated wax (Sasol H1 hard wax) inside the reactor. The FTS conditions employed were 240-270 °C, 20 bar, commercial synthesis gas as feed of composition: 50-60 vol% H<sub>2</sub>, 25-35 vol% CO and 10 vol% inerts. The synthesis gas flows were regulated by Brooks mass-flow controllers and was adjusted to keep the conversion levels the same. Samples of the spent catalysts tested at various temperatures were taken from the slurry-phase CSTR at the end of the reaction. The catalyst/wax mixture was allowed to congeal under an inert nitrogen environment. The catalyst was then wax extracted in an inert argon environment and then subjected to a TPH at 350 °C and held there for 1h (as in Chapter 5). A TPO was then done to determine the remaining hydrogen-resistant carbon.



#### 6.2.4 FTS run in a CSTR with interrupted $H_2$ flow.

An FTS run was conducted as described above at 230 °C, 20 bar, commercial synthesis gas as feed of composition: 50-60 vol%  $H_2$ , 25-35 vol% CO and 10 vol% inerts. After 40h the  $H_2$  flow was stopped for 2h. Thereafter the  $H_2$  flow was reintroduced and the reaction was run for a total of 134 hours. After completion of the reaction the catalyst/wax mixture was allowed to congeal under an inert nitrogen environment. The catalyst was then analysed by XRD.

#### 6.2.5 Boudouard reaction at various temperatures.

To simulate the effect of very high carbon coverages and upset conditions, about 1g of a 15 wt% Co/Pt/ $Al_2O_3$  catalyst was first reduced at 450 °C and then exposed to CO for 4 h at 250, 350 and 400 °C in a flow reactor coupled to a mass spectrometer. The catalyst was then cooled to room temperature and passivated in a dilute 0.1% $O_2$ /Ar mixture. Thereafter TPH, XPS and TEM analysis was performed to characterize the carbonaceous phases formed on the catalyst.

#### 6.2.6 X-ray photoelectron spectroscopy measurements

The passivated catalyst samples were crushed finely with a pestle and mortar and the powder was pressed into an indium layer on top of standard stainless steel XPS stubs. The XPS measurements were carried out using a VG Escalab 200 MKII spectrometer. An aluminum anode ( $K_\alpha = 1486.6$  eV) was used to generate the X-ray radiation (240 W (20 mA; 12kV)). Measurements were carried out with a 0.1 s dwell time and 0.1 eV step for the selected regions. To obtain sufficient signal-to-noise ratio the Co 2p region was scanned 50 times. During the measurements the pressure in the main chamber remained below  $10^{-8}$  mbar.

#### 6.2.7 X-ray diffraction measurements

The experiments were done using an Anton Paar HTK600 coupled to the Philips X'Pert Pro multi-purpose diffractometer (XRD-1). The XRD patterns of the catalyst coated in wax were obtained in a dry nitrogen atmosphere at 120 °C. At this

temperature the crystalline wax on the catalyst is melted and its strong diffraction features can be eliminated allowing detection of other crystalline phases. Use was made of X-rays generated from a fine focus cobalt tube (wavelength 1.79 Å). The peaks on the diffractograms were identified using the JCPDS database.

#### *6.2.8 TEM measurements*

Thin samples for TEM were prepared by crushing the passivated catalyst with a mortar and pestle, followed by dispersion in ethanol using an ultrasound bath. Then an appropriate amount of sample was placed onto a copper microscope grid covered with carbon windows. Samples were studied using a Fei Tecnai 20F (type Sphera) microscope with an acceleration voltage of 200 keV.

### **6.3 Results and Discussion**

#### *6.3.1 Effect of FTS temperature on carbon deposition*

##### *(a) Model conditions*

The effect of temperature on the amount and type of carbon deposited on a 20 wt% Co/Pt/Al<sub>2</sub>O<sub>3</sub> catalyst was investigated under model conditions: a relatively low H<sub>2</sub>/CO ratio of 0.75, 1 bar total pressure, to enhance the carbon deposition in the short reaction time of 3 h. The temperature was varied between 200 and 260 °C in steps of 20 °C. After the model FTS reactions a TPH profile was measured. The impact of the temperature on carbon can be seen in Figure 6.1. It is clear that reaction temperature during these model FTS conditions has an influence on the amounts and nature of carbon formed on the catalyst. The first noticeable feature in the TPH profile is the decrease in the methane peak around 195 °C and increase in amount of methane produced after 240 °C at higher temperatures. The carbon produced at higher reaction temperatures becomes more difficult to hydrogenate as indicated by a shift in the methane evolution to higher temperatures (See inset Figure 6.1). Increasing temperature results in the transformation of reactive species to less reactive species. The inset shows the evolution of various carbon species at the higher FTS temperatures. Polymeric carbon, which according to literature is hydrogenated at 430 ± 10 °C [30, 31] seems to form during FTS at 240 °C and to a greater extent at 260 °C.

The total amount of carbon on the catalyst seems to decrease with increasing FTS temperature at 220 and 240 °C (Figure 6.2a). At higher FTS temperatures more methane is produced and also the amount of hydrocarbon species on the catalyst is reduced due to enhanced desorption and hydrogenation. However, at 260 °C the active carbon formed from CO dissociation is rapidly transformed to more stable species and the carbon amount on the catalyst increases. An increased transformation of reactive carbon species to more stable species with higher FTS temperatures (> 220 °C) can clearly be seen in Figure 6.2b.

The exact mechanism of this transformation of reactive atomic carbon to more stable polymeric carbon is not clear. McCarty and Wise [31] observed a slow transformation of active carbon to the inactive carbon species on Ni/Al<sub>2</sub>O<sub>3</sub> upon prolonged exposure to an inert atmosphere. Winslow and Bell [32] proposed a reversible transformation of the active carbon species to the inactive form through a CH<sub>x</sub>-type intermediate. The forward and reverse rates of this transformation are assisted by adsorbed hydrogen. However it was also argued that the transformation of the active (C<sub>α</sub>) carbon to inactive (C<sub>β</sub>) carbon is assisted by gas-phase CO [12, 33]. Regardless of the exact mechanism of the transformation of active carbon to stable carbon, these model experiments indicate that to prevent unwanted carbon formation, FTS should be performed at temperatures as low as possible.

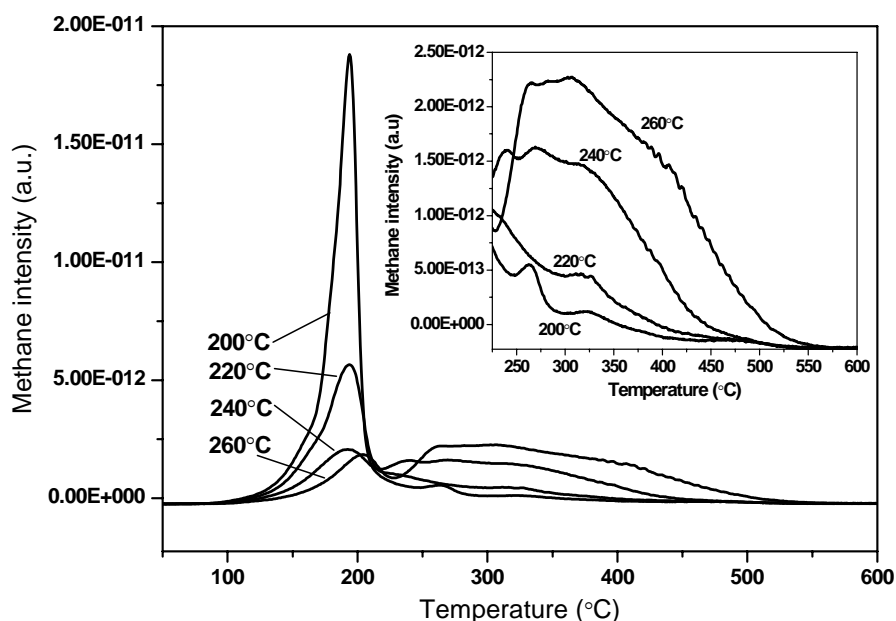


**Figure 6.1** Methane TPH profiles of 20 wt% Co/Pt/Al<sub>2</sub>O<sub>3</sub> catalysts after 3 hours of FTS at various temperatures using a H<sub>2</sub>/CO ratio of 0.75 at 1bar.

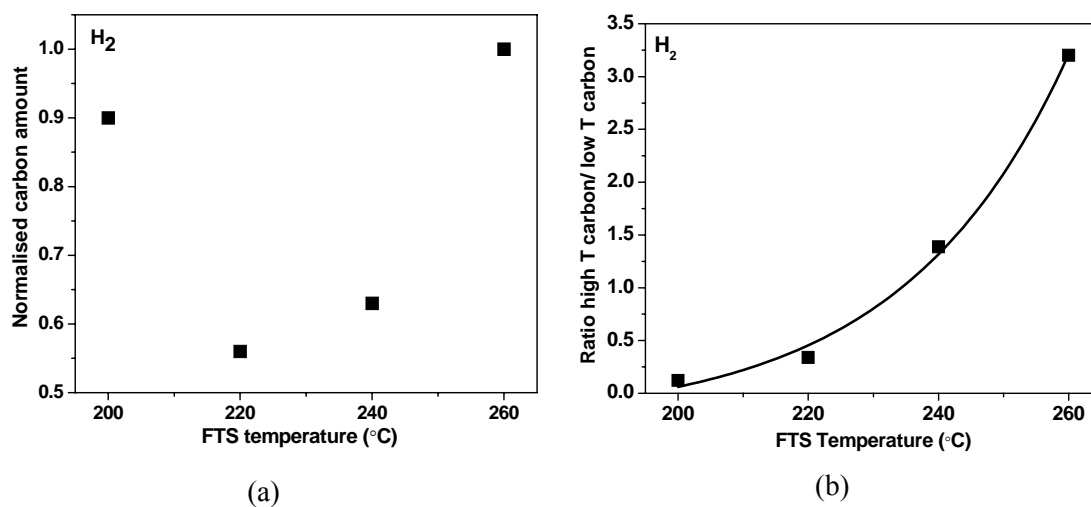


**Figure 6.2** (a) Normalised total carbon amount based on area under TPH curves. (b) The ratio of high temperature carbon (hydrogenated > 250 °C) to low temperature carbon (hydrogenated < 250 °C) as a function of FTS temperature (H<sub>2</sub>/CO = 0.75, 1 bar).

(b) *Effect of temperature on carbon in runs at realistic FTS pressures in a CSTR*

FTS runs were conducted close to realistic conditions in a slurry reactor. The runs were conducted at 240, 260 and 270 °C for around 20 days. The conversion was kept constant during the runs by adjusting the flow rate of synthesis gas. This will prevent changes in  $P_{H_2}$  and  $P_{CO}$  that may occur at higher conversions as described in the experiment in Section 6.1. The partial pressures of  $H_2$ ,  $CO$  and  $H_2O$  were more or less constant during the three runs (Table 6.1) and any effects seen are thus due to temperature and not partial pressures. An increase in methane is expected with an increase in reaction temperature and this is indeed observed. Afterwards the catalysts were unloaded, then wax-extracted, subjected to a TPH at 350 °C for 1 h, cooled to RT, flushed with He and then subjected to a TPO to determine the polymeric carbon present on the catalyst (As described in Chapter 5). It can be seen from Figure 6.3 that the amount of polymeric carbon increases with increasing reaction temperature. An activation energy of 69 kJ/mol for the formation polymeric carbon was calculated from the data.

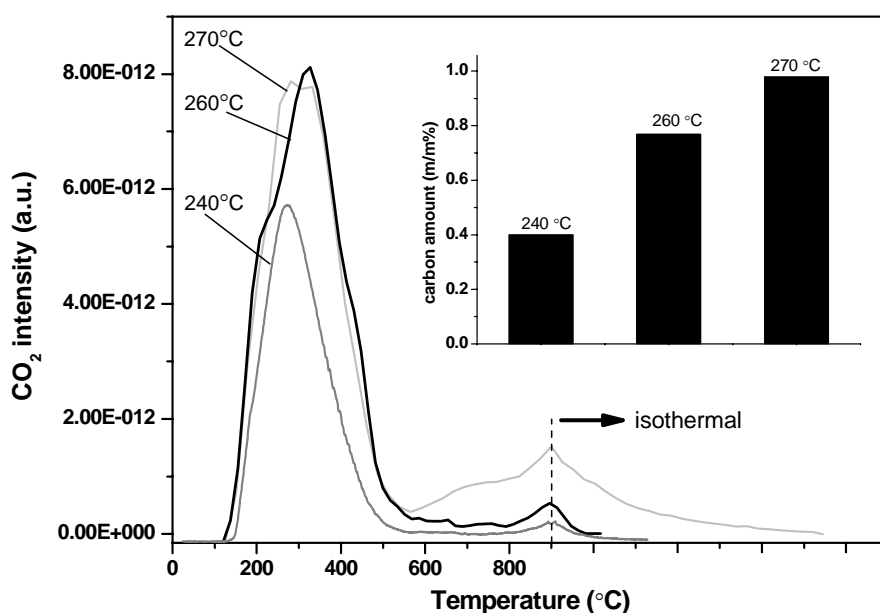


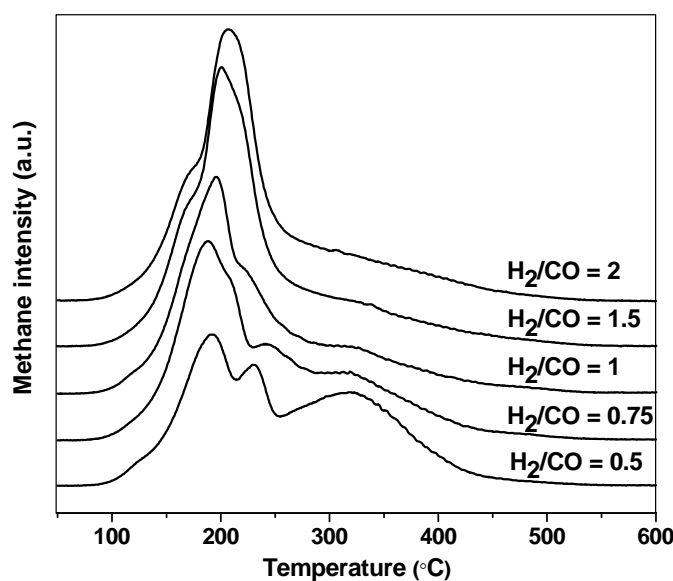
**Figure 6.3** TPO (after TPH to 350 °C) of 20 wt% Co/Pt/Al<sub>2</sub>O<sub>3</sub> catalysts tested in three FTS runs conducted at various temperatures (240-270 °C, 20 bar,  $H_2/CO = 1.6$ ). Inset: carbon amounts on the catalyst determined from CO<sub>2</sub> evolution.

**Table 6.1** *Partial pressures, methane selectivity and amount of polymeric carbon on 20 wt% Co/Pt/Al<sub>2</sub>O<sub>3</sub> catalysts for FTS runs at various temperatures. (Inlet H<sub>2</sub>/CO ratio = 1.6, 20 bar)*

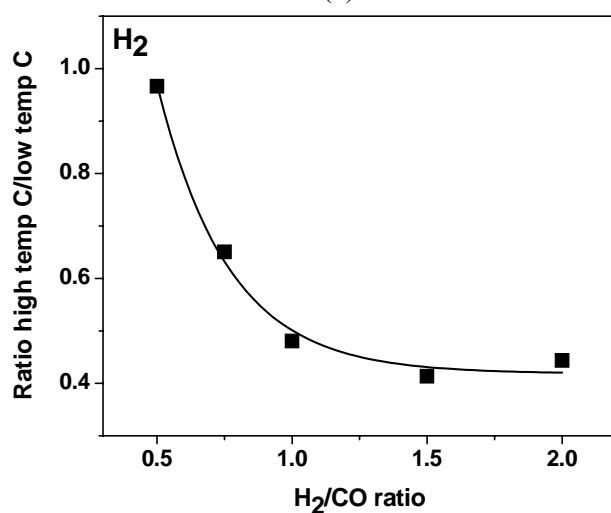
Temperature	$P_{H_2}$	$P_{CO}$	$P_{H_2O}$	Av. CH <sub>4</sub> selectivity (%)	polymeric carbon (wt%)
	(bar)				
240	4.1	3.7	4.2	7.9	0.40
260	4.3	3.7	4.0	15.5	0.77
270	4.1	3.9	4.3	19.0	0.98

### 6.3.2 Effect of H<sub>2</sub>/CO ratio (model FT conditions)

Model experiments were performed on a 20 wt% Co/Al<sub>2</sub>O<sub>3</sub> catalyst to study the impact of H<sub>2</sub>/CO ratio on the formation of carbon. The experiments were executed at 230 °C, 1 bar, and varying the H<sub>2</sub>/CO ratio between 0.5 and 2.0. The TPH profiles are shown in Figure 6.4a. Various types of carbon species, based on their reactivity to hydrogen are observed. The amount of reactive carbon that is hydrogenated below 250 °C decreases with decreasing H<sub>2</sub>/CO ratio. The main peak at ~200 °C is probably associated to an extent with the hydrogenation of surface carbide (atomic carbon) which is known to hydrogenated at 190 ± 10 °C [30]. It is also noted that the shoulder peak at around 220 °C becomes more pronounced at lower ratios and could be due to the hydrogenation of longer hydrocarbons that are favoured at lower H<sub>2</sub>/CO ratios. There is not a large difference between the methane profiles for H<sub>2</sub>/CO ratios of 2 and 1.5. The fraction of harder to remove carbon (320 °C) is most pronounced at H<sub>2</sub>/CO ratios of 0.75 and 0.5. The total amount of carbon on the catalysts, based on the area under the methane curves is very similar. However, it is clear from Figure 6.4b that more stable species are formed at the expense of more reactive species at lower H<sub>2</sub>/CO ratios. It is therefore implied that lower H<sub>2</sub>/CO ratios (< 0.75) favour higher amounts of difficult to remove carbon which might have a negative impact on both the selectivity stability and the activity stability.



(a)



(b)

**Figure 6.4** (a) TPH profile of 20 wt% Co/Pt/Al<sub>2</sub>O<sub>3</sub> catalysts tested in model FTS at different H<sub>2</sub>/CO ratios (230 °C, 1 bar). The P<sub>CO</sub> was kept constant at 0.33 bar while P<sub>H<sub>2</sub></sub> was varied between 0.17-0.66 bar. (b) The ratio of high temperature carbon (hydrogenated > 250 °C) to low temperature carbon (< 250 °C) as a function of H<sub>2</sub>/CO ratio during FTS at 230 °C, 1 bar.

### 6.3.3 Effect of interruption of hydrogen

During a laboratory FTS run at 230 °C and 20 bar in a CSTR, using a 20 wt% Co/Al<sub>2</sub>O<sub>3</sub> catalyst, the H<sub>2</sub> flow was stopped for around 2 h and then continued again. This was done in order to monitor changes that may occur in catalyst activity when the catalyst is exposed to CO only for a brief period. Figure 6.5 shows the activity profile and methane selectivity during the run. After the hydrogen flow is stopped there is a dramatic decrease (70%) in the catalyst activity. Upon reintroduction of hydrogen flow, the activity increases slowly, but the catalyst does not fully recover from the upset for the duration of the run. The selectivity to methane also increases after the catalyst is exposed to CO only. The stopping of the H<sub>2</sub> flow had a severe

effect on catalyst activity, which could not be reversed by switching back to the standard  $\text{H}_2/\text{CO}$  ratio.

The spent catalyst was analyzed by XRD (Figure 6.6) to observe changes that may have occurred and showed the presence of peaks characteristic of Co, CoO, and alumina, but also of cobalt carbide (i.e.  $\text{Co}_2\text{C}$ ). A large portion of the cobalt was in the form of bulk carbide (Table 6.2). This experiment illustrates that the formation of bulk carbide, facilitated by upset conditions can be accompanied by deactivation and selectivity changes. Although bulk cobalt carbide is reported to metastable [34], if it forms it seems to be stable in the presence of  $\text{H}_2/\text{CO} = 2$  at 230 °C for a considerable period of time. The bulk carbide can be removed by hydrogenation in pure  $\text{H}_2$  as previously reported which results in hcp cobalt and methane [10].

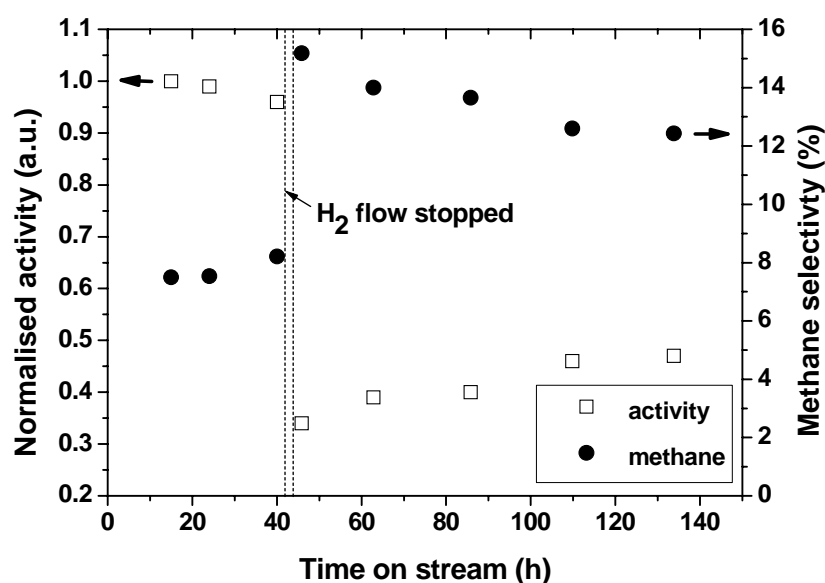


**Figure 6.5** Activity profile and methane selectivity of a FTS run at 230 °C,  $\text{H}_2/\text{CO} = 2$ , 20 bar showing drop in activity after stopping  $\text{H}_2$  flow for 2h. The  $\text{H}_2$  flow was reintroduced thereafter.



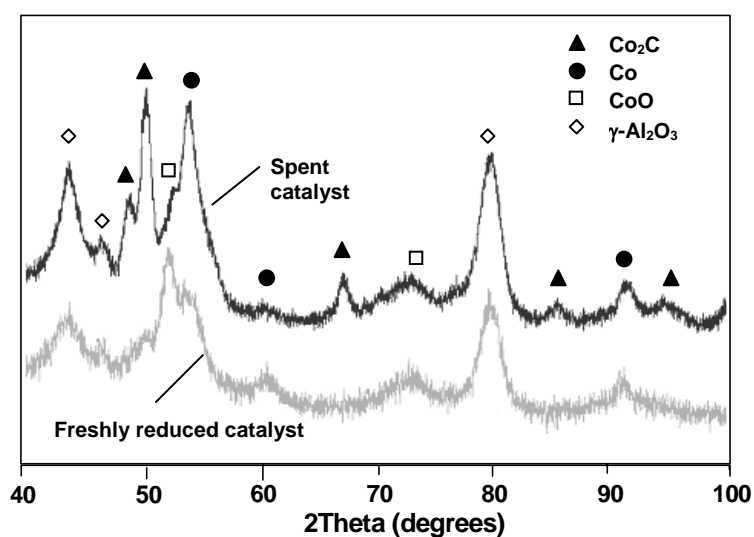


**Figure 6.6** X-ray diffractograms of the spent 20 wt% Co/Pt/ $\text{Al}_2\text{O}_3$  catalyst from the run shown in Figure 6.5, compared to a freshly reduced catalyst in wax. The wax was melted in-situ in nitrogen at 120 °C to remove interfering diffraction patterns.

**Table 6.2** Phase decomposition and average crystallite sizes of spent 20 wt% Co/Pt/ $\text{Al}_2\text{O}_3$  sample.

Phase	Composition (Mass %)
CoO	6.4
Co	3
$\text{Co}_2\text{C}$	10.3
$\gamma\text{-Al}_2\text{O}_3$	80.3

#### *6.3.4 The effect of temperature on carbon deposition from CO disproportionation*

The influence of temperature on the formation and reactivity of carbon deposits from CO disproportionation was studied on reduced 15 wt% Co/Al<sub>2</sub>O<sub>3</sub> catalysts at 250, 350 and 400 °C for 4h. In the absence of H<sub>2</sub>, carbon is deposited via the Boudouard reaction ( $2\text{CO} \rightarrow \text{C} + \text{CO}_2$ ). The formation of CO<sub>2</sub> was monitored during the reaction and confirmed the deposition of carbon on the samples.

The carbon deposited samples were then subjected to a TPH step to determine the reactivity of the formed carbon deposits. Figure 6.7 shows TPH profiles for catalysts with carbon deposited at various temperatures. After CO exposure at 250 °C two broad types of carbonaceous species are noted (Figure 6.7a). Carbon deposited at these temperatures were ascribed to atomic (185 °C) and polymeric (445 °C) forms of carbon by Lee et al. [30] who performed similar experiments. Additionally there is shoulder peak evident around 200 °C which could possibly correspond to the hydrogenation of bulk cobalt carbide. It has also been reported that hydrogenation of carbon from adsorbed CO is observed around this temperature [35]. At 350 °C it is observed that reactivity of the deposited carbon has been considerably decreased (Figure 6.7b). The complete absence of the atomic type of carbon is noted, which is different from the work of Lee et al. [30]. The hydrogenation temperature of carbon indicates the presence of both polymeric and graphitic carbon [36]. A further increase in CO disproportionation temperature resulted in an even more stable carbon specie which only can be removed by a hold at 900 °C in hydrogen (Figure 6.7c). Lee et al. [30] reported on carbon that could not be hydrogenated at 600 °C but did not comment on its nature nor its effect on catalyst morphology.

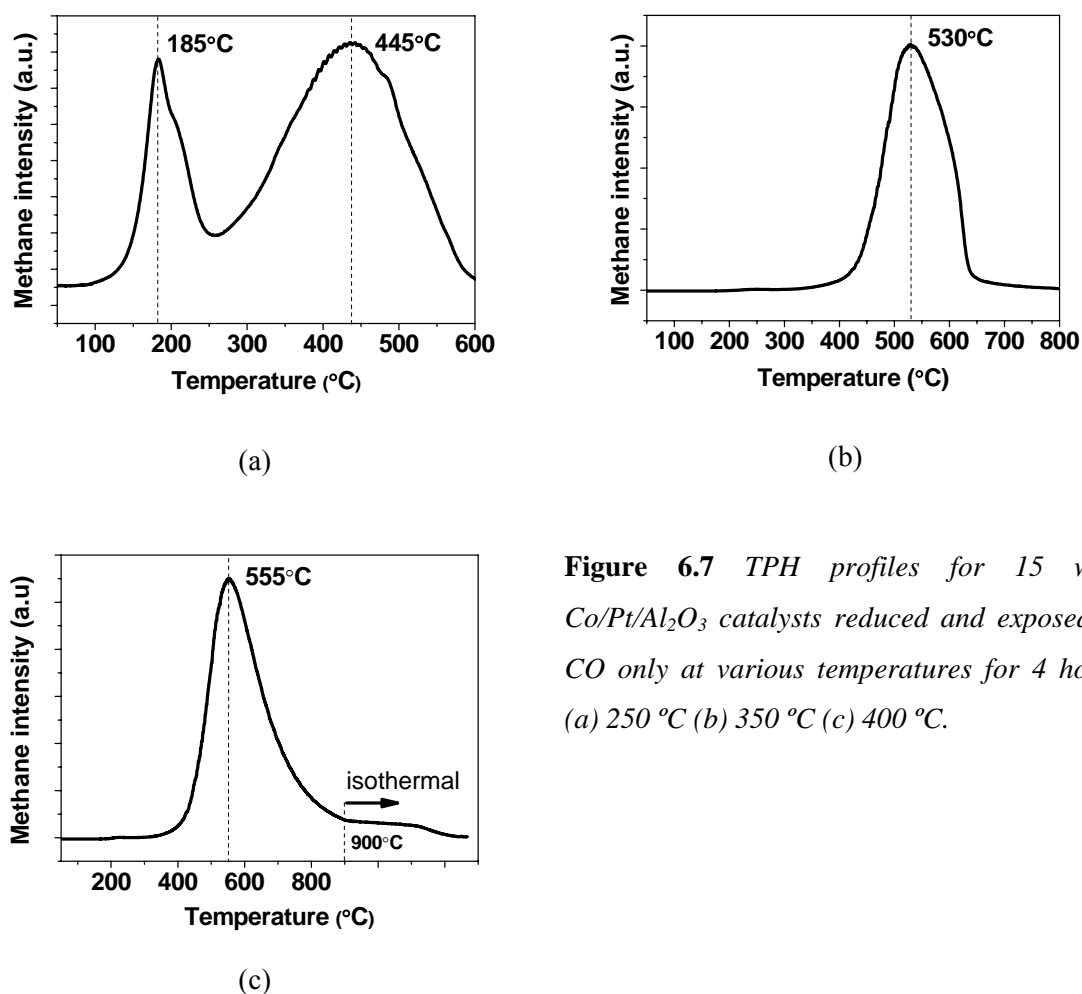


**Figure 6.7** TPH profiles for 15 wt% Co/Pt/Al<sub>2</sub>O<sub>3</sub> catalysts reduced and exposed to CO only at various temperatures for 4 hours (a) 250 °C (b) 350 °C (c) 400 °C.

XPS was used to understand the surface properties of the catalyst after carbon deposition. The C 1s spectra (Figure 6.8) show a feature at 284.5 eV which is characteristic of C-C bonds (both in graphite [37] and ubiquitous hydrocarbon contamination [38]). In the case of the catalyst exposed to higher temperatures at 350 °C and 400 °C a new feature at 283.1 eV is noted. This indicates the possible presence of cobalt carbide [39]. Normally, since cobalt carbide is metastable it is difficult to observe with ex-situ techniques. However it has been reported that cobalt carbide was visible with TEM when in an encapsulated state [34]. As the temperature is increased to 400 °C cobalt carbide is believed to be decomposed/transformed to cobalt and graphite [37], which is a major component of the C 1s spectrum. It was reported by Volkova et al. [40] that bulk cobalt carbide decomposes at 390-400 °C in flowing CO. The Co 2p spectra (Figure 6.8) for the catalyst exposed to 250 °C, resembles a passivated catalyst and the predominant phase here is cobalt (II) oxide. At

350 °C and 450 °C we see new features at 778 eV which corresponds to metallic cobalt [41]. The fact that this is visible suggests that carbon has caused encapsulation and thus protected some of the metallic cobalt from oxidation. The amount of carbon increases exponentially with increasing CO disproportionation temperature in the range tested. The XPS C 1s/Co 2p ratio, corrected with sensitivity factors, for the catalyst exposed to CO at 250 °C is 4.8 while it is 16.8 and 42.3 for the catalysts exposed at 350 °C and 400 °C respectively.

TEM analysis of the sample exposed to 400 °C shows the presence of carbon nanostructures including filaments and encapsulated particles (Figure 6.9). The carbon filaments have clearly resulted in the break up of the catalyst particles. Similar nanostructures were observed for a Co/SiO<sub>2</sub> catalyst activated in a H<sub>2</sub>/CO ratio of 1 at 400 °C [42]. Borko et al. [9] suggested that the formation of these carbon nanostructures may have importance in deactivation of cobalt catalysts in a H<sub>2</sub> deficient FTS process. These conditions and temperatures are however rather extreme, and might be a bigger issue in a fixed bed reactor than in a slurry bed system. The interaction of the CO with surface cobalt generates surface carbon and CO<sub>2</sub>. This carbon may diffuse into the cobalt surface to form metastable bulk carbides; the bulk carbides may decompose to form carbon filaments and other carbon nanostructures. During the course of the growth of filaments cobalt particles are encapsulated and detached from the support and this results in the disintegration of the catalyst.

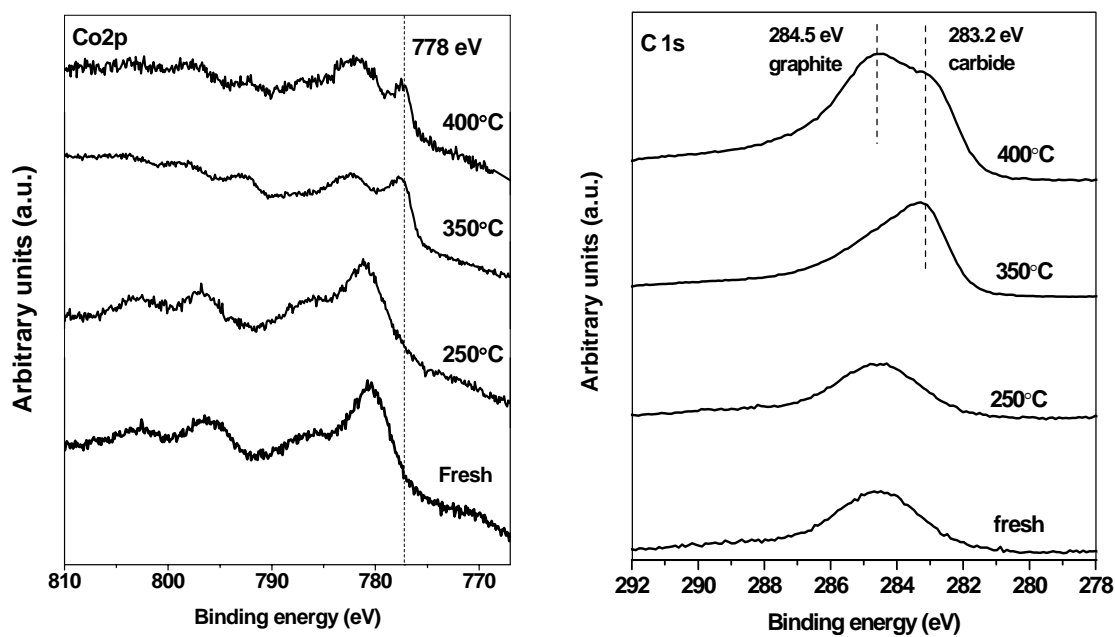


**Figure 6.8** *Co 2p and C 1s regions of the XPS spectrum of fresh (reduced and passivated) and carbon deposited 15 wt% Co/Pt/Al<sub>2</sub>O<sub>3</sub> catalysts*

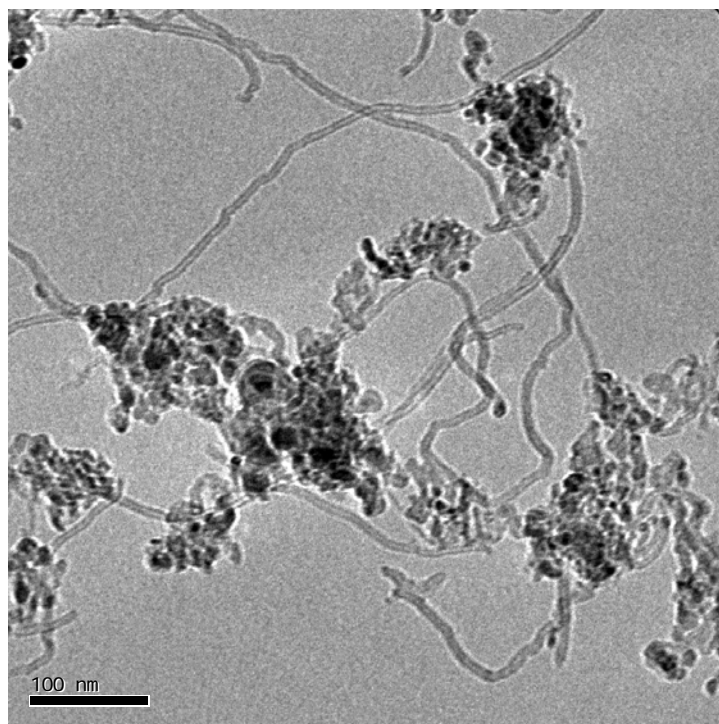


**Figure 6.9** *TEM image of 15 wt% Co/Pt/Al<sub>2</sub>O<sub>3</sub> catalyst reduced and exposed to CO at 400 °C at 1 bar for a period of 4 hours*

## 6.4 Conclusions

The effect of temperature and gas composition on carbon deposits was investigated on FTS catalysts at model and realistic conditions. Temperature programmed hydrogenation and oxidation (TPH/O), X-ray diffraction (XRD), X-ray photoelectron spectroscopy and transmission electron microscopy (TEM) were used to characterise the carbonaceous phases. It was found that both temperature and gas composition play important roles in determining the amount and reactivity of carbon deposits on Co/Pt/Al<sub>2</sub>O<sub>3</sub> catalysts. An important factor in determining carbon deposition is the rate of hydrogenation of active carbon compared to the rate of transformation to more stable carbon species. Transformation of active carbon to more stable species occurs faster at higher reaction temperatures and lower H<sub>2</sub>/CO ratios. Upset conditions even if they occur over short periods result in production of carbon phases (Co<sub>2</sub>C, encapsulating carbons and filaments) that are detrimental to catalyst activity.

## Acknowledgements

The authors thank M.J. Overett, J. Maloka and B. Sigwebela for conducting the FTS runs at high pressure. Sasol Technology's Materials Characterisation group is acknowledged for the XRD measurements.

## 6.5 References

- [1] T.H. Fleisch, R.A. Sills, M.D. Briscoe, *J. Nat. Gas Chem.* 11 (2002) 1.
- [2] B.H. Davis, *Ind. Eng. Chem. Res.* 46 (2007) 8938.
- [3] P.G. Menon, *J. Mol. Catal.* 59 (1990) 207.
- [4] J.J.H.M. Font Freide, T.D. Gamlin, R.J. Hensman, B. Nay; C. Sharp, *J. Nat. Gas Chem.* 13 (2004) 1.
- [5] V. Gruver, R. Young, J. Engman, H.J. Robota, *Prepr. Pap.-Am. Chem. Soc., Div. Pet. Chem.* 50 (2005) 164.
- [6] M. Ojeda, F.J. Pérez-Alonso, P. Terreros, S. Rojas, T. Herranz, M.L. Granados, J.L.G. Fierro, *Langmuir* 22 (2006) 3131.
- [7] M.K. Niemela, A.O.I. Krause, *Catal. Lett.* 42 (1996) 161.
- [8] D.J. Moodley, J. van de Loosdrecht, A.M. Saib, J. W. Niemantsverdriet, *Prepr. Pap.-Am. Chem. Soc., Div. Pet. Chem.* 53 (2) (2008) 122.
- [9] L. Borko, Z.E. Horvath, Z. Schay, L. Guczi, *Stud. Surf. Sci. Catal.* 167 (2007) 231.
- [10] V. Gruver, X. Zhan, J. Engman, H.J. Robota, *Prepr. Pap.-Am. Chem. Soc., Div. Pet. Chem.* 49 (2004) 192.
- [11] H. Schulz, *Pure Appl. Chem.* 51 (1979) 2225.
- [12] S. Mukkavilli, C. Witman, *Ind. Eng. Chem. Proc. Des. Dev.* 25 (1986) 487.
- [13] G.R. Fredriksen, E.A. Blekkan, D. Schanke, A. Holmen, *Chem. Eng. Technol.* 18 (1995) 125.
- [14] J. Nakamura, K. Tanaka, I. Toyoshima, *J. Catal.* 108 (1987) 55.
- [15] J. Lahtinen, T. Anraku, G. A. Somorjai, *J. Catal.* 142 (1993) 206.
- [16] J. Lahtinen, T. Anraku, G.A. Somorjai, *Catal. Lett.* 25 (1994) 241.
- [17] D.C. Gardner, C.H. Bartholomew, *Ind. Eng. Chem. Prod. Res. Dev.* 20 (1981) 80.
- [18] C.H. Bartholomew, M.V. Strasburg, H.-Y. Hsieh, *Appl. Catal.* 36 (1988) 147.

- [19] D. Bianchi, C.O. Bennet, J. Catal. 86 (1984) 433.
- [20] H. Ahlafi, D. Bianchi, C.O. Bennett, Appl. Catal. 66 (1990) 99.
- [21] D. Tristantini, S. Lögdberg, B. Gevert, Ø. Borg, A. Holmen, Fuel Proc. Tech. 88 (2007) 643.
- [22] G. Calleja, A. de Lucas, R. van Grieken, Fuel 4 (1995) 445.
- [23] W. Zhou, J.-G. Chen, K.-G. Fang, Y.-H. Sun, Fuel Proc. Tech. 87 (2006) 609.
- [24] P.J. van Berge, J. van de Loosdrecht, J.L. Visagie, United States Patent 6 806 226 (2004), to Sasol.
- [25] P.J. van Berge, J. van de Loosdrecht, E. Caricato, S. Barradas, B.H. Sigwebela, United States Patent 6 455 462 (2002), to Sasol.
- [26] P.J. van Berge, J. van de Loosdrecht, E. Caricato, S. Barradas, United States Patent 6 638 889 (2004), to Sasol.
- [27] R.L. Espinoza, J.L. Visagie, P.J. van Berge, F.H. Bolder, United States Patent 5 733 839 (1998), to Sasol.
- [28] P.J. van Berge, J. van de Loosdrecht, J.L. Visagie, T.J. van der Walt, H. Veltman, C. Sollié, European Patent 1 444 040 B1 (2003), to Sasol.
- [29] J. van de Loosdrecht, S. Barradas, E.A. Caricato, N.G. Ngwenya, P.S. Nkwanyana, M.A.S. Rawat, B.H. Sigwebela, P.J. van Berge, J.L. Visagie, Top. Catal. 26 (2003) 121.
- [30] D.-K. Lee, J.-H. Lee, S.-K. Ihm, Appl. Catal. 36 (1988) 199.
- [31] J.G. McCarty, H. Wise, J. Catal. 57 (1979) 406.
- [32] P. Winslow, A.T. Bell, J. Catal. 86 (1984) 158.
- [33] A.D. Moeller, C.H. Bartholomew, Ind. Eng. Chem. Prod. Res. Dev. 21 (1982) 390.
- [34] F. Tihay, G. Pourroy, M. Richard-Plouet, A. C. Roger, A. Kiennemann, Appl. Catal. A 206 (2001) 29.
- [35] W.H. Lee, C.H. Bartholomew, J. Catal. 120 (1989) 256.
- [36] D. Potoczna-Petru, Carbon, 29 (1991) 73.
- [37] J. Nakamura, I. Toyoshima, K.-I. Tanaka, Surf. Sci. 201 (1988) 185.
- [38] J.W. Niemantsverdriet, Spectroscopy in Catalysis, Third ed., Wiley-VCH, Weinheim, 2007.
- [39] J. Xiong, Y. Ding, T. Wang, L. Yan, W. Chen, H. Zhu, Y. Lu, Catal. Lett., 102 (2005) 265.
- [40] G. G. Volkova, T. M. Yurieva, L. M. Plyasova, M. I. Naumova, V. I. Zaikovskii, J. Mol. Cat. A 158 (2000) 389.
- [41] R.L. Chin, D.M. Hercules, J. Phys. Chem. 86 (1982) 360.
- [42] V.A. de la Peña O'Shea, N. Homs, J.L.G. Fierro, P. Ramírez de la Piscina, Catal. Today 114 (2006) 422.

---

# Chapter 7

---

## **Opportunities to study the behaviour of cobalt nanoparticles by using model FTS catalysts: *Initial results and outlook***

---

*The work described in this thesis, thus far, has focused on attempting to understand the deactivation of complex industrial cobalt-based FTS catalysts that have been tested under realistic conditions. However, a reductionist approach is necessary to understand more fundamental issues relating to the behaviour of supported cobalt nanoparticles in the FTS. This can potentially be achieved by using model supported cobalt catalysts tested at model FTS conditions. In this chapter we report on two potential techniques to investigate the behaviour of cobalt nanoparticles by applying supported cobalt model catalysts. Spherical model cobalt catalysts were prepared by slurry “impregnation” of Stöber silica spheres. These were then investigated under different gas environments using in-situ TEM. Secondly, planar model catalysts were prepared by spincoating of preformed cobalt nanoparticles onto silica TEM grids and imaged after thermal treatment. Initial results obtained on the two model systems are discussed. The potential of applying model cobalt catalysts using these two techniques and possible future applications are outlined.*

---



## 7.1 Introduction

In industry, development and optimization of FTS catalysts is based largely on empirical knowledge [1]. Cobalt catalysts are complex mixtures of different phases and wide varieties of compounds for example; a modified porous support, chemical and structural promoters and active cobalt phase [2]. Understanding cobalt catalysts on a fundamental level creates further opportunities to develop, tune and optimise catalysts. Deeper fundamental understanding requires the application of advanced spectroscopic and microscopic techniques on the (active) catalyst, coupled with catalyst testing. The cobalt catalysts as used in industry, however, are often not suitable for systematic fundamental studies for a few reasons. Firstly, the active surface of a catalyst is often hidden in the pore structure of supports and the surface area exposed for characterization is often too low. Secondly, as already mentioned, industrial catalyst systems are complex. In the case of cobalt FTS catalysts the entire cobalt phase (the surface of which contains active sites) typically consists of only 15-20 wt% of the catalyst and may be difficult to distinguish from inactive phases.

In order to partially overcome these problems, a reductionist approach may be used by applying simplified model catalysts. A model catalyst is an idealized version of an existing industrial catalyst system that has been prepared to gain information on certain aspects of the catalyst that cannot be gained from the conventional system. The design of a model catalyst is a compromise between achieving a simple well definable and controllable catalyst and resembling the original industrial catalyst to maintain relevance [3].

There are various possibilities that exist when it comes to the design of model cobalt FTS catalysts and two of these are illustrated in Figure 7.1. Spherical model catalysts have been used previously by Datye and co-workers [4]. The nonporous support has active particles on their external surface and this facilitates profile views of supported nanoparticles which are useful for study with HRTEM. Planar model catalysts can also be applied to bridge the gap between high surface area catalysts and single crystals. The planar model consists of a conducting substrate, for example silica, on top of which is deposited an active phase usually by spincoating. Advances in the preparation of TEM substrates have resulted in production of silica TEM grids

which have back-etched "membrane windows" of 10 nm, which facilitate TEM imaging [5]. Recently, nanoparticles have been deposited on these planar silica TEM grids to produce well-defined model catalysts [6]. Planar model catalysts are advantageous as the deposited particles are directly accessible to many characterization techniques and since the particles are directly exposed to synthesis gas there are no transport limitations [7]. It can be clearly seen from Figure 7.1 that the model catalysts substantially reduce the complexity of a supported, porous industrial catalyst. The cobalt (darker features) and alumina support are difficult to differentiate using standard bright field TEM imaging in the industrial catalyst.

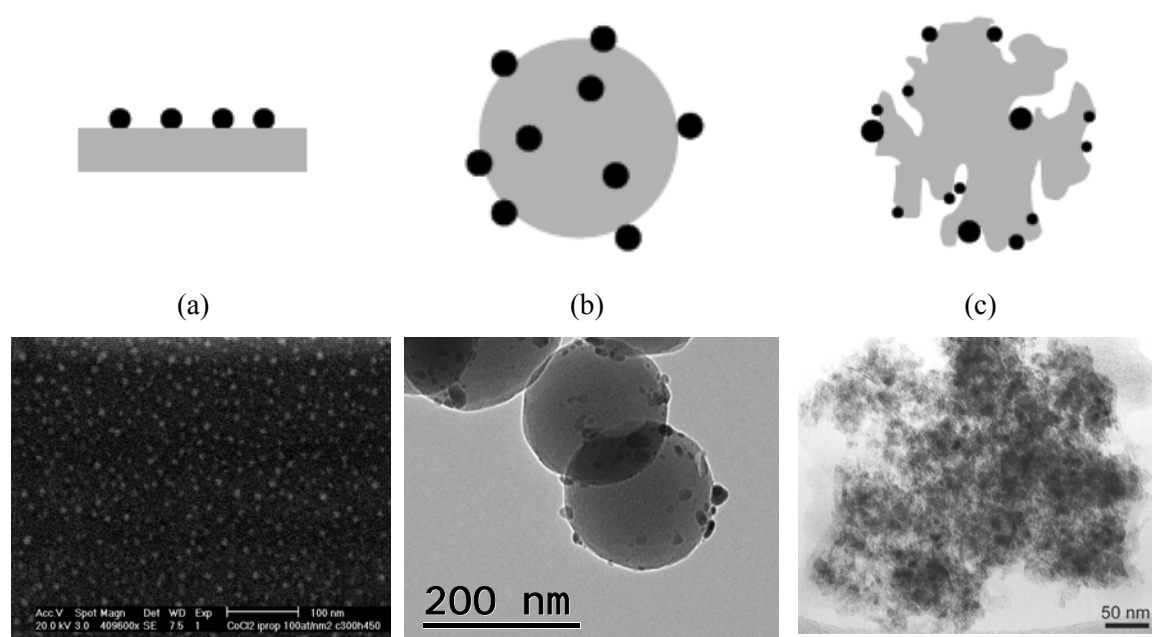


**Figure 7.1** *Representation of industrial and model catalysts (a) Planar model cobalt/SiO<sub>2</sub> catalyst and corresponding SEM image (b) Cobalt model catalyst supported on non-porous Stöber silica spheres and corresponding TEM image (c) Typical cobalt on alumina catalyst similar to that used industrially and corresponding TEM image.*

Over the last few years important fundamental information of the reactivity of cobalt FTS catalysts have been obtained by using a model catalyst approach. Bezemer et al. showed that there was a decrease in TOF for particles smaller than 6-8 nm, which was due to particle shape changes and restructuring of the cobalt under synthesis gas, which they observed by X-ray absorption spectroscopy (XAS) [8]. This

was accomplished by using model Co/carbon nanofibre (CNF) catalysts and would be difficult to show with refractory oxide-supported catalysts as cobalt in these traditional systems have strong metal support interaction and it is difficult to reduce smaller particles. Spherical model Co/SiO<sub>2</sub> catalysts have been used recently by Saib et al. to study the crystallite size dependency of cobalt oxidation under model FTS conditions [9]. Kuipers et al. used planar model Co/SiO<sub>2</sub> catalysts to study secondary reactions during FTS [7]. The surface oxidation behaviour of cobalt was also studied by near edge X-ray absorption fine structure (NEXAFS) on planar model cobalt catalysts consisting of uniform 4-5 nm cobalt particles prepared by spin-coating of aqueous solutions of the metal nitrate onto a SiO<sub>2</sub>/Si (100) substrate [10].

## **7.2 Investigation of cobalt particle behaviour using in-situ TEM on spherical model cobalt catalysts**

### **7.2.1 Experimental**

#### *Preparation of spherical model catalyst*

The catalyst chosen was 5 wt% Co promoted with 0.01 wt% platinum, supported on nonporous silica spheres. The first step involved the preparation of Stöber silica spheres which was done based on a published method [11] which involves mixing appropriate quantities of water, TEOS, 25% NH<sub>4</sub>OH and EtOH. After stirring for 24 h the excess solvent was evaporated off under reduced pressure. The obtained spheres were dried overnight at 110 °C and calcined at 500 °C for 1h in a muffle furnace to remove organic material and ammonia. The BET surface area of the spheres was determined to be 24.2 m<sup>2</sup>/g. The calcined spheres were finely crushed and “impregnated” by mixing with an aqueous cobalt nitrate and ammonium-platinum-nitrate solution and thereafter the excess water was removed in a rotary evaporator at 75 °C. The catalyst was then calcined at 250 °C (ramp 1 °C/min) for 2h in 25%O<sub>2</sub>/Ar. A portion of the catalyst was reduced at 450 °C (5 °C/min) for 4h and then passivated at room temperature in a 1%O<sub>2</sub>/He mixture.

### *Characterization by TEM and Temperature programmed reaction (TPR)*

Thin samples for TEM were prepared by crushing the reduced and passivated catalyst with a mortar and pestle, followed by dispersion in ethanol using an ultrasound bath. Then an appropriate amount of sample was placed onto a copper microscope grid covered with carbon windows. Samples were studied using a FEI Tecnai 20F high resolution microscope with an acceleration voltage of 200 keV. The cobalt crystallite size was obtained from several TEM images (in excess of 200 particles). Metal particle sizes obtained from TEM were corrected for the presence of a ~3-4 nm CoO layer on the passivated Co particles. For TPR a 50 mg sample of the calcined catalyst was loaded into a quartz TPR reactor and dried at 250 °C (5 °C/min) under nitrogen for 2h to remove moisture. The reactor was cooled to 25 °C and the catalyst was then reduced using a linear temperature program (10 °C/min to 800 °C) in 5% H<sub>2</sub>/N<sub>2</sub>.

### *In-situ TEM imaging under reactive gases*

The experiments were performed in a FEI CM 300 microscope at Haldor Topsøe AS, Denmark which was equipped with the necessary differential pumps, gas lines (CO, H<sub>2</sub> and H<sub>2</sub>O) and an in-situ sample holder with a heating filament [12]. The microscope is equipped with a FEG, a quadrupole mass spectrometer (QMS), a Gatan image filter (GIF), and a Tietz F144 CCD camera for data acquisition. The instrument is capable of providing images with a resolution of 0.14 nm during exposure of the sample to reactive gases and elevated temperatures. The maximum pressure that was used was around 5 mbar. Measurements were performed with a stainless steel grid. Samples were crushed and mounted directly onto the grids without solvent to prevent any contamination. Data analysis was conducted using either Digital Micrograph or ImageJ software.

## **7.2.2. Results**

### *Characterization of spherical model catalyst by TEM and TPR*

The prepared model catalyst was characterized using TEM and TPR. The cobalt particle size distribution of the catalyst was determined by TEM and it is evident that

a fairly wide particle size distribution was obtained with particle varying from 5-25 nm (Figure 7.2). The average cobalt particle size of the reduced and passivated catalyst was determined to be around 15 nm.

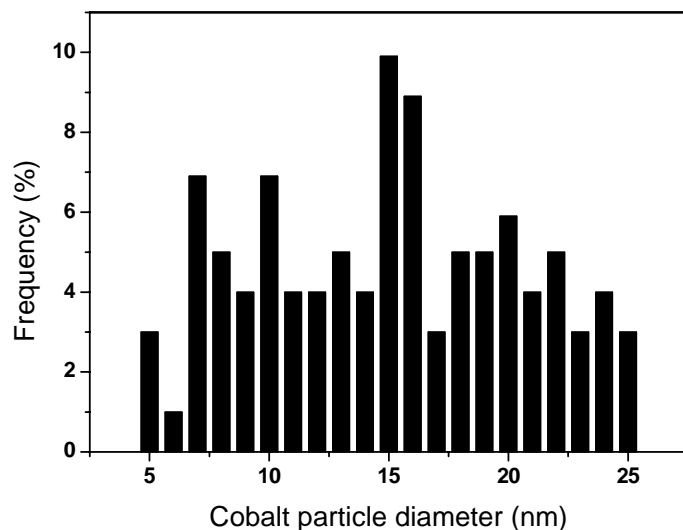


**Figure 7.2** *Metallic cobalt crystallite size distribution for spherical 5 wt% Co/Pt/SiO<sub>2</sub> model catalyst as determined by TEM. The catalyst has been reduced at 450 °C in pure hydrogen and passivated at room temperature in a 1%O<sub>2</sub>/He mixture.*

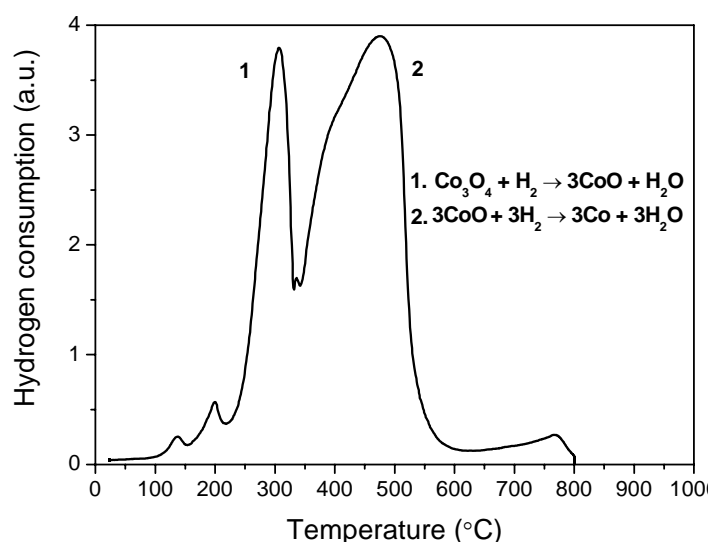


**Figure 7.3** *A TPR profile of a spherical 5 wt% Co/Pt/SiO<sub>2</sub> model catalyst prepared by slurry “impregnation” of Stöber spheres followed by calcination at 250 °C.*

TPR was also conducted on the catalyst (Figure 7.3). The two reduction steps of Co<sub>3</sub>O<sub>4</sub> (Co<sub>3</sub>O<sub>4</sub> → CoO → Co) which is the main phase expected in the calcined catalyst are observed as the main two peaks at around 300 and 450 °C [13]. This is supported by the fact that the area ratio between peak 2 and peak 1 is 2.8, close to the stoichiometric ratio for hydrogen consumption expected during the two reduction steps. The smaller peaks below 200 °C could possibly correspond to the hydrogenation of residual cobalt nitrate [8]. The peak at around 760 °C is likely due to the reduction of a silicate-like species [9].

*In-situ imaging of reduced cobalt particles under hydrogen at 450 °C, 2 mbar*

As done in previous in-situ TEM studies [14], the reduced and passivated catalyst was re-reduced in the TEM at 425-450 °C (20 °C/min) and allowed to equilibrate for 1h. Figure 7.4 shows high resolution (x 235k) in-situ TEM images of cobalt particles that have been reduced under hydrogen at 450 °C.

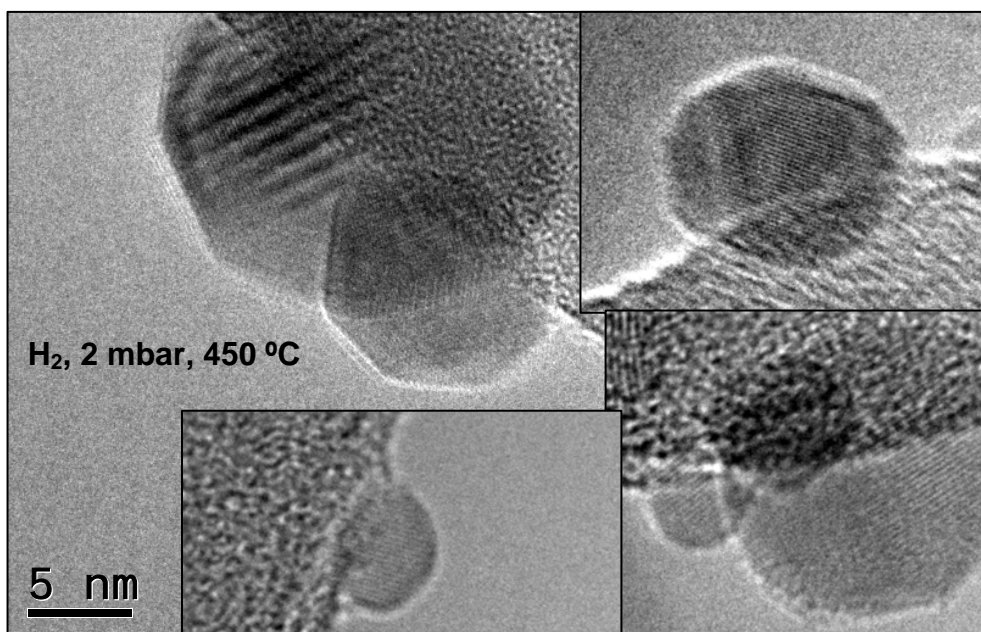


**Figure 7.4** *Lattice-resolved in-situ TEM images of various metallic cobalt particles, on a reduced 5 wt% Co/Pt/SiO<sub>2</sub> model catalyst under hydrogen (2 mbar) at 450 °C. The scale bar is valid for all images.*

Lattice spacings were measured to ascertain which phase of cobalt was present on the reduced catalysts. The lattice spacing's obtained (2.03-2.05 and 1.77 Å) compare well with that of fcc cobalt metal (see Table 7.1). This is in agreement with expectations, as it has been reported that fcc is the predominant phase for cobalt particles under 40 nm [15]. It was noted that even most of the smaller cobalt particles (~5 nm) appear to be in the metallic state, implying that the catalyst is well (re)reduced under conditions in the TEM. The larger particles have a more faceted shape while the smaller particles seem more spherical. Images of particles were also taken at 100 and 250 °C in 2 mbar hydrogen and were similar to those at 450 °C.

**Table 7.1** *Reference values for d-spacings of relevant cobalt compounds*

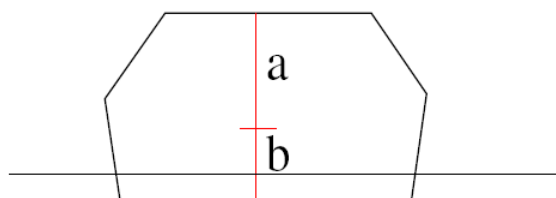
Compound	Orientation	d-spacing (Å)
fcc cobalt	111	2.05
	200	1.77
hcp cobalt	002	2.04
	101	1.94
CoO	111	2.46
	200	2.13
CoSiO <sub>4</sub>	120	2.79
	131	2.53
	112	2.47

*Wulff construction based on in-situ TEM images under hydrogen*

The equilibrium shape of a metal particle (which is a function of the surface energy) can be determined by the Wulff construction [16]. Wulff construction can provide knowledge about particles in TEM images by providing a corresponding three-dimensional picture. The various exposed planes can be visualised and possibly be linked to activity. Earlier the surface energies for an fcc cobalt particle under hydrogen environment were calculated [17]. To determine the equilibrium shape of a supported particle these surface energies as well as an additional interface energy is needed. Here the interface energy (between the cobalt particle and the silica support) is evaluated based on the shapes of the particles in the TEM images. The procedure involves measuring the distance from the centre of the particle (determined by a circular approximation) to the interface as well as the distance to one of the surfaces. The ratio of the two distances (which are perpendicular to the tangents) is equal to the ratio of the interface/surface energies (Scheme 7.1).

For example, if the surface energy of the plane at the distance  $a$  from the centre of the particle is  $\gamma$ , the interface energy ( $i$ ) situated at the distance  $b$  is  $i = \gamma \times a/b$ . This calculated interface energy is used in the Wulff construction along with the other calculated surface energies. The result for such a particle is shown in Figure 7.5. The image was taken in a 2 mbar hydrogen atmosphere. The particles lies with the

(100) orientation on the surface. The approximation gives an indication of the 3-dimensional shape of the particle in the TEM image. Restructuring of a surface may result in the stabilisation of different planes which can affect activity and selectivity. This methodology can be extended to particles in other gas environments.



**Scheme 7.1** *Evaluating the interface energy*

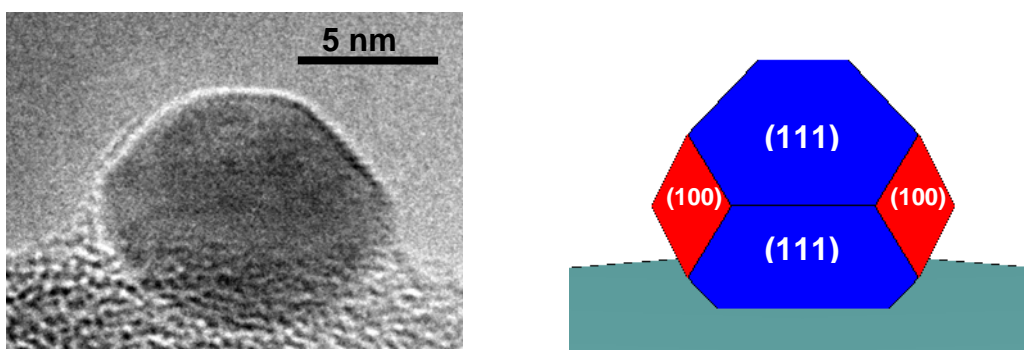


**Figure 7.5** *In-situ TEM image of a cobalt particle on a reduced 5 wt% Co/Pt/SiO<sub>2</sub> model catalyst (imaged in H<sub>2</sub>, 2 mbar) in profile view and the corresponding Wulff shape based on the interface energy determined from the in-situ TEM image (0.78 eV/surface atom) and calculated surface energies in hydrogen.*

#### *Imaging under H<sub>2</sub>/CO (model FTS conditions)*

The reduced 5 wt% Co/Pt/SiO<sub>2</sub> model catalyst was cooled under hydrogen (2 mbar) to 250 °C and then imaged. Thereafter CO (1 mbar) was introduced to give a H<sub>2</sub>/CO ratio of 2:1 which represents model FTS conditions. After around 1 h of equilibration time the catalyst was imaged again to observe if any changes have occurred in morphology and shape of particles. In general, in the time frame of the experiments the observed shape particles seem to be unaffected by this treatment. As an example, Figure 7.6 (a and b) shows the same cobalt particle under a H<sub>2</sub> environment and under a synthesis gas at H<sub>2</sub>/CO = 2. Exposing the catalyst to lower H<sub>2</sub>/CO ratios (1) for



prolonged periods resulted in the formation of amorphous carbonaceous layer on some of the particles (Figure 7.6d).

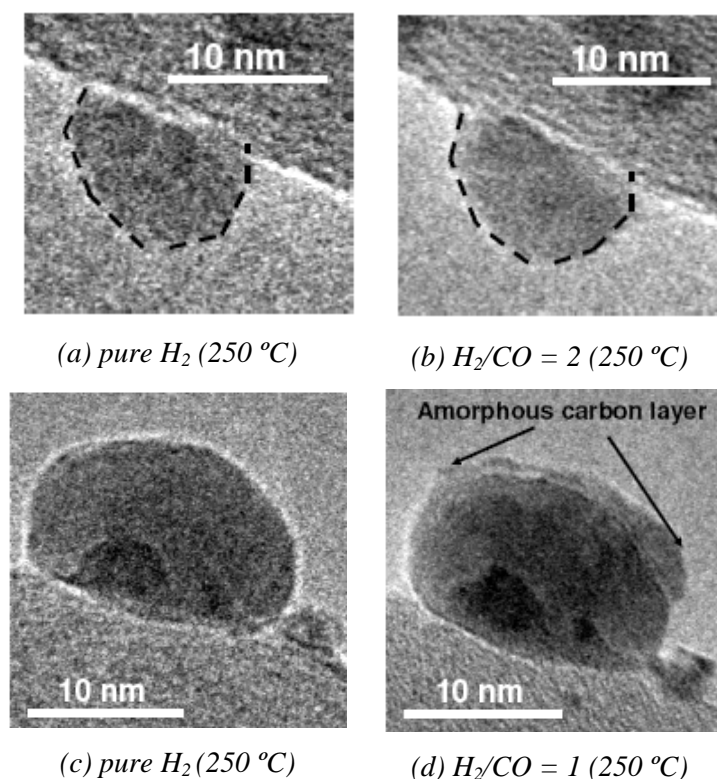


**Figure 7.6** In-situ TEM images of two cobalt particles on a spherical 5 wt% Co/Pt/SiO<sub>2</sub> model catalyst. A 10 nm particle under (a) pure H<sub>2</sub> at 250 °C, and (b) H<sub>2</sub>/CO = 2, H<sub>2</sub> = 2 mbar, CO = 1 mbar at 250 °C. A 20 nm particle under (c) pure H<sub>2</sub> at 250 °C and (d) H<sub>2</sub>/CO = 1, H<sub>2</sub> = 1 mbar, CO = 1 mbar at 250 °C

In summary, spherical model cobalt catalysts have been prepared and successfully reduced and imaged via in-situ TEM under various gas environments. It has been shown that the combination of Wulff construction with in-situ TEM can provide information on exposed faces under different reaction conditions. It seems from preliminary measurements that cobalt particles on these silica-supported model catalysts do not change shape markedly under model FTS environments. This could be due to the low pressures (mbar range) in the TEM. Lower H<sub>2</sub>/CO ratios resulted in some carbon deposition on the cobalt particles.

### **7.3 Preparation of model catalysts by supporting pre-formed cobalt nanoparticles on silica TEM grids.**

#### **7.3.1 Experimental**

##### *Preparation of planar model catalysts*

Silica TEM grids are promising for application as supports for planar model catalysts. The silica TEM grid consists of a silica window suspended in a silicon framework [5]. Silicon nitride is deposited at the back of a standard silicon 100 wafer. The nitride is patterned to form an appropriate mask which facilitates anisotropic etching of the silicon, until the oxide is left suspended in its framework. The silica window allows for the transmission of the electron beam. There are a few options available for preparing cobalt catalysts supported on silica TEM grids. The particles can be formed in-situ by the technique of grafting /spincoating of a solution of cobalt salts as done earlier by Kuipers et al. [7] and Saib et al. [9]. The catalyst may also be prepared by grafting preformed metal particles onto the silica TEM grid as been shown recently [6]. The advantage of the preformed particle route is that it seems that the particle size, shape and phase can be manipulated more easily as compared to the in-situ formation route. Preformed particles of cobalt have been previously prepared by decomposition cobalt carbonyl in the presence of capping surfactants [18]. Many of the used capping agents contain phosphorous and nitrogen which may act as poisons for cobalt [18]. If possible it would be advantageous to prepare preformed particles that contain only carbon, hydrogen and oxygen in the surfactants, which could later be removed in a calcination step.

##### *(a) Preformed nanoparticles*

Oleic acid (3.2 ml, 10 mmol), adamantane carboxylic acid (2.0 g, 10 mmol) and diphenyl ether (90 ml), were added to a 250 ml round bottom flask under nitrogen and heated to 170 °C. In a separate flask, the cobalt carbonyl (3.42 g, 10 mmol) was suspended in octyl ether (40 ml) and was heated to 60 °C to dissolve the cobalt carbonyl. This solution was transferred rapidly to the hot mixture and heated at 220 °C for 80 min until no further carbon monoxide could be detected. After such time the

mixture was left to cool, and ethanol (~ 200 ml) was added to precipitate the nanoparticles. The particles were transferred from the reaction mixture using a magnetic rod and washed into a clean flask using heptane. The heptane was removed and the particles stored as an oily residue. The nanoparticles were re-suspended in heptane (20 ml) and washed 3 times with ethanol to yield a grey-black precipitate. These particles were then suspended in heptane and TEM analysis was performed (Figure 7.7). An average particle diameter of around 8 nm was obtained. Not all particles are spherical and a few triangle and rod shaped particles were also observed. It is expected that the technique will yield predominately metallic particles, encapsulated with the surfactant [18]. Additionally, a passivated oxide layer may be present.

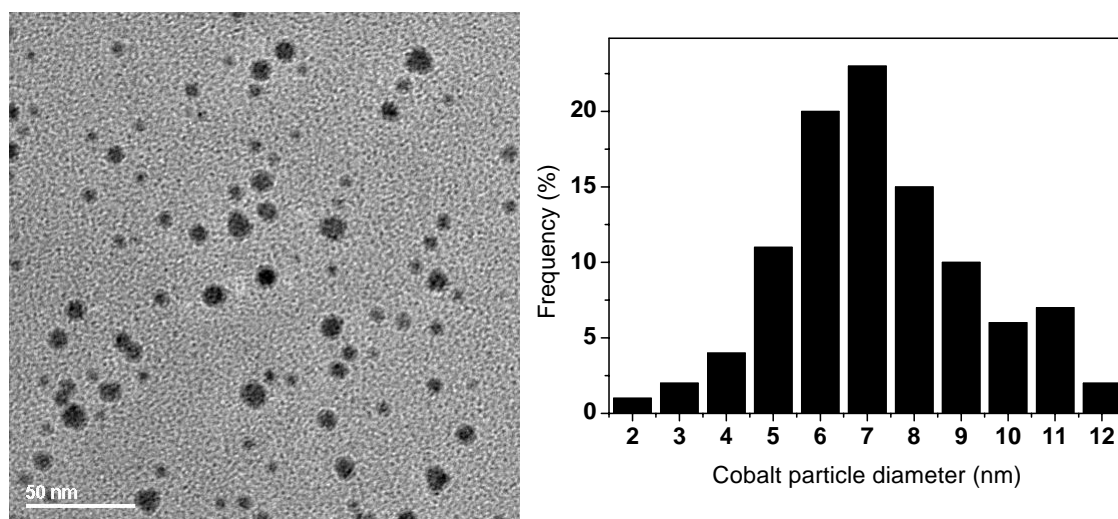


**Figure 7.7** *TEM image of prepared cobalt nanoparticles in a heptane solution and corresponding particle size distribution of the prepared nanoparticles.*

*(b) Supporting performed particles on silica TEM grids, imaging and calcination*

The silicon TEM grids were first calcined at 750 °C for 24 hours and then etched with a 1:2 mixture of H<sub>2</sub>O<sub>2</sub>/NH<sub>4</sub>OH for 20 min at room temperature and 10 min at 35 °C, to clean and hydroxylate the surface. Thereafter they were placed in boiling water to remove excess ammonium hydroxide. A small portion of the cobalt nanoparticle solution was suspended in heptane and then spin-coated onto the TEM grid under flowing nitrogen. The TEM grid was cut into appropriate sizes to fit into a TEM holder and then placed onto a glass boat into a quartz reactor and calcined in a 20% O<sub>2</sub>/He mixture at 350 °C (2°C/min) for 2 hr. Previous TGA analysis confirmed that the surfactant groups could be removed around 300 °C in air. Samples of the spincoated and calcined catalysts were analysed by TEM (FEI Tecnai 20, 200 kV, type Sphera).

### **7.3.2 Results**

The distribution of the spin coated (Figure 7.8) particles on the TEM grid is rather sparse and this can be remedied by increasing the concentration of the nanoparticle in heptane spincoating solution. There is a halo/shell around the cobalt nanoparticles (not a focus effect) which could indicate a passivation layer of CoO (Figure 7.8, inset) of about 3 nm around a metallic cobalt core. The fact that the brim shows lighter contrast than the core points towards the presence of an oxide (mass-thickness contrast). This shell is not evident in the calcined samples (Figure 7.9) which suggests that Co/CoO is converted to Co<sub>3</sub>O<sub>4</sub> during calcination. There also seems to be “sintering” of close lying nanoparticles after calcination. Another feature of the calcined samples is that very small nanoparticle (2-3 nm) satellites are present around the larger particles. The 2-3 nm crystallites actually appear to be primary particles that make up the larger crystallites. Here it is evident that calcination leads to major changes in the structure/stability of these nanoparticles.

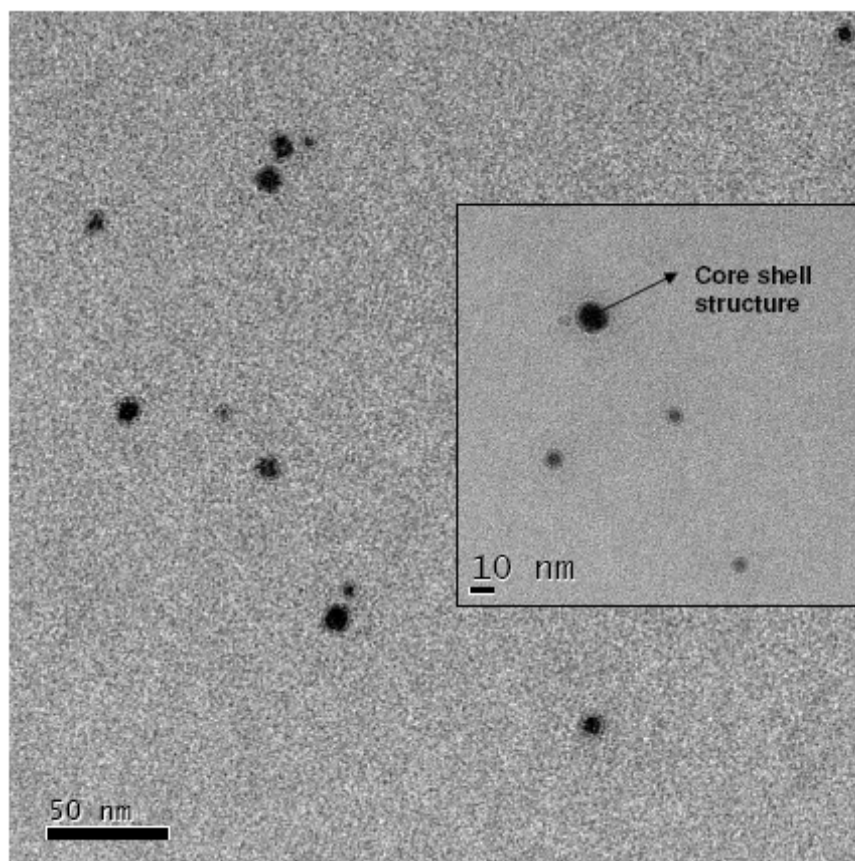


**Figure 7.8** *TEM images of spin coated samples of cobalt nanoparticles on silica TEM grids*

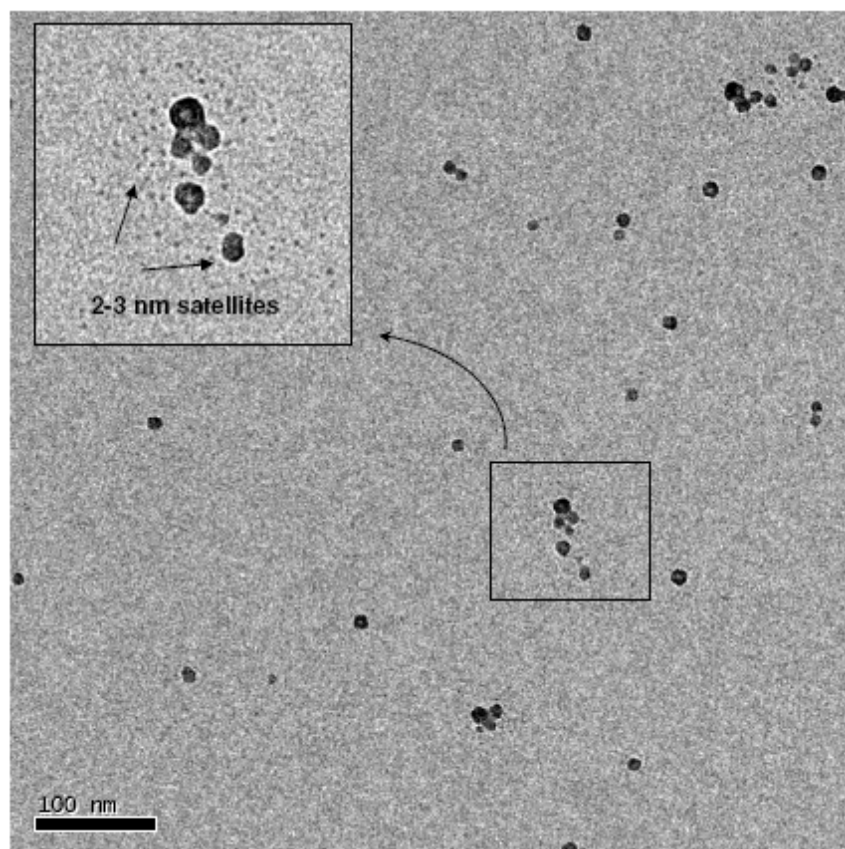


**Figure 7.9** *TEM images of calcined samples (350 °C) of cobalt nanoparticles on silica-TEM grids*

Another powerful application of catalysts supported on silica TEM grids is that it is possible to revisit the exact same area before and after pre-treatment. This enables one to image the same particles and thus track changes making data collection less rigorous in terms of statistics. Figure 7.10 shows images of the same set of cobalt nanoparticles after spincoating and calcination. The calcined particles appear larger than particles in the spin coated state, which are expected to consist of cobalt metal with a small passivated CoO layer (Figure 7.8). This could be due to the increase in volume that occurs upon oxidation. It is known that the diameter of Co is 0.75 times the diameter of  $\text{Co}_3\text{O}_4$  which coincides with the observed increase in size. High resolution images of the calcined particles showed  $d$ -spacings of 2.45 Å which is close to that of  $\text{Co}_3\text{O}_4$ . The redispersion of cobalt into the primary nanoparticles upon thermal treatment can also be seen.

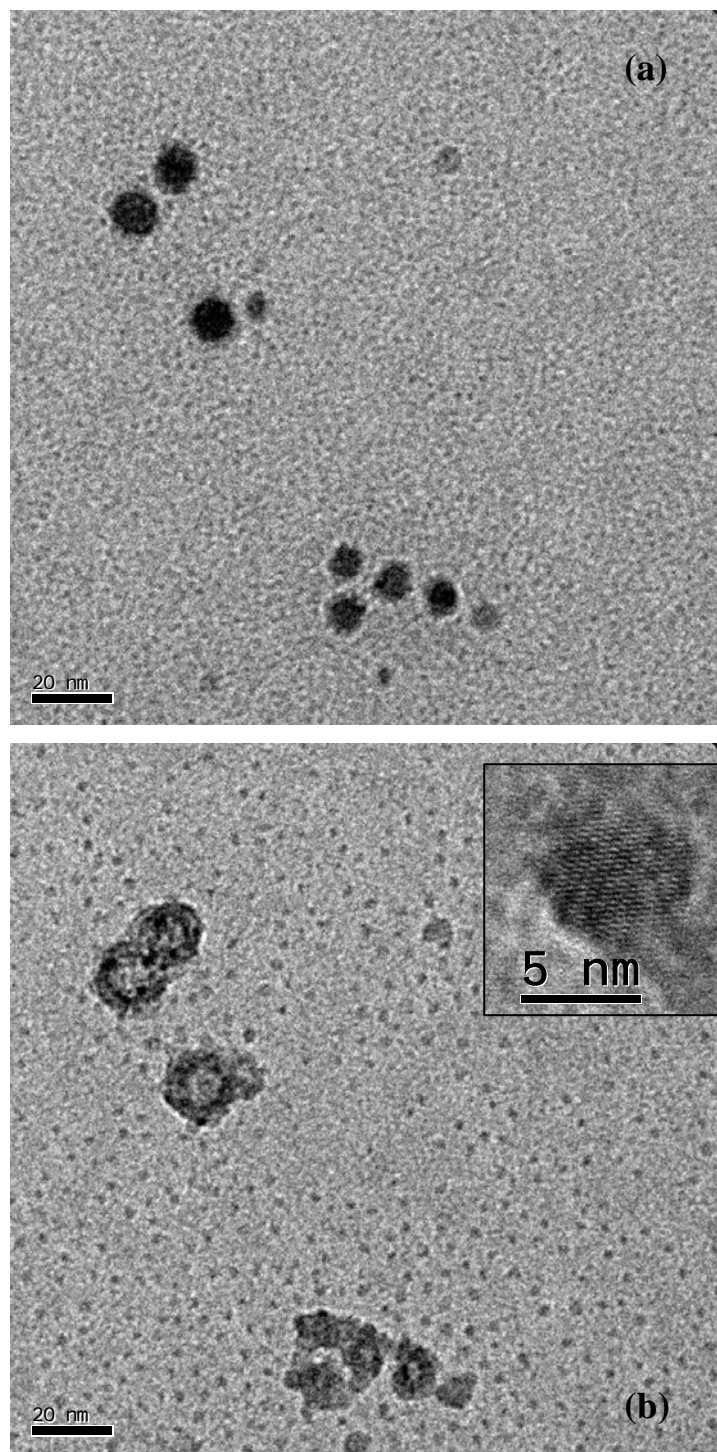


**Figure 7.10** *TEM images of the same set of preformed cobalt nanoparticles on silica TEM grid (a) after spincoating and (b) after calcination in a 20% O<sub>2</sub>/He mixture at 350 °C (2°C/min) for 2 hr. Inset: High resolution image of a calcined cobalt nanoparticle.*

In this section, planar model catalysts on silica TEM grids were prepared by using preformed cobalt particles with reasonably good size distribution. Large scale

rearrangements seem to occur upon calcination of these preformed catalysts. Although the preformed cobalt particles described here may not be ideal model systems, model cobalt catalysts on silica TEM grids are promising in terms of tracking particle behaviour after treatment at under various gases. An alternative method of preparing cobalt planar model catalysts samples that can be explored include spin coating of solutions of cobalt nitrate salts onto the substrate as done by Saib et al. [10].

#### **7.4 Conclusions and outlook**

The purpose of this chapter was to briefly highlight some recent developments that may be further exploited in future work. In-situ TEM on spherical model catalysts has high potential to provide information on the reactivity of particles under model FTS environments. This technique in combination with the Wulff construction can provide a three dimensional picture of the reactive surface during model FTS conditions. Furthermore in future, the technique will be able to be used under more relevant conditions since recent advances have allowed in-situ TEM to be carried out at 1 bar [19].

Cobalt planar model catalysts supported on silica TEM grids provide a way to study extensively the morphology and structure of cobalt after treatment in model FTS environments with TEM. An advantage of applying this system is that it is possible to revisit the same area after treatments. The use of a TEM transfer cell which enables the transport of the cobalt model catalyst in protected environments is also possible. It is envisaged that in future, the two techniques will be able to provide fundamental information on model systems. A few examples of future applications are given below.

##### *In-situ TEM on model systems:*

- Although the effect of promoters on the catalytic FTS activity and reaction kinetics is easily measured, structural information is not readily obtained. Very often reduction promoters are present in relatively small amounts and are not



found as crystalline structures, which complicates the structural characterization. Conventional TEM analysis may not be that useful as it is often conducted in passivated samples where the promoter may be masked by an oxidic layer. Furthermore, it may be expected that mobility of promoters occurs in the reduced state. Insight into the location, state, and function of a promoter in a reduced state in hydrogen or under model FTS conditions can be obtained through atomic-resolution in-situ transmission electron microscopy.

*Planar model catalysts on silica TEM grids:*

- In this thesis it was shown that carbon deposition plays a role in the deactivation of cobalt-based catalysts. A fundamental understanding of the interaction of carbon with cobalt nanoparticles can be gained by applying TEM on planar model catalysts prepared on silica TEM grids that have been carburised at model FTS conditions.
- Sintering of cobalt has been put forward as a possible deactivation mechanism. The mobility of particles can be tracked after treatment under relevant gas atmospheres and temperatures. Particle size distributions obtained in this manner could be used to elucidate mechanisms of sintering which is extremely difficult to determine with complex cobalt industrial catalysts. The effect of reaction conditions on the rate of sintering could also be investigated in this way.

**Acknowledgments**

We acknowledge Haldor Topsøe AS (Dr Alfons Molenbroek) for use of their in-situ TEM facility. Dr Stig Helveg and Dr Fernando Cano are thanked for performing the in-situ TEM measurements. Dr Grant Forman (Sasol Technology, UK) is acknowledged for preparing the preformed cobalt nanoparticles. We are grateful to Dr Peter Thüne and Mrs Prabashini Moodley for the introduction to planar model catalyst preparation.

## **7.5 References**

- [1] J. Collings, Mind over matter-The Sasol story: A half-century of technological innovation, Sasol Ltd, Rosebank, 2002, p. 57.
- [2] R. Oukaci, A.H. Singleton, J.G. Goodwin Jr., Appl. Catal. A 186 (1999) 129.
- [3] P.L.J. Gunter, J.W. Niemantsverdriet, F.H. Ribeiro, G.A. Somorjai, Catal. Rev. 39 (1997) 77.
- [4] A.K. Datye, A.D. Logan, N.J. Long, J. Catal. 109 (1988) 76.
- [5] F. Enquist, A. Spetz, Thin Solid Films 145 (1986) 99.
- [6] P. Moodley, J. W. Niemantsverdriet, P.C Thune, Towards the “ideal” iron nanoparticle model catalyst; in Book of Abstracts, IXth Netherlands' Catalysis & Chemistry Conference, Noordwijkerhout, Netherlands, O71 (2008). p. 135.
- [7] E.W. Kuipers, C. Scheper, J.H. Wilson, I.H. Vinkenburg, H. Oosterbeek, J. Catal. 158 (1996) 288.
- [8] G.L. Bezemer, J.H. Bitter, H.P.C.E. Kuipers, H. Oosterbeek, J.E. Holewijn, X. Xu, F. Kapteijn, A.J. van Dillen, K.P. de Jong, J. Am. Chem. Soc. 128 (2006) 3956.
- [9] A.M. Saib, A. Borgna, J. van de Loosdrecht, P.J. van Berge, J.W. Geus, J.W. Niemantsverdriet, J. Catal. 239 (2006) 326.
- [10] A.M. Saib, A. Borgna, J. van de Loosdrecht, P. van Berge, J.W. Niemantsverdriet, J. Phys. Chem. B 110 (2006) 8657.
- [11] W. Stöber, A. Fink, E. Bohn, J. Colloid Interface Sci. 26 (1968) 62.
- [12] S. Helveg, P.L. Hansen, Catal. Today 111 (2006) 68.
- [13] J. van de Loosdrecht, S. Barradas, E.A. Caricato, N.G. Ngwenya, P.S. Nkwanyana, M.A.S. Rawat, B.H. Sigwebela, P.J. van Berge, J.L. Visagie, Top. Catal. 26 (2003) 121.
- [14] T.W. Hansen, J.B. Wagner, P.L. Hansen, S. Dahl, H. Topsøe, C.J.H. Jacobsen, Science 294 (2001) 1508.
- [15] O. Kitakami, H. Sato, Y. Shimada, F. Sato, M. Tanaka, Phys. Rev. B 56 (1997) 13849.
- [16] G. Wulff, Z. Kristallogr. 34 (1901) 449.
- [17] Theoretical calculations by Dr. I. M. Ciobîcă (Sasol Technology).
- [18] C.B. Murray, S. Sun, W. Gaschler, H. Doyle, T.A. Betley, C.R. Kagan, IBM J. Res. Dev. 45 (2001) 47.
- [19] J.F. Creemer, S. Helveg, G.H. Hoveling, S. Ullmann, A.M. Molenbroek, P.M. Sarro, H.W. Zandbergen, Ultramicroscopy 108 (2008) 993.



---

# Summary

---

## On the Deactivation of Cobalt-based Fischer-Tropsch Synthesis Catalysts

The catalytic conversion of synthesis gas, derived from natural gas, into liquid hydrocarbon fuel via the Fischer-Tropsch synthesis (FTS), is currently receiving much attention due to the demand for environmentally friendly liquid fuel and the rising costs of crude oil. From an industrial perspective, both cobalt and iron catalysts have been applied. However, cobalt catalysts are preferred for gas-to-liquid (GTL) processes as they have high activity for FTS, high selectivity to linear hydrocarbons and low activity for the water-gas shift (WGS) reaction. As cobalt is relatively expensive, high catalyst stability is desired. Understanding deactivation is therefore an important objective in the field of cobalt-based FTS and was the main focus of this thesis.

In Chapter 3, X-ray adsorption near-edge spectroscopy (XANES) was used to investigate the role of cobalt aluminate formation on the deactivation of Co/Pt/Al<sub>2</sub>O<sub>3</sub> FTS catalysts. These catalysts, which were protected in a wax layer, were removed at various intervals from a 100-barrel/day slurry bubble column reactor, operated at commercially relevant FTS conditions. The amount of cobalt aluminate formed was small and it appeared that its formation was difficult during realistic FTS conditions. Using laboratory CSTR runs it was shown that water does seem to enhance aluminate formation but even at high water partial pressures of 10 bar,  $\leq 10$  wt% cobalt aluminate formed and a reduction was still observed compared to a fresh catalyst. It was proposed that the cobalt aluminate that formed resulted from existing CoO. The results obtained led to the conclusion that cobalt aluminate formation does not significantly influence the deactivation of cobalt-based catalysts during realistic FTS conditions.

Following this finding, a review (Chapter 4) was undertaken on the topic of carbon deposition, which was postulated as another potential deactivation mechanism.

It was clear that the FTS over cobalt-based catalysts occurred in the presence of an active surface carbidic over layer and in the presence of various hydrocarbon products. However, the conversion of active surface carbidic carbon to other inactive forms (for example bulk carbide, polymeric carbon and graphene) over time could result in deactivation and selectivity loss of the catalyst. Additionally, it is evident that non-desorbing, heavy hydrocarbon wax could lead to pore plugging and deactivation. From the available literature and regeneration patents it did seem that deactivation by carbon deposits is an important deactivation pathway for cobalt-based FTS catalysts under realistic conditions that warranted further study.

In order to test the hypothesis that carbon deposition was a potential deactivation mechanism, a study was conducted on Co/Pt/Al<sub>2</sub>O<sub>3</sub> FTS catalysts covered in a wax layer, taken from a 100-barrel/day slurry bubble column reactor operated at commercially relevant FTS conditions for an extended period and is described in Chapter 5. A wax-extraction procedure was developed and applied, enabling characterization of the catalyst by both surface techniques like X-ray photoelectron spectroscopy (XPS) as well as bulk techniques such as transmission electron microscopy (TEM) and temperature programmed (TP) hydrogenation and oxidation. The carbon deposits on the wax extracted catalysts were studied using TP techniques and it was found that there was a slow accumulation of a polymeric type of carbon species on the catalyst during the extended FTS run. This carbon was resistant to hydrogen treatments at temperatures above that used in realistic FTS. High sensitivity, low energy ion scattering (HS-LEIS), energy filtered transmission electron microscopy (EFTEM) and chemisorption analysis of samples containing this resistant polymeric carbon showed that it was dispersed largely over the support as well as on the cobalt phase. A large part of the activity of the catalyst could be recovered by removal of these polymeric carbon deposits and it was thus postulated that these play a role in deactivation of cobalt-based FTS catalysts in extended runs.

Understanding the factors that contribute toward carbon deposition is an important step in trying to extend the lifespan of cobalt-based FTS catalysts. In Chapter 6, the impact of temperature and H<sub>2</sub>/CO ratio on the build-up of carbonaceous species on Co/Pt/Al<sub>2</sub>O<sub>3</sub> catalysts was investigated using both model and realistic FTS tests. The influence of upset conditions on carbon deposition and its subsequent effect

on catalyst structure was also investigated. It was found that both temperature and gas composition play important roles in determining the amount and reactivity of carbon deposits on Co/Pt/Al<sub>2</sub>O<sub>3</sub> catalysts. An important factor in determining carbon deposition was the rate of hydrogenation of active carbon compared to the rate of transformation to more stable carbon species. The transformation of active carbon to more stable species occurred faster at higher reaction temperatures and lower H<sub>2</sub>/CO ratios. Upset conditions resulted in the production of carbon phases (Co<sub>2</sub>C, encapsulating carbons and filaments) that are detrimental to catalyst activity.

Most of the work in the preceding chapters dealt with the study of deactivation using complex industrial catalysts. Chapter 7 discusses some preliminary results of new potential techniques that are able to shed light on the reactivity and morphology of cobalt nanoparticles by using both spherical and planar model catalysts. Spherical model cobalt catalysts were prepared by supporting cobalt nanoparticles on Stöber silica spheres. These were then investigated under different gas environments using in-situ TEM. Secondly, planar model catalysts were prepared by spincoating of preformed cobalt nanoparticles onto silica TEM grids and imaged after thermal treatment. Initial results obtained on the two model systems showed that there is a lot of potential for applying these techniques in future to obtain fundamental information on the reactivity and structure of cobalt FTS catalysts.



---

# Samenvatting

---

## Deactivering van Kobaltkatalysatoren voor de Fischer-Tropsch Synthese

De katalytische omzetting van synthese gas, gemaakt uit aardgas, in vloeibare transport brandstoffen door middel van de Fischer-Tropsch Synthese (FTS), krijgt op dit moment veel aandacht vanwege de vraag naar milieu vriendelijke brandstoffen en de structureel hoge prijs van ruwe olie. Zowel kobalt als ijzerkatalysatoren worden industrieel toegepast. Echter, kobalt katalysatoren hebben de voorkeur voor “gas-to-liquid” (GTL; van gas naar vloeistof) processen vanwege hun hoge activiteit hebben voor FTS, hoge selectiviteit naar lineaire koolwaterstoffen en een lage activiteit voor de water-gas shift (WGS) reactie. Vanwege de relatief hoge prijs van kobalt is een erg stabiele katalysator gewenst. Het begrijpen van katalysator deactivering is daarom een belangrijk onderwerp voor kobalt katalysatoren voor de FTS en het hoofddoel van dit proefschrift.

In Hoofdstuk 3 is X-ray adsorption near-edge spectroscopy (XANES) toegepast om de invloed van de vorming van kobalt aluminaat op de deactivering van Co/Pt/Al<sub>2</sub>O<sub>3</sub> FTS katalysatoren te bestuderen. Deze katalysatoren, die door een laagje was werden bedekt en beschermd, werden gehaald uit een 100 vaten per dag slurrie fase reaktor, waarin commerciële FTS condities werden toegepast. De hoeveelheid kobalt aluminaat dat werd gevormd was gering en de vorming van deze fase gedurende realistische FTS is moeilijk. Er werd ook waargenomen dat extra water, toegevoegd tijdens laboratorium CSTR tests, de vorming van kobalt aluminaat versnelt, maar zelfs tijdens tests met 10 bar water werd er minder dan 10 % kobalt aluminaat gevormd. Vergeleken met de verse katalysator vond er nog steeds reductie plaats. Het gevormde kobalt aluminaat kwam waarschijnlijk van het bestaande CoO in de verse katalysator. De behaalde resultaten hebben geleid tot de conclusie dat de vorming van kobalt aluminaat geen waarneembare invloed heeft op de deactivering van kobalt katalysatoren voor de FTS tijdens realistische condities.



Hoofdstuk 4 omvat een literatuur overzicht over de invloed van koolstofvorming op de deaktivering van kobaltkatalysatoren. Het is duidelijk dat gedurende FTS met kobalt katalysatoren er actieve koolstof en koolwaterstoffen op het oppervlak aanwezig moeten zijn om de FTS reactie uit te voeren. Echter, de omzetting van actieve koolstof op het kobalt oppervlak in andere niet-actieve koolstof vormen (bijvoorbeeld polymerische koolstof en grafiet) zou tot deaktivering en selectiviteitveranderingen kunnen leiden. Verder zouden erg lange koolwaterstoffen kunnen leiden tot het blokkeren van poriën en dus deaktivering. Uit de open literatuur en uit octrooien blijkt dat koolstofvorming een belangrijk deaktiverings mechanisme zou kunnen zijn voor kobaltkatalysatoren in de FTS, waarnaar meer onderzoek gedaan zou moeten worden.

Om de hypothese te testen dat koolstof vorming de katalysator deactiveert (Hoofdstuk 5), werden gebruikte Co/Pt/Al<sub>2</sub>O<sub>3</sub> FTS katalysatoren bestudeerd die uit een 100 vaten per dag slurrie fase reaktor gehaald werden. FTS werd in deze reaktor uitgevoerd onder industrieel relevante condities voor langdurige periodes. Een extraktie procedure werd ontwikkeld om de overtollige was (“wax”) te verwijderen, waarna de karakterisering van de katalysator kan worden uitgevoerd met oppervlakte gevoelige technieken zoals X-ray photo-electron spectroscopy (XPS) en ook met “bulk” technieken zoals transmission electron microscopy (TEM) en temperatuur geprogrammeerde (TP) hydrogenering and oxidatie. De gevormde koolstof op de geextraheerde katalysator werd bestudeerd met de TP technieken en het was duidelijk dat er een langzame toename was van polymere koolstof op de katalysator tijdens lange FTS tests. Deze koolstof was stabiel tijdens waterstofbehandelingen bij temperaturen hoger dan de gebruikelijke temperaturen tijdens FTS. Waterstof chemisorptie, high sensitivity, low energy ion scattering (HS-LEIS), en energy filtered transmission electron microscopy (EFTEM) analyses aan deze katalysatoren met stabiele polymere koolstof laten zien dat de koolstof was verdeeld over zowel de drager als de actieve kobalt fase. Een groot gedeelte van de katalysator aktiviteit werd hersteld door het verwijderen van deze polymerische koolstof. Op grond hiervan is gepostuleerd dat deze polymerische koolstof een belangrijke rol speelt in de deaktivering van kobaltkatalysatoren tijdens langdurige FTS tests.

Het begrijpen van de factoren die een rol spelen tijdens koolstofvorming (Hoofdstuk 6) is belangrijk met betrekking tot het verlengen van de tijd dat kobalt katalysatoren gebruikt kunnen worden in de FTS. De invloed van temperatuur en de  $H_2/CO$  verhouding op de vorming van koolstof verbindingen op de  $Co/Pt/Al_2O_3$  katalysatoren werd bestudeerd door middel van model FTS reacties en realistische FTS tests. De invloed van “upset” condities op de koolstof vorming en de katalysator structuur werd ook bestudeerd. Het was duidelijk dat zowel de temperatuur als de gassamenstelling belangrijk zijn voor de hoeveelheid en het type koolstof dat wordt gevormd op  $Co/Pt/Al_2O_3$  katalysatoren. Een belangrijke parameter is de snelheid van de hydrogenering van actieve koolstof in verhouding tot de snelheid van de omzetting van actieve tot niet-actieve koolstof. De omzetting van actieve koolstof in meer stabiele koolstof gebeurt sneller bij hogere temperaturen en lagere  $H_2/CO$  verhoudingen. “Upset” condities zorgen voor de vorming van koolstoffases ( $Co_2C$ , koolstof dat de actieve fase bedekt en filamenten) die de katalysator deaktiveren.

Het werk beschreven in de vorige hoofdstukken gaat over complexe, industriële katalysatoren. In Hoofdstuk 7 worden de eerste resultaten besproken die behaald zijn met nieuwe technieken gemeten aan zowel sferische als vlakke model katalysatoren. Deze resultaten kunnen mogelijk duidelijkheid verschaffen over de reactiviteit en de morfologie van kobalt nanodeeltjes. Allereerts werden sferische kobalt model katalysatoren bereidt door het afzetten van kobalt nanodeeltjes op Stöber silica bollen. Deze katalysatoren werden bestudeerd onder variërende gas samenstellingen door middel van een in-situ TEM. Vervolgens werden vlakke model katalysatoren bereidt door middel van spincoating van voorgevormde kobalt nanodeeltjes op silica TEM grids en bestudeerd na thermische behandelingen. De eerste resultaten op beide model systemen laten zien dat er veel mogelijkheden zijn om deze technieken in de toekomst toe te passen om fundamentele informatie te krijgen over de reactiviteit en structuur van kobalt FTS katalysatoren.



---

# Acknowledgments

---

The completion of this thesis and the enjoyable stay that I had in Eindhoven over the last three and a half years would not have been possible without the contribution of many people and it is my pleasure to thank them here.

At the outset I would like to thank my employer, Sasol Technology and especially my group leader at the time, Peter van Berge for offering me the opportunity to come to the Netherlands. Thank you, Philip Gibson, my departmental manager, for ensuring that we were well taken care of and for your regular visits. I am indebted to Jan van de Loosdrecht, who fulfilled a dual role as my co-promoter and line manager for most of my stay, for his scientific input, sound leadership and for allowing me the necessary freedom in the project. I extend my sincere gratitude to Hans Niemantsverdriet, my promoter, for his guidance and hospitality during our stay in Eindhoven. Hans, I especially appreciate the time you took when we first arrived, to teach us about some fundamental concepts of catalysis. Your tips on scientific presentations also helped to secure a presentation award at NCCC 2008!

I was fortunate to have many research collaborations during the course of this project. I wish to express my gratitude to Abhaya Datye of the University of New Mexico for the EFTEM work and useful discussions. Alfons Molenbroek and Stig Helveg of Haldor Topsøe AS are thanked for their collaboration on in-situ TEM. Stig, your enthusiasm behind the microscope was certainly an inspiration. I also enjoyed the evenings out in Lyngby. My thanks also go to Hidde Brongersma of Calipso BV for the HS-LEIS measurements and insightful discussions on the application of the technique to real catalysts. Grant Forman (Sasol Technology, UK) is thanked for collaboration on cobalt nanoparticles and chats on cobalt FT catalysis in general. I would also like to thank the members of my group and colleagues in Sasolburg, for all their input.

To my friend and predecessor Abdool Saib, thank you for your assistance during the project handover, especially for introducing me to X-ray absorption spectroscopy and for the good company during work visits to Italy, Denmark and Scotland. Thanks also for your useful comments on most of the chapters in this thesis. Thank you, Thehzeeb for all the favours and also for your hospitality during my visits

to Sasolburg. Thanks to Ionel, Sorinela and Ana Ciobîcă for your friendship and for the wonderful Romanian dinners we enjoyed. Ionel, I really appreciate the time you took discussing fundamental aspects of catalysis and helping me with the theoretical work and drawings. Bruce Anderson (*Big guy*) thanks for your input both while you were at Eindhoven and Sasolburg (facilitating the LEIS work) and for the entertaining evening we had with you and Michelle in Nuenen.

I thank Sanne Wijnans for the wax extraction and XPS work she did in her graduation project and for transferring her knowledge. Thank you, Tiny Verhoeven (*de Twaalfde Man*) for your expert technical assistance, especially with XPS and TP and the great help you provided during the two visits to Synchrotron Trieste. We also enjoyed some moments of “high tension” in front of the TEM. Peter Thüne is thanked for useful discussions on model catalysts, XPS and for performing TEM measurements. I thank Thérèse-Anne for all her organisational and administrative tasks and for the pleasant conversations. Emiel Hensen and Christian Müller are thanked for the use of their labs.

Dilip, (*Mate*) you are the most “interesting” Indian guy I ever met. Your love for the Aussie cricket team and heavy metal music really confounded me. Thank you for the many memories (watching the 2007/08 Champions league final stands out) and for introducing me to the TP equipment. Neelesh, I will always remember that you were the first person who made an effort to befriend us. I enjoyed your company. Soon, you’ll be a married man and I hope your wife will be able to convince you to eat spicy food. Thank you to my Albanian colleague, Adelaida Andoni (*happy Ad*), for your close friendship and also for ensuring that we had some excitement in Turku. Ad, I haven’t met a person who was as perseverant and well-prepared as you. Success with the defence! Han Wei, my Chinese friend, I enjoyed your company at many events like the stick dance, braai and the Asian cook-out. Thanks most of all for cycling back on the tandem-bike with Prabashini from Nederwetten! I thank Davy Nieskens, who was my roommate in STW 3.59 for six months, for the pleasant company and interesting conversations and Emiel van Kimmenade for his friendship and eagerness to help. Vijay (*Mr. Ruthenium*), it was nice to know you and talk about catalysis to you. I hope that you have a lot of success in your project and of course lots of publications! Akhtar, you were a friendly colleague and I wish you well with your modelling work. Maarten (*nearest neighbour, with many questions*) and Freek (*who always seemed to be in an excited state*), you gave us company during our first trip on a night train. Best wishes to you both with the DFT calculations and surface science experiments. Gilbère, thanks for your company and willingness to help,

especially with the new XPS machine. Best wishes with your project. Ash and Greg, thanks for the lovely dinners, entertaining evenings with Suhina and for the nice chats that made us reminisce about SA. Best wishes to both of you with the writing-up.

I'd like to thank all my friends and colleagues, past and present in SKA for their company or assistance at one time or another. Thanks to Dani, Ben, Michel, Pieter vG, Luis, Robert, Pijus, Ramesh, Srilakshmi, Volkan, Alessandro, Arjan, Wout, Elize, Marianne, Marion, Yejun, Jie, Sami, Farid, Svetlana, Sander, Noor, Dianna, Merijn, Van-Anh, Ton, Evgeny, Ojwang, Sharan, Kaushik, Subu, Brahim, Pieter M., Gabriella, Ramona, Thijs, Jos, Michèle, Gijsbert, Lianne, Laura, Leandra, Bart, Patrick, Jarno, Jarl Ivar, Barry, Paul, Marcel, Bert and Katharina.

I thank all the members of my church family at IBC Eindhoven for their warm fellowship and friendship during our time there. I express my gratitude to Sadesh Sookraj, Holger Friedrich and Abdool Saib who encouraged me to continue with my studies in chemistry. I am grateful to all my family members and my in-laws, Ronnie and Rose for their moral support and assistance. I acknowledge the support of Freddy Narainsamy, Lily Gengan and my grandmother, people dear to me who passed on while we were in Eindhoven. I especially thank my sister, Camy and my parents, Ronnie and Savy for their encouragement and support. Mum and Dad, I would have never got this far without your influence. I dedicate this book to you.

Last, but by no means least, I must reserve thanks for my lovely wife, Prabashini, who had to make sacrifices to go on this adventure with me. I am glad that we could share so many new experiences together. Thank you also, for your love and support which has carried me through all the difficult times. It was exciting to watch your project progress and see how you turned something “small” into something of substance. All the best with wrapping up your thesis!

A handwritten signature in black ink, reading "Denzil". The signature is written in a cursive style with a large, stylized 'D' and a horizontal line underneath.

Eindhoven, Fall 2008

## *Acknowledgments*

---

# List of Publications

---

D.J. Moodley, C. van Schalkwyk, A. Spamer, J.M. Botha, A.K. Datye, Appl. Catal. A 318 (2007) 157.

D.J. Moodley, J. van de Loosdrecht, A.M. Saib, M.J. Overett, A.K. Datye, J. W (Hans) Niemantsverdriet, “*Carbon deposition as a deactivation mechanism of cobalt-based Fischer-Tropsch synthesis catalysts under realistic conditions*”, Submitted to Appl. Catal A (2008).

D.J. Moodley, J. van de Loosdrecht, A.M. Saib, J. W (Hans) Niemantsverdriet, *The Formation and influence of carbon of cobalt based Fischer-Tropsch Synthesis catalysts: An integrated review*, Prepr. Pap.-Am. Chem. Soc., Div. Pet. Chem. 53 (2) (2008) 122.

D.J. Moodley, J. van de Loosdrecht, A.M. Saib, J. W (Hans) Niemantsverdriet, *The Formation and influence of carbon of cobalt based Fischer-Tropsch Synthesis catalysts: An integrated review*, submitted for publication in B.H. Davis, M.L. Occelli (Eds.), *Advances in Fisher Tropsch Synthesis, Catalysts and Catalysis*, CRC, 2008.

D.J. Moodley, A.M. Saib, J. van de Loosdrecht, J. W (Hans) Niemantsverdriet, *The impact of cobalt aluminate formation on the deactivation of cobalt-based Fischer-Tropsch synthesis catalysts*, to be submitted to Applied Catal. A (2008).





---

# Curriculum Vitae

---

Denzil James Moodley was born in Port Shepstone, a small town on the east coast of South Africa on March 12, 1977. After he finished high school in his home town in 1994, he started his tertiary studies at the University of Natal, Durban in the School of Pure and Applied Chemistry. He was introduced to the field of catalysis during his BSc (Hons) project which involved the study of alcohol oxidation using supported ruthenium catalysts.

Upon graduation with a BSc Hons (Chemistry) degree he began working for Sasol Technology R&D in South Africa, where he was involved in hydrocarbon transformation research utilizing Fischer-Tropsch derived feed streams. Here, he worked on projects involving heterogeneous olefin metathesis and alcohol dehydration. During this time he completed his MSc Chemistry degree (cum laude) at the Potchefstroom University for Christian Higher Education under the supervision of Prof. Manie Vosloo with a thesis entitled “The metathesis activity and deactivation of heterogeneous metal oxide catalytic systems”.

He then moved to the Fischer-Tropsch catalysis group at Sasol Technology R&D in 2004, where he was involved in the study of cobalt-based catalysts. In June 2005, he was seconded to Eindhoven University of Technology to the group of Prof. Dr. Hans Niemantsverdriet. His research here mainly involved aspects of deactivation of cobalt-based Fischer-Tropsch synthesis catalysts. The most important results of the research are described in this thesis.